

SCUOLA DI SCIENZE

Corso di Laurea Magistrale in Geologia e Territorio

Dipartimento di Scienze Biologiche, Geologiche ed Ambientali

Tesi di Laurea Magistrale

Thermal rock properties of geothermal reservoirs
and caprocks in the Danish Basin – prerequisites
for geothermal applications

Candidato:
Roberto Miele

Relatore:
Prof. Marco Antonellini

Correlatore:
Dr. Sven Fuchs

Acknowledgments

First of all, I would like to warmly thank my external supervisor, Dr. Sven Fuchs (GFZ Helmholtz Centre Potsdam), who gave me the opportunity to join his research team and work at the GFZ institute. His patient guidance, enthusiastic encouragement and useful critiques have been essential for the realisation of this work.

I would also like to express my deepest gratitude to Dr. Andrea Förster (GFZ), for the studentship position and for the financing of this project, as well as for the valuable advice she gave me during my time at the GFZ.

Furthermore, my deep gratitude goes to my supervisor Prof. Marco Antonellini (University of Bologna) for his assistance and advice that have been of great importance in the realization of this work.

I am also particularly grateful for the work of Christian Cunow and Matthias Kreplin (GFZ) in sample preparation and for the assistance in all the laboratory procedures. They were always available whenever I needed help or had a question.

Many thanks also to Dr. Ben Norden and Dr. Hans-Jürgen Förster (GFZ) for sharing their knowledge with me and giving me useful advice in several occasions.

I want to thank also my friends and my beloved flatmates, who listened to me while continuously rambling about this dissertation.

Finally, I want to express my very profound gratitude to my parents, Lorenzo and Giuliana, for providing me with unfailing support and continuous encouragement throughout these years of study. My curiosity and interest for science and my love for nature I owe them especially to them.

This accomplishment would not have been possible without all of them.

Thank you.

Table of contents

Acknowledgments	i
Abstract in Italian	v
Abstract in English	vi
1. Introduction	1
1.1. <i>GEOTHERM project</i>	2
1.2. <i>Aim of this study</i>	2
2. Theoretical framework	4
2.1. <i>Heat Storage</i>	4
2.2. <i>Heat transport</i>	5
3. Overview of the study area	6
3.1. <i>Geographical location</i>	6
3.2. <i>Geology</i>	7
3.2.1. Tectonic setting	7
3.2.2. Evolution of the Norwegian-Danish Basin	8
3.2.3. Late Triassic – Early Cretaceous lithostratigraphy	10
3.2.3.1. Gassum Formation	11
3.2.3.2. Fjerritslev Formation	12
3.2.3.3. Haldager Sand Formation	13
3.2.3.4. Flyvbjerg Formation	14
3.2.3.5. Børglum and Frederikshavn Formations	14
3.2.3.6. Cretaceous Chalk Members and Neogene sedimentation	15
3.3. <i>Geothermics</i>	16
3.3.1. Potential reservoirs in the Danish Basin	16
4. Material and methods	18
4.1. <i>Samples compilation</i>	18
4.1.1. Aars-1	18
4.1.2. Farsø-1	20
4.1.3. Stenlille-1	22
4.1.4. Lavø-1, Sæby-1 and Gassum-1 samples	23
4.1.5. Classification by major components	24
4.2. <i>Laboratory analyses</i>	25
4.2.1. Drying process	26
4.2.2. Saturation procedure	27
4.2.3. Archimedes' method	28
4.2.4. Optical Scanning method	29
4.2.4.1. Theoretical background	29
4.2.4.2. Required corrections	31
4.2.4.3. Measuring procedures	32

4.3.	<i>Data processing</i>	34
4.3.1.	Geometric mean model	34
4.3.2.	Final data set	36
4.3.3.	Software	36
5.	Results	37
5.1.	<i>Petrophysical properties and lithology</i>	37
5.1.1.	Porosity and density	37
5.1.2.	Bulk thermal conductivity and bulk thermal diffusivity	40
5.1.3.	Specific heat capacities	43
5.1.4.	Anisotropy	44
5.1.5.	Geometric mean model application on bulk thermal properties	45
5.1.6.	Matrix thermal properties from geometric mean model	48
5.2.	<i>Characteristics by formations</i>	50
6.	Discussions and conclusions	53
6.1.	<i>Bulk thermal diffusivity and geometric mean model</i>	53
6.2.	<i>Matrix thermal properties as indicators of the composition of the rocks</i>	55
6.3.	<i>Variability of the investigated properties and comparison with literature</i>	57
6.3.1.	Variability within the Danish Basin	57
6.3.2.	Variability with saturating fluid	60
6.4.	<i>Summary of the main results</i>	62
	Appendix A	64
	Appendix B	65
	References	66

Abstract in Italian

Il sottosuolo danese offre un grande potenziale per l'utilizzo del calore geotermico a bassa entalpia e, quindi, per modificare la struttura di teleriscaldamento nazionale, fornendo un carico di base al sistema. Nell'ultimo decennio sono state condotte nuove campagne di esplorazione e ricerca per rimuovere gli ostacoli geologici, tecnici e commerciali per un uso significativo di queste risorse geotermiche. Uno degli ostacoli principali è la conoscenza delle proprietà termiche delle rocce quali conduttività, diffusività e capacità termica. Le condizioni termiche del sottosuolo, nonché la capacità produttiva e il ciclo di vita degli impianti di teleriscaldamento geotermico dipendono in gran parte, tra gli altri parametri, da queste proprietà. Per il bacino danese in particolare sono disponibili solo pochi set di dati pubblicati e quasi totalmente limitati alla conduttività termica delle rocce. I valori di diffusività termica e calore specifico sono in gran parte sconosciuti. Per superare questa lacuna, sono state effettuate nuove misurazioni di laboratorio. La conduttività termica e la diffusività termica sono misurate su sezioni di carota, mentre il calore specifico è calcolato in base a questi valori e alla densità della roccia. Gli obiettivi geologici dello studio sono le arenarie del bacino del Mesozoico (Formazioni del Gassum, Frederikshavn e Haldager Sand), così come rocce argillose e calcari appartenenti a formazioni che fungono da caprocks (Formazioni di Fjerritslev, Vedsted e Unità Gessose). La suite di 43 campioni studiata comprende rocce di sei pozzi: Aars-1, Farsø-1, Stenlille-1, Lavø-1, Gassum-1 e Sæby-1. Le misurazioni sono eseguite su rocce secche e sature in acqua pura, utilizzando il metodo di scansione ottica (Thermal Conductivity Scanner, [Popov et al., 1999](#)). Inoltre, sono ricavati i valori di conduttività e diffusività termica di matrice attraverso l'utilizzo del modello di media geometrica. Pertanto sono individuati i *range* di valori caratteristici per ogni litologia e viene fornita un'indagine qualitativa sulla composizione mineralogica dei campioni sulla base dei dati di matrice. Ulteriori osservazioni sono fatte sul comportamento della diffusività termica e l'applicazione relativa della modello di media geometrica.

Questo studio è stato reso possibile grazie al supporto del progetto "GEOTHERM", finanziato dalla Innovation Fund Denmark.

Parole chiave: *bacino danese, conduttività termica, diffusività termica, capacità termica, optical scanning, geotermia a bassa entalpia, GEOTHERM.*

Abstract in English

The Danish subsurface provides a large potential for the use of low-enthalpy geothermal heat and, thereby, to change the national district heating structure by providing a base load power to the system. In the past decade, new exploration and research campaigns were performed to remove geological, technical and commercial obstacles for a significant use of these geothermal resources. One of the obstacles is the lack of knowledge on the thermal-related physical rock properties. Subsurface thermal conditions as well as the production capacity and lifecycle of geothermal district heating plants largely depend, among other parameters, on these properties. For the Danish Basin only few published data sets are available and mostly limited to thermal conductivity. Values of thermal diffusivity and specific heat capacity are mostly unknown. In order to overcome this gap, new laboratory measurements were conducted. Thermal conductivity and thermal diffusivity were measured on drill cores sections, while specific heat capacity was calculated based on these values and on rock density. Geological targets for the study are Mesozoic reservoir sandstones (Gassum Fm., Frederikshavn Fm., Haldager Sand Fm.), but also mud-/claystones and limestones of seal rocks (Fjerritslev Fm., Vedsted Fm.). The rock suite of 43 specimens studied was sampled in six wells: Aars-1, Farsø-1, Stenlille-1, Lavø-1, Gassum-1 and Sæby-1. The measurements are performed under dry and saturated conditions using the optical scanning method (Thermal Conductivity Scanner; [Popov et al., 1999](#)). Furthermore, the values of conductivity and thermal diffusivity of the matrix were obtained by geometric mean averaging. Therefore, the ranges of characteristic values for each lithology were identified and a qualitative survey on the mineralogical composition of the samples on the basis of the matrix data was assembled. Further observations on the behaviour of thermal diffusivity and the relative application of the geometric mean model are also provided.

This study was possible thanks to the "GEOTHERM" project, funded by the Innovation Fund Denmark.

Keywords: Danish Basin, thermal conductivity, thermal diffusivity, specific heat capacity, optical scanning, low enthalpy geothermal, GEOTHERM.

1. Introduction

The reduction of CO₂ emissions in the atmosphere and limitation of fossil fuel usage is a key global issue. Therefore, the general interest in using renewable energy sources is constantly growing. Geothermal systems represents a fundamental element for this goal, as they can be used for different applications (from energy production to storage of gas or energy itself). More than one hundred geothermal plants are currently operating in the European territory and this number is destined to grow in the next years (EGEC, 2017).

Denmark, is investing in this field, in order to become entirely based on green energy. Currently, geothermal energy plays an important role in district heating systems and gas storage in this country. As pointed out by several authors (e.g. Balling, 1992; Nielsen et al., 2004; Mahaler & Magtengaard, 2010; Mathiesen et al., 2010), the Danish subsurface is currently not believed to be sufficiently efficient for direct electricity production, mainly due to the low permeability of the deeper and warmer aquifers. Nonetheless, the basin has a great potential in terms of low-enthalpy. Moreover, increasing technologies and research may lead to the production of electricity from these systems in the future (van Wees et al., 2013; Røgen et al., 2015). Past and recent research is focused on the characterization of petrophysical and geochemical properties of sandstone reservoirs in geothermal systems and the definition of their spatial distribution in the basin. Particular interest was focused on the Jurassic and Triassic formations, where several units were identified as potential reservoir originally by Balling et al. (1981) and Balling et al. (1992):

- Frederikshavn Member (Upper Jurassic);
- Haldager Sand Member (Middle Jurassic);
- Gassum Formation (Upper Triassic - Lower Jurassic);
- Skagerrak Formation (Lower to Upper Triassic);
- Fjerritslev Formation (Middle Triassic);
- Bunter Sandstone Formation (Lower Triassic).

These Mesozoic formations are related to two Permian–Cenozoic tectonic structures, which extend in northern Europe: the Norwegian-Danish Basin and the North German Basin.

Three geothermal plants are already in operation in Thisted, Copenhagen and Sønderborg, while several other sites are under investigation for the construction of new plants (Danish Energy Agency, 2014). The first geothermal heating plant started the production in Thisted in 1984. The heat is produced using 15 % saline water at 43 °C, taken from the Gassum Formation at a depth of 1.25 km. Currently, the plant has a capacity of 7 MWt (75 TJ/yr). The second plant is located in Copenhagen (Margretheholm). It takes water from a well at 2.6 km of depth from the Bunter Sandstone reservoir. The water has a salinity of 19 % and a temperature of 74 °C. The production of the plant started in 2005 and currently produces 14 MWt (180 TJ/yr). The latest plant, at up to 12 MWt (100 TJ/yr) started production at Sønderborg in 2013. It uses water at 48°C from 1.2 km depth, from Gassum Formation. The salinity of the water is 21 % (Mahler & Magtengaard, 2010; Røgen, et al., 2015). These plants have one injection well producing heat through a heat exchanger and/or based absorption heat pumps. The driving heat primarily comes from external sources (such as biomass boilers). Considering the shallow geothermal heat production (around 27,000 installation), the total installed capacity of the country is 353 MWt, with an annual energy use of 3,755 TJ/yr (Røgen, et al., 2015).

1.1. GEOTHERM project

The first studies on detailed reservoir extension, reservoir properties and temperatures on regional scale were carried since the 1970s. The Dansk Olie & Naturgas A/S (DONG A/S) and the Geological Survey of Denmark and Greenland (GEUS; former “DGU”) were involved in exploration, research, advisory and consultancy for geothermal energy in Denmark.

The GEOTHERM project is an on-going multi-disciplinary research project, carried out jointly by GEUS (as coordinator of the project), the University of Aarhus, the Geological Survey of Sweden, the German Research Centre for Geosciences (GFZ), and the DONG Energy. This project aims to remove remaining geological, technical and commercial obstacles, by analysing in details the Danish subsurface. Properties such as depth to reservoir, thickness, permeability and temperature of geothermal reservoirs were analysed, combining new data with those already available. In particular, one of the main project goals is to study and investigate petrophysical rock properties of major geothermal reservoir sandstones and adjoining cap rocks. A second aim is to identify the variability of these properties according to the lithological composition and to determine the geological formations that are most suitable for geothermal applications. The final goal is the production of geological and geophysical models, for the understanding of lateral and vertical variations in reservoir quality and temperature.

1.2. Aim of this study

The work herein presented reflects parts of the Work Package 4 of the GEOTHERM project and consists in the measurement and investigation of the petrophysical properties of 42 drill-core samples, collected from six wells of the Danish onshore (Aars-1, Farsø-1, Stenlille-1, Lavø-1, Sæbey-1 and Gassum-1). Most of the analysed rocks belong to the Mesozoic formations of the Danish Basin: Gassum, Fjerritslev, Haldager Sand, Flyvbjerg, Frederikshavn, and Vedsted Formations. A smaller part of the collection represents the Upper Cretaceous chalk units, which was sampled in the adjacent Skagerrak–Kattegat Platform.

The last petrophysical data of the sedimentary units in the Danish Basin date back to 1992 (Balling et al., 1992) and are representative of wide depth intervals within the basin. This work contributes to the resolution of this problem by providing new results from detailed laboratory analyses. A thermal characterization of the specimens is provided, including bulk thermal conductivity and bulk thermal diffusivity, measured at ambient conditions, using the Optical Scanning method (Popov et al., 1999). The samples were analysed in dry and saturated conditions. Moreover, effective porosity and density of each sample were defined through the Archimedes method. Secondly, the geometric mean model (Woodside & Messmer, 1961a,b) was applied for the calculation of matrix thermal properties and conversion of the bulk values. Such parameters underpin the numerical modelling for the geothermal potential of the Danish Basin, which will be computed by the colleagues from Aarhus University in a subsequent Work Package of the GEOTHERM project.

The main objective of this work is the investigation of the relationships between rock type and their thermal properties. In particular, the variations of these characteristics with the lithology, main mineralogical components and porosity were examined, in order to define the characteristic ranges. Finally, the measurements here presented were compared with the data available in the literature, in order to evaluate the variability of these properties within the Danish Basin.

This thesis is organized in six chapters, as follows:

1. **Introduction** (current chapter).
2. **Theoretical framework:** this chapter provides a brief outline of the thermal parameters investigated, focusing the attention on the underlying theory.
3. **Overview of the study area:** the geographical location of the wells from which the rock samples are collected is described. Moreover, the tectonic and sedimentary context in which these rocks formed are outlined. Finally, the attention is focused on the thermal regime of the Danish territory and the geothermal systems currently used.
4. **Material and methods:** In this chapter the samples taken under examination are first listed and described. Subsequently, all laboratory procedures and data analysis are described, briefly integrating the underlying theory.
5. **Results:** all results achieved in the measurement phase of the petrophysical properties and data analysis are shown here.
6. **Discussion and Conclusions:** the main results obtained in this thesis are analysed and discussed here, including a comparison with the available literature. The chapter ends with a brief summary of the results achieved in this work.

2. Theoretical framework

Variations in the temperature field are generally linked to the variation of terrestrial heat flow, the thermal conductivity, stratigraphy, and the radioactive-heat sources in the basin. For geothermal modelling, it is fundamental to define different thermal properties of the Earth subsurface. For this purpose, two main characteristics of a geothermal system are investigated: how the heat is absorbed and how it is transferred within the rocks of the system. In the first case, it is necessary to quantify the heat capacity of reservoirs and contiguous cap rocks. In the second case, thermal conductivity, thermal diffusivity and heat flow density are the main parameters to define (e.g. Clauser, 2006; Fuchs & Förster, 2010; Fuchs et al., 2015). These properties vary both laterally and with depth, depending on several factors such as petrography and porosity of the rocks, the saturating fluids in pores and fractures, tectonic setting of the area, and paleoclimate history. For a more detailed dissertation on this topic, see e.g. Clauser (2006, 2009, 2011) and Robertson (1988).

2.1. Heat Storage

The heat capacity C quantifies the amount of heat that can be stored in a rock volume. It is determined by the amount of heat (ΔQ) required to raise the temperature of a body by (ΔT).

$$C = \frac{\Delta Q}{\Delta T} \quad \left[\frac{J}{K} \right] \quad (1.1)$$

When considering a unit mass (M) of a substance, the specific heat capacity c is defined.

$$c = \frac{\Delta Q}{M * \Delta T} \quad \left[\frac{J}{kg * K} \right] \quad (1.2)$$

In geothermal modelling, it is useful to consider isobaric specific heat capacity (c_p). As defined e.g. by Clauser (2006), this parameter can be inferred considering the following state function for a closed system

$$dH(P, T) = dE + PdV + VdP \quad [J] \quad (1.3)$$

where the variation of the enthalpy of the system (dH) is given by variation of internal energy (dE) and work ($PdV + VdP$). Assuming dE as the sum of change in heat (dQ) and the work delivered to the system (dW), and dW as only volume expansion work

$$dE = dQ + dW \quad [J] \quad (1.4)$$

$$dW = -PdV \quad [J] \quad (1.5)$$

it is finally possible to define the isobaric specific heat capacity as

$$c_p = \frac{dQ}{dT} = \left(\frac{\partial H}{\partial T} \right)_P \quad \left[\frac{J}{K} \right] \quad (1.6)$$

Thus, isobaric specific heat capacity is the first derivative of enthalpy with respect to temperature. Finally, by comparing equations (1.2) and (1.6) it is possible to settle their equivalency for $dQ=\Delta Q/M$ and define that c_p is equal to the specific heat content (ΔH):

$$c_p = \Delta H = \frac{\Delta Q}{M} \quad \left[\frac{J}{kg * K} \right] \quad (1.7)$$

Nonetheless, the total heat capacity of a rock is defined by heat capacities of both rock and saturating fluids in pores and fractures. Thus, a common way to calculate the heat capacity is on a volumetric basis, using the volumetric heat capacity (or thermal capacity) ρc .

$$\rho c = \lambda / \alpha \quad \left[\frac{J}{m^3 * K} \right] \quad (1.8)$$

where ρ is the density in kg/m³, λ is the thermal conductivity in W/(m*K) and α is the thermal diffusivity [m²/s] (see the following section) of the specific phase considered. Moreover, the difference between isobaric and isochoric specific heat capacity is negligible for crustal rock at temperatures below 1000K.

2.2. Heat transport

In Earth's crust, the heat is transported mainly by diffusion and conduction. Advection occurs only when a sufficiently large hydraulic permeability is available and the contribution of radiation is relevant only when the ambient temperature is greater than ca. 600 °C. Thus to define the transport of heat through a rock, two fundamental parameters must be specified: thermal conductivity and thermal diffusivity.

The thermal conductivity (λ) is an intrinsic physical property of the rocks for steady state conditions. This quantity defines the amount of heat that flows across a unit cross-section of rock, along a unit distance, per unit temperature decrease, per unit time [W/(m*K)].

In transient state conditions, the thermal diffusivity α describes the heat diffusion in a rock. Clauser (2011) defines the thermal diffusivity as “the ratio of heat flowing across the face of a unit volume and the heat stored in the unit volume per unit time” [m²/s]. It is also possible to define this quantity as the ratio of thermal conductivity and volumetric heat capacity, considering Eq. (1.7).

As previously mentioned, the heat-flow density (q_i , later referred to be the “heat flow”) has a pivotal role for thermal characterization of a site. When observed at the surface, it counts as surface heat flow (q_s). When unaffected by paleoclimate, terrain effects such as heat refraction or similar effects, it counts as terrestrial surface heat flow and reflects the “real” heat flow from the Earth's interior. For steady state conditions, the heat flow is defined by Fourier's law

$$q_i = \lambda_{ij} \frac{\partial T}{\partial x_j} \quad \left[\frac{W}{m^2} \right] \quad (1.9)$$

where $(\partial T / \partial x_j)$ is the thermal gradient vector. The heat flow itself is a vector, depending on the thermal conductivity tensor (λ_{ij}). In fact, the layering of sedimentary rocks, as well as the foliation in general, defines differences of thermal conductivity between the directions parallel and perpendicular to bedding. Thus, the thermal conductivity tensor is related to the anisotropy of the rocks. For isotropic rocks, the heat flow will be predominantly vertical and it is sufficient to consider only its vertical component. On the contrary, for many sedimentary and metamorphic rocks the lateral heat flow is significant, due to their inhomogeneity (Clauser, 2011).

3. Overview of the study area

3.1. Geographical location

The study area is the Danish Basin, a buried extensional basin that approximately covers the vast majority of the Danish territory, both onshore and offshore. In particular, the samples analysed in this project were collected from six wells shown in Fig. 3.1, in the north-eastern part of Denmark. The names of the wells indicate the six cities in which they were drilled, which are located in the Midtjylland (Gassum-1), Norjyland (Farsø-1, Aars-1 and Sæby-1), Sjælland (Stenlille-1) and Hovedstaden (Lavø-1) regions. The wells are in different tectonic structures of the basin, as shown in Fig. 3.2:

- Aars-1, Farsø-1, Gassum-1 and Stenlille-1 are placed in the Danish Basin
- Sæby-1 is located on the northern part of the Skagerrak-Kattegat-Platform
- Lavø-1 is located on the Ringkøbing-Fyn High area in the South

Such tectonic structures are described in the following paragraph.

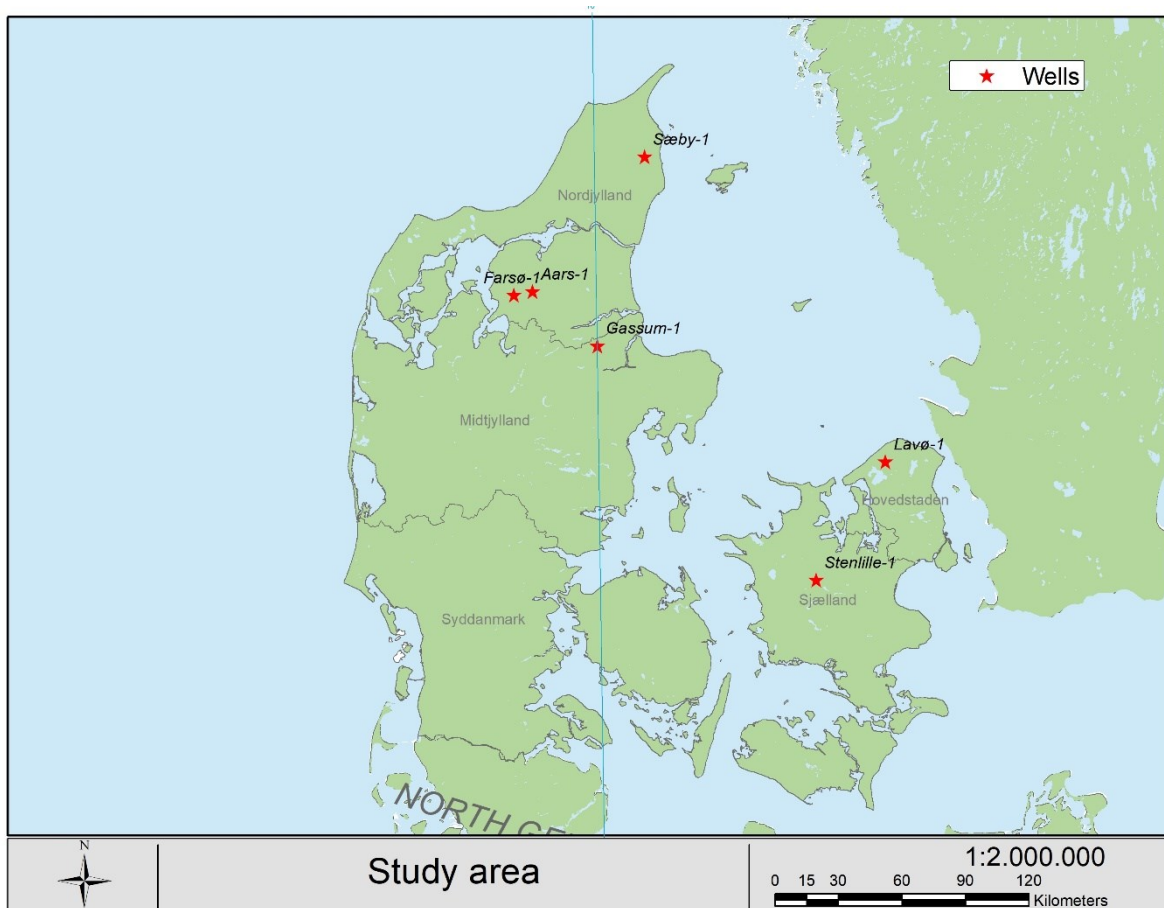


Figure 3.1: Area of interest of this work. The red stars represent the location of the wells from which the samples of this work were collected (Coordinate System: ED50/UTM Zone 32). Data: GEUS.

3.2. Geology

3.2.1. Tectonic setting

The Danish Basin constitutes the eastern part of the Norwegian-Danish Basin, comprising the Danish Embayment and the Danish Sub-basin. It is an intra-cratonic, Permian–Cenozoic structure, trending WNW–ESE (Michelsen et al., 2003; Michelsen & Nielsen, 1993; Nielsen, 2003). The Norwegian-Danish Basin, in turn, belongs to the eastern part of the North Sea Basin, which is made up of several fault-bounded basins, interspersed with structural highs (Balling, 1992). Five major structural elements, generally oriented NW–SE, are distinguished in the study area (Fig. 3.2):

- The North German Basin and the Ringkøbing–Fyn High to the south
- The Danish Basin
- The Sorgenfrei–Tornquist Zone and the Skagerrak–Kattegat Platform to the north-east

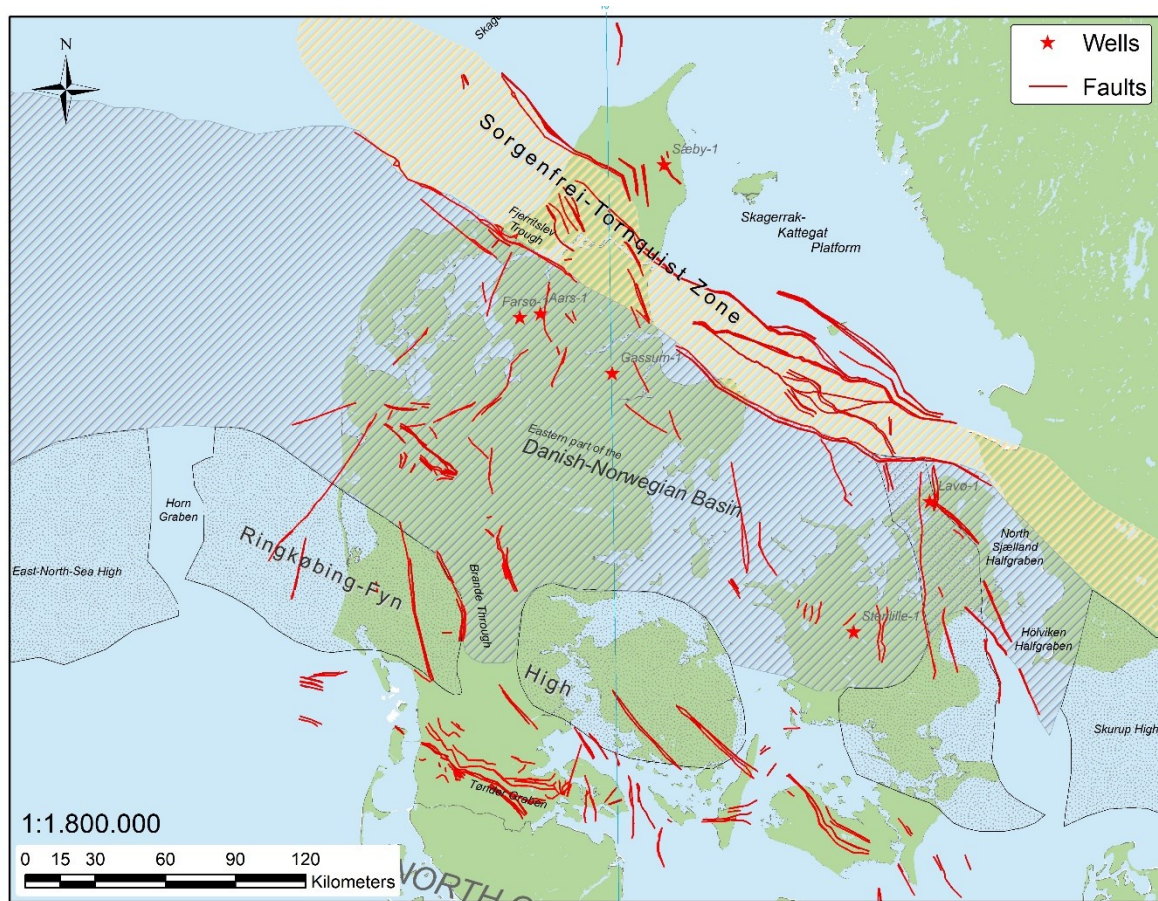


Figure 3.2: main tectonic elements of the Danish area (Coordinate System: ED50/UTM Zone 32). Data: GEUS.

The Ringkøbing–Fyn High separates the Danish Basin from the Northern German Basin. It consists of shallow faulted blocks of Precambrian basement. To the northeast, the Skagerrak–Kattegat Platform and the Sorgenfrei–Tornquist Zone separate the basin from the Precambrian Baltic Shield and together constitute the Fennoscandian Border Zone (EUGENO-S Working Group, 1988; Michelsen et al., 2003; Nielsen, 2003). The Sorgenfrei–Tornquist Zone is a block-faulted zone, 30–50 km wide, with tilted Palaeozoic rocks. It runs from the North Sea in the Skagerrak area to the Rønne Graben in the Baltic Sea and converges to the Teisseyre–Tornquist Zone in the offshore Bornholm. It originated during

the Late Carboniferous – Early Permian times and defines a rift zone. The adjacent and eastern Skagerrak-Kattegat Platform is a more stable area composed by Lower Permian, Lower Palaeozoic and Precambrian crystalline rocks (EUGENO-S Working Group, 1988; Nielsen, 2003; Vejbæk, 1989).

The syn-rift succession is separated from the post-rift one by a basin-wide unconformity: the pre-Zechstein surface. It mainly covers Precambrian crystalline rocks on the Ringkøbing–Fyn High and Skagerrak–Kattegat Platform and lower Palaeozoic deposits in most of the Danish Basin and Sorgenfrei–Tornquist Zone. Eventually, Late Carboniferous – Early Permian syn-rift clastic rocks (Rotliegend group) are found under this unconformity (Michelsen & Nielsen, 1993; Nielsen, 2003). The Upper Triassic – Jurassic succession is 5 – 6.5 km thick along the Danish Basin and more than 9 km thick in the Sorgenfrei–Tornquist Zone. It is possible to distinguish two main tectono-stratigraphic units, separated by an intra-basinal unconformity:

- The Norian – Lower Aalenian succession, formed under relative tectonic tranquillity. In this succession, the sediments are relatively undisturbed and define a layered-cake geometry, except for areas where local faulting or diapir movements occurred. The sedimentation is mainly controlled by sea level changes;
- The Late Middle – Jurassic succession, influenced by a fault controlled subsidence and sea level changes.

These deposits represent various environments, from dominantly fluvial to paralic and coastal in the east, to deep marine in the west (Michelsen et al., 2003; Nielsen, 2003). According to the EUGENO-S working group (1988), the crustal thickness varies between 28 and 30 km in the Norwegian-Danish Basin and Sorgenfrei–Tornquist Zone, whereas it is 32–36 km thick in the Skagerrak-Kattegat Platform and Ringkøbing–Fyn High.

3.2.2. *Evolution of the Norwegian-Danish Basin*

The formation of the Norwegian-Danish Basin is caused by regional thermal cooling that followed a Late Carboniferous – Early Permian rifting phase. Erosion followed the rifting, causing the formation of the top pre-Zechstein surface (EUGENO-S Working Group, 1988; Michelsen & Nielsen, 1993; Vejbæk, 1989). A marine transgression in the Upper Permian led to the deposition of thick layers of calcareous and salt deposits (Zechstein Formation) in the central part of the basin. The halokinetic movements of the Zechstein's salt influenced the geometry and the sedimentation of the following successions (Nielsen 2003; Petersen et al., 2008; Vejbæk, 1989).

From Lower to Middle Triassic, thick layers of mainly continental sediments were deposited (Michelsen & Nielsen, 1993; Nielsen 2003; Petersen et al., 2008). The Norian stage is characterised by the beginning of a transgression phase. The Danish Basin was covered by a shallow marine – paralic environment, which defined the sedimentation of limestones and claystones of the Vinding Formation in the central basin and shallow marine sandstones and mudstones of the Skagerrak Formation in the Sorgenfrei–Tornquist Zone. A regression phase during Rhaetian times caused the coastal progradation and the deposition of mainly shallow marine to fluvial sands towards the centre of the basin, defining the Gassum Formation.

In the earliest Hettangian, a new transgressive phase defined the deposition of marine muds of the Fjerritslev Formation (FI member) in the southwest and the regression of the coastline towards north-east (Fig. 3.3). The Gassum Formation was progressively overstepped until the earliest Sinemurian, when the open marine environment took over in the Sorgenfrei–Tornquist Zone. An overall sea level rise, interspersed by smaller sea level fluctuations lasted until the Early Toarcian and defined the deposition of FI, FII and FIII

members of the Fjerritslev Formation (Michelsen et al., 2003; Nielsen, 2003; Petersen et al., 2008). During Aalenian – Bajocian, a regional uplift influenced the

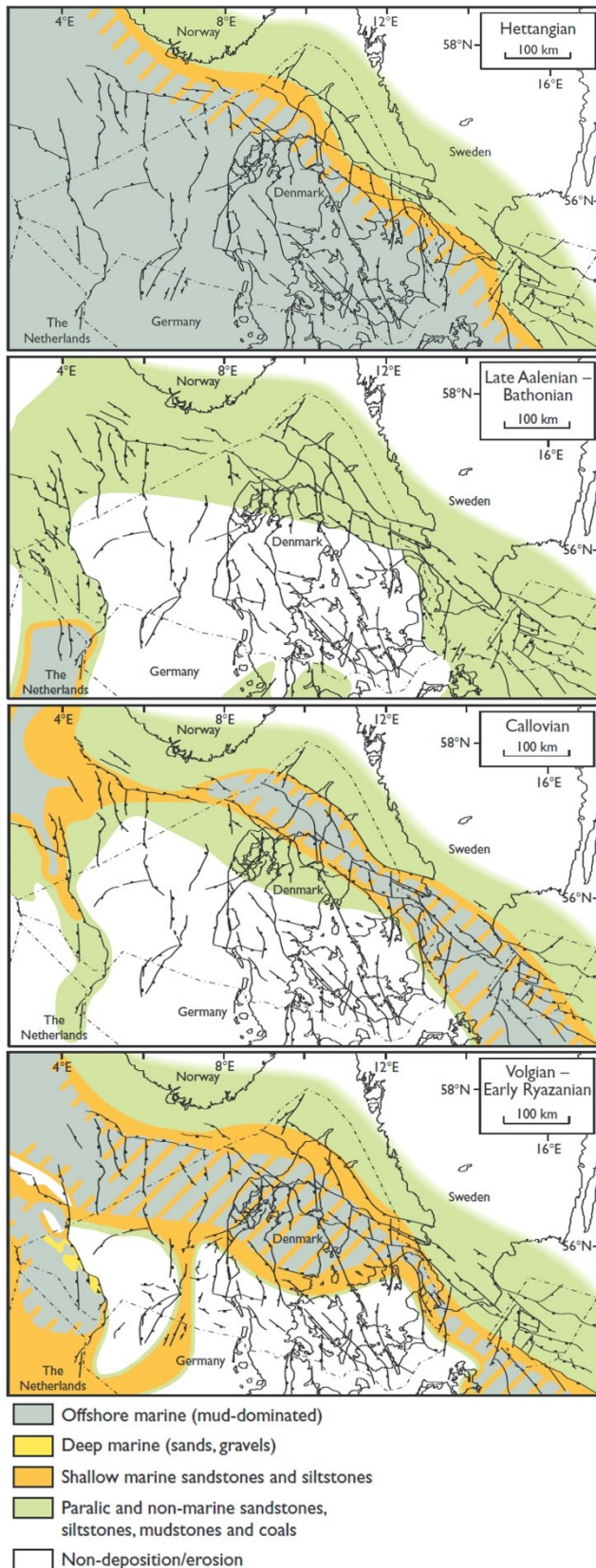


Figure 3.3: Environmental succession of the Norwegian-Danish Basin pre, during and post Middle Jurassic uplift (modified from Michelsen et al., 2003).

Ringkøbing-Fyn High and the Danish Basin. The Triassic – Lower Jurassic succession in the Ringkøbing-Fyn High was totally eroded, as well as part of the Fjerritslev Formation in the Danish Basin. The Sorgenfrei–Tornquist Zone continued to subside at a slower rate, permitting the deposition of the FIV member. A regressive phase during Upper Aalenian defined the deposition of paralic and fluvial sands of the Haldager Sand Formation (Fig. 3.3; Michelsen & Nielsen, 1993; Mogesen & Korstgård, 2003; Nielsen, 2003). The uplift was followed by a regional subsidence that lasted until Volgian times and the Fennoscandian Border Zone was characterized by shallow marine to non-marine environments, and was strongly influenced by repeated transgressive–regressive cycles.

The Oxfordian Age is characterised by the deposition of offshore clay-dominated deposits in the basin, while lagoonal deposition dominated the remaining highs (Flyvbjerg Formation). The deposition of marine claystones of the Børglum Formation followed in the Kimmeridgian. The Frederikshavn Formation was deposited in Volgian–Ryazanian times, in a shallow marine to offshore environment. Non-marine conditions prevailed in the Skagerrak–Kattegat Platform and Sorgenfrei–Tornquist Zone in this period (Michelsen et al., 2003; Petersen et al., 2008). The expansion of the marine environment in Early Cretaceous times caused a deposition of marine mud over most of the study area. The tectonic tranquillity ended during Late Cretaceous–Palaeogene times, giving way to an inversion in the Sorgenfrei–Tornquist Zone. Significant uplift and erosion occurred over parts of the Norwegian-Danish Basin and the Ringkøbing-Fyn High in the Neogene (Michelsen & Nielsen, 1993; Mogesen & Korstgård, 2003; Petersen et al., 2008).

3.2.3. Late Triassic – Early Cretaceous lithostratigraphy

In the Norwegian-Danish Basin, the Zechstein evaporites (Fig. 3.4) represent the first post-rift deposit. This succession is present at various depths due to the salt movements. During Early – Middle Triassic, the depositional environment was mainly continental, controlling the deposition of Bunter Sandstone, Skagerrak, Ørslev, Falster and Tønder Formations. See e.g. Petersen et al. (2008) for a more detailed description of these formations and their relative depositional environments. In Norian Age, 40–90 m of marls and oolitic carbonates were deposited, defining the Vinding Formation. (Nielsen, 2003; Petersen et al., 2008). The Upper Triassic – Jurassic succession of the Danish Basin includes Skagerrak, Vinding, Gassum, Fjerritslev, Haldager Sand, Flyvbjerg, Børglum and Frederikshavn Formations (Michelsen et al., 2003; Nielsen, 2003; Petersen et al., 2008).

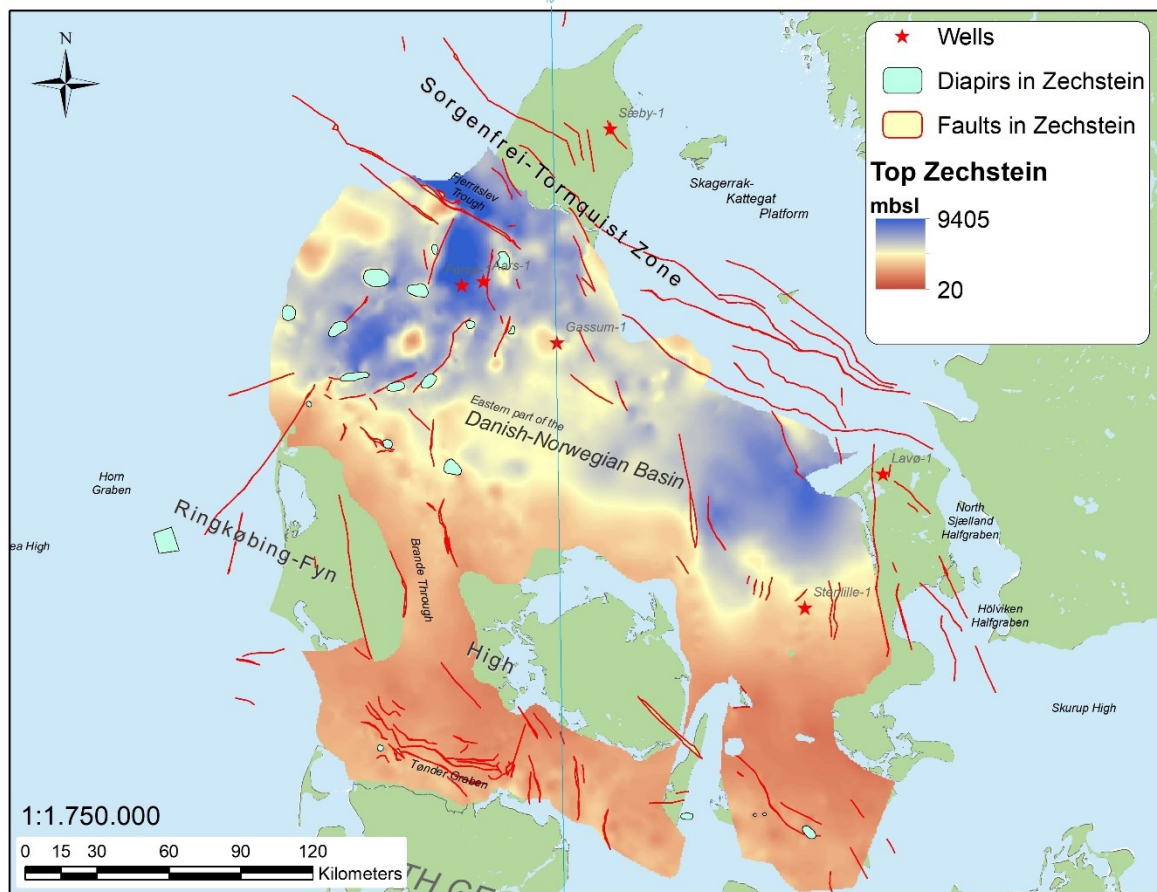


Figure 3.4: Extension and depth of the top of the Zechstein units, including main faults and salt diapirs that occur within the surface (Coordinate System: ED50/UTM Zone 32). Data: GEUS.

3.2.3.1. Gassum Formation

The Gassum Formation formed during Late Norian – Rhaetian times over most of the basin (Fig. 3.5). Its upper limit is dated to the latest Rhaetian over most of the central part of the Danish Basin, and it progressively youngs to earliest Sinemurian Age towards the Fennoscandian–Border Zone. It interfingers with the Vinding Formation at its base, and its upper part (in the north-eastern part of the basin) is contemporaneous to the Fla member of the Fjerritslev Formation (Michelsen et al., 2003; Nielsen, 2003). In general, the thickness of the formation is between 50 and 150 m in the Danish Basin and between 170 and 200 m in the Sorgenfrei-Tornquist Zone. The maximum thickness of 300 m is reached in this fault bounded area. The Gassum Formation occurs throughout most of Denmark at typical depths of 2,500–3,000 m. Locally, the depth can increase to 2,000–4,000 m. Along the structural highs it is found at 500–1,000 m depth (Balling, 1981). The lithology consist of interbedded white-grey and fine- to medium- grained (occasionally coarse-grained and pebbly) sandstones, greenish-grey heteroliths, mudstones, dark mudstones and few beds of coal. The general porosity of the sandstones is 15–25 % (Michelsen et al., 2003; Nielsen, 2003; Petersen et al., 2008). The formation presents the evidence of repeated sea level fluctuation that strongly influenced the sedimentation, which occurred in a fluvio-deltaic to tidally influenced shallow marine environment (Nielsen, 2003).

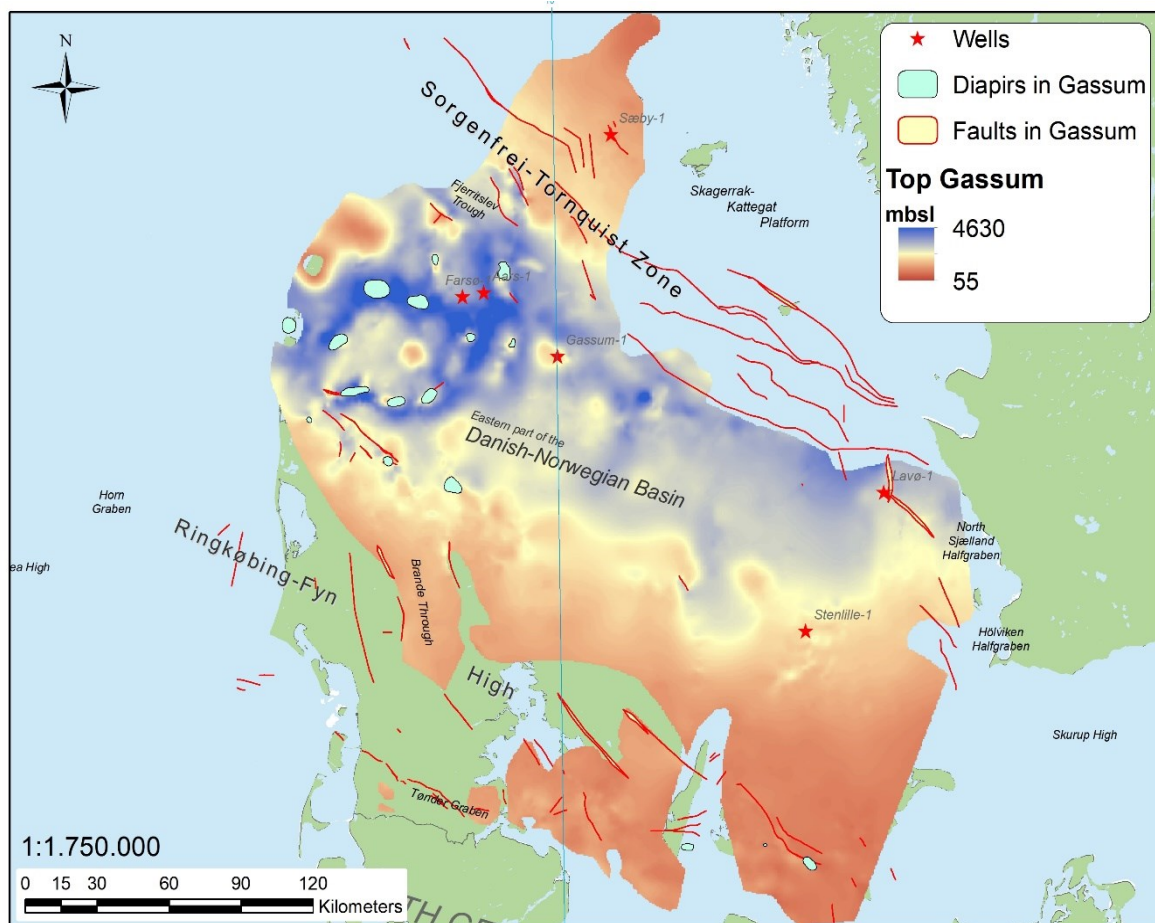


Figure 3.5: Extension and depth of the top of the Gassum Formation in the Danish Basin, including main faults and salt diapirs that occur in the formation (Coordinate System: ED50/UTM Zone 32). Data: GEUS.

3.2.3.2. Fjerritslev Formation

The Fjerritslev Formation (Fig. 3.6) overlies the Gassum, generally presenting an abrupt shift. The Aalenian–Bajocian erosion altered the original thickness of the succession. The maximum thickness of 1,000 m is recorded in the Fjerritslev Trough. Locally the formation includes mudstones of latest Rhaetian and Early Aalenian age (Michelsen & Nielsen, 1993; Michelsen et al., 2003; Nielsen, 2003). The formation is subdivided into four informal members (FI – FIV), the lowermost of which can be subdivided into two units, FIa and FIb. It consists in a relatively uniform succession of marine, dark grey to black, slightly calcareous claystones, with a varying content of silt and siltstone laminae. On the Skagerrak–Kattegat Platform, siltstones and fine-grained sandstones form a minor portion of the succession. Around 20–30 m of fine-grained muddy sandstones dominate the F-II member, located on the Skagerrak–Kattegat Platform. They have a porosity of 10–25 % and are frequently interfingering with mudstones. These sandstones were deposited during different sea level minor fluctuations (Michelsen et al., 2003; Nielsen, 2003; Petersen et al., 2008).

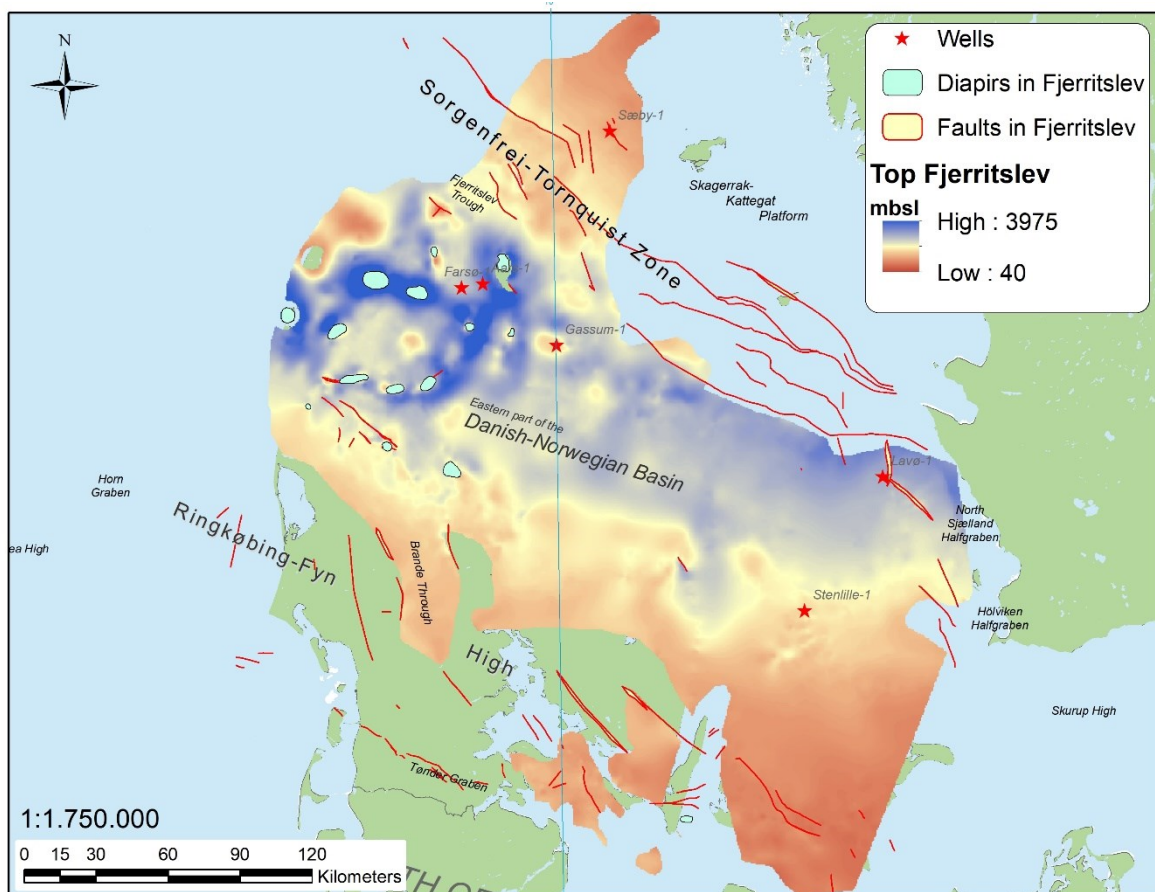


Figure 3.6: Extension and depth of the top of the Fjerritslev Formation, including main faults and salt diapirs that occur in the formation (Coordinate System: ED50/UTM Zone 32). Data: GEUS.

3.2.3.3. Haldager Sand Formation

The Haldager Sand Formation (Fig. 3.7) was deposited in a Bajocian–Bathonian period in the Danish Basin and from Aalenian to Callovian in the Sorgenfrei-Tornquist Zone (Michelsen & Nielsen, 1993; Michelsen et al., 2003; Nielsen, 2003). The formation is distributed in the central and northern part of the Danish Basin (restricted to North Jylland), in the Sorgenfrei-Tornquist Zone and on the Skagerrak-Kattegat Platform. The lateral continuity, the thickness and the facies are significantly altered where the salt structures occur. In the Danish sub-basin, the top of the Haldager Sand Formation reaches depths of 2,000–3,000 m. The thickness of the formation is 15–50 m in the Skagerrak-Kattegat Platform, 30–175 m in the Sorgenfrei-Tornquist Zone, and 25–50 m in the central part of the basin. The distribution in the south-western area is patchy and reduced to less than 10 m. The formation is absent on and along the Ringkøbing–Fyn High. This formation consists of light olive-grey, fine- to very coarse grained, occasionally pebbly sandstones, siltstones, mudstones and coaly beds. The sandstones are generally well sorted and their porosity varies between 15 and 30 %. In the Sorgenfrei–Tornquist Zone, the formation is made of thick fluvial-estuarine and marine sandstones separated by marine and lagoonal-lacustrine mudstones. In the south-western part of the basin the formation is characterized by sandstones of braided rivers, 1–10 m thick (Michelsen et al., 2003; Nielsen, 2003; Petersen et al., 2008).

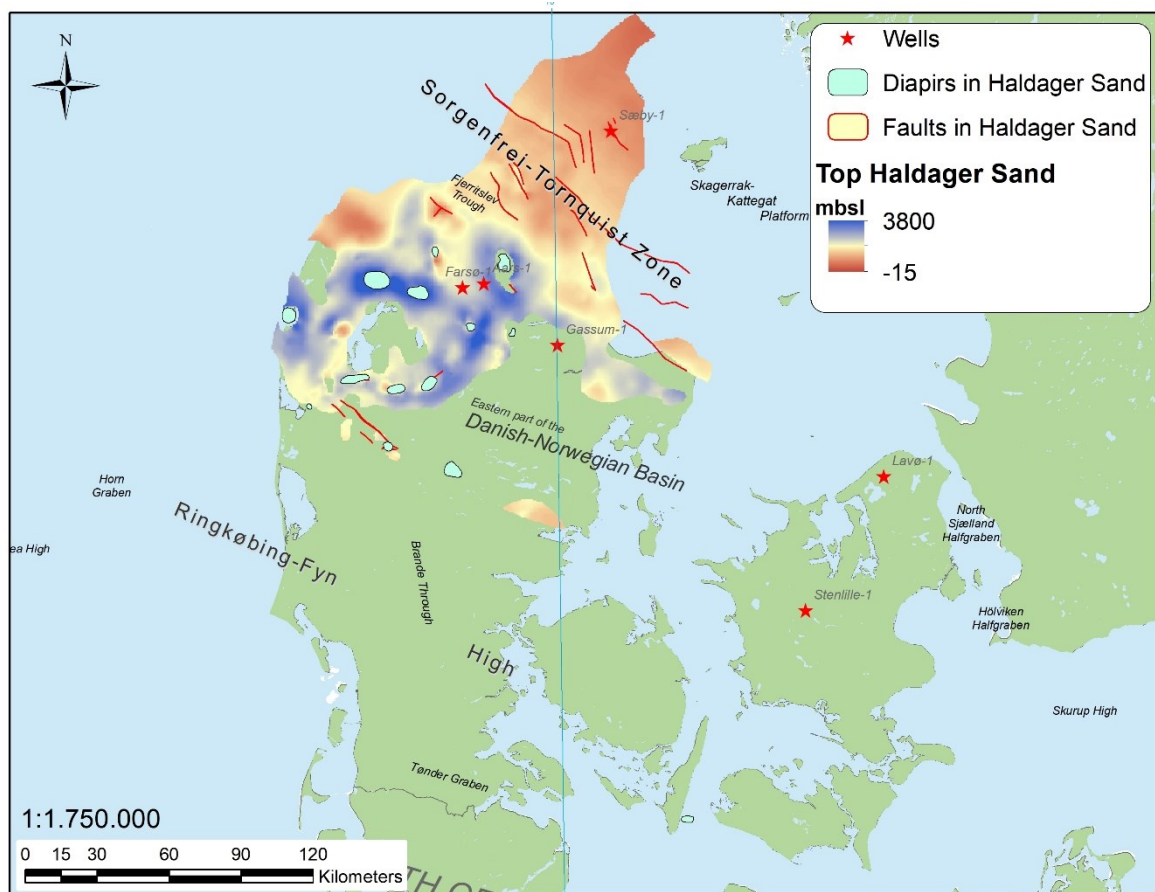


Figure 3.7: Extension and depth of the top of the Haldager Sand, including main faults and salt diapirs that occur in the formation (Coordinate System: ED50/UTM Zone 32). Data: GEUS.

3.2.3.4. Flyvbjerg Formation

Both the base and top of the Flyvbjerg Formation are diachronous all over the basin, younging towards the north-eastern margin. It was deposited from Middle Oxfordian to Late Kimmeridgian. The formation extends from the central basin to the northern part of the Danish Basin and on the Fennoscandian Border Zone (approximately the same distribution as the Haldager Sand Formation). It forms a wedge thickening north-eastward. Maximum thicknesses of 50 m are found over the Fennoscandian Border Zone. It consists of lightly coaly sandstones and siltstones in its lower part. The sediments trend to a more calcareous sandstones interbedded with claystones. In the upper part, fine-grained calcareous sandstones dominate the formation. The succession formed in a shallow to deep marine environment (Michelsen et al., 2003; Nielsen, 2003; Petersen et al., 2008).

3.2.3.5. Børglum and Frederikshavn Formations

The lower boundary of the Børglum Formation is located at the top of the thick sandstone beds uppermost in the Flyvbjerg Formation. This formation consists of a relatively uniform succession of slightly calcareous, homogeneous claystones and mudstones, with varying contents of silt, mica and pyrite. The sediments were mainly deposited in an offshore marine environment. The transition from the claystones of the underlying Børglum Formation to the more coarse-grained Frederikshavn Formation is dated Kimmeridgian–Ryazanian. Although, the Frederikshavn is time-equivalent with the upper part of the Børglum Formation in the central and western parts of the Norwegian–Danish Basin (Michelsen et al., 2003; Nielsen, 2003; Petersen et al., 2008).

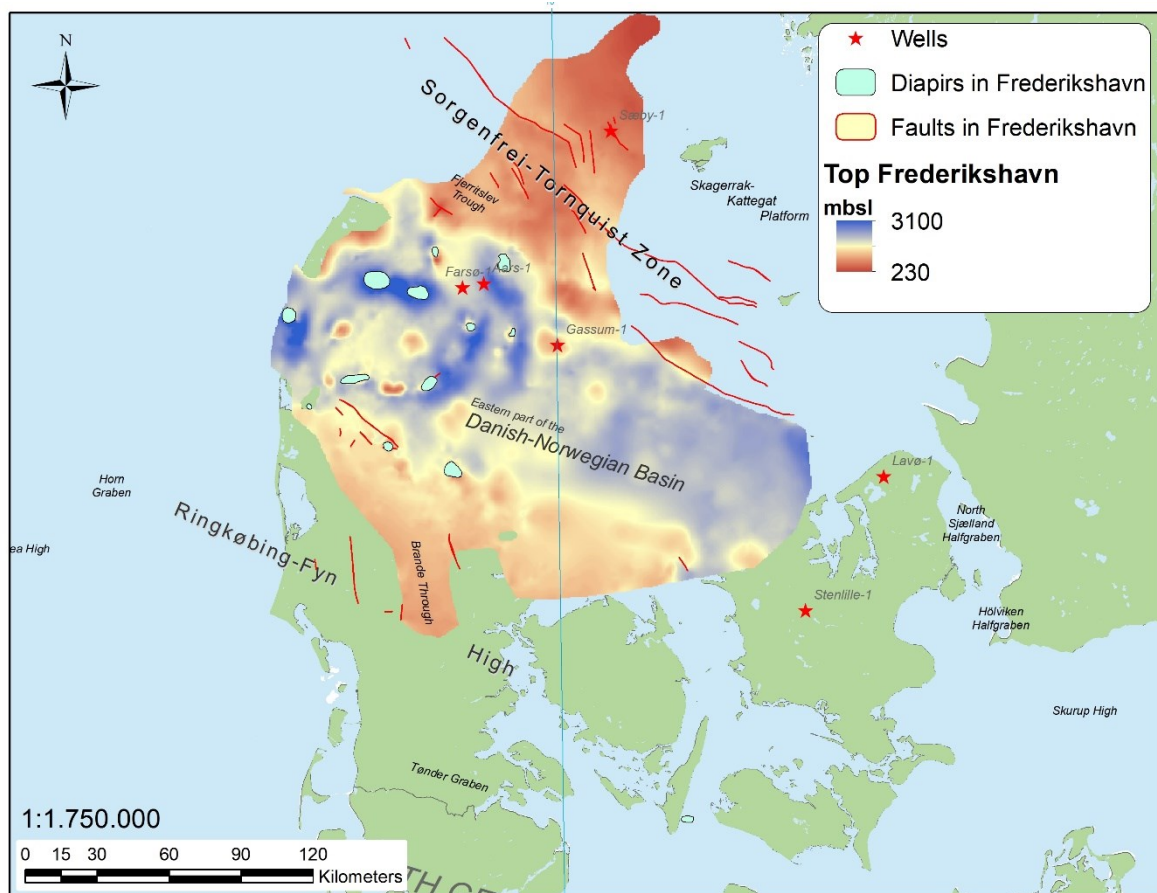


Figure 3.8: Extension and depth of the top of the Frederikshavn Formation, including main faults and salt diapirs that occur in the formation (Coordinate System: ED50/UTM Zone 32). Data: GEUS.

The Frederikshavn Formation deposited in the north-eastern part of the Danish Basin (Fig. 3.8). It shows large variations in thickness (75–230 m). The maximum thickness recorded is more than 230 m in the Sorgenfrei-Tornquist Zone. The formation consists of siltstones and fine-grained, slightly calcareous, sandstones interbedded with claystones, deposited in a paralic environment (Balling et al., 2002; Petersen et al., 2008).

3.2.3.6. Cretaceous Chalk Members and Neogene sedimentation

The claystones of the Frederikshavn Formation gradually give way to the Lower Cretaceous mudstones of the Vedsted Formation (Fig. 3.9). These mudstones present sandy intercalations (most common towards the northeast) and the entire formation is divided into four depositional units (Petersen et al., 2008; Michelsen & Nielsen, 1993).

Until the Cenomanian-Turonian, marine greensands were deposited in the easternmost part of the basin and within the Fennoscandian Border Zone, whereas intermittent deposition of marls and mudstones occurred in the south-west. In Late Cretaceous – Danian times, a pelagic chalk deposition over the entire study area took place. In the Sorgenfrei–Tornquist Zone, 1.5–2 km of chalk was deposited, while 500–750 m accumulated over the Ringkøbing–Fyn High. Late Cretaceous – Palaeogene inversion and erosion, masks the original thickness of the chalk succession. During the Palaeocene, deep marine sedimentation of fine-grained hemipelagic deposits took place, while in the Oligocene, major clastic wedges began to build out from the Baltic Shield. Coarse-grained sediments reached the southern part of the basin and the Ringkøbing–Fyn High in Neogene times. Up to 500 m of sediments were deposited in the Norwegian–Danish Basin during the Late Miocene and Pliocene. (Petersen et al., 2008).

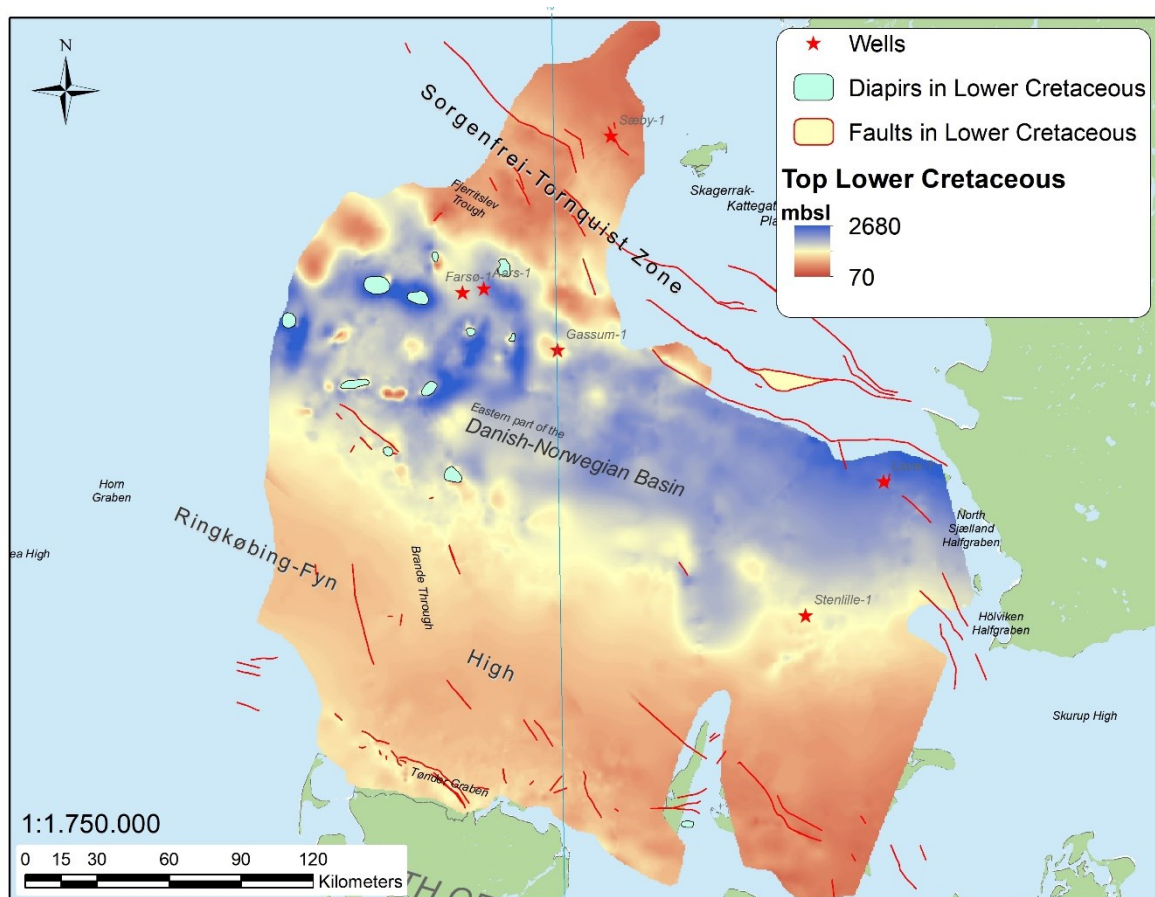


Figure 3.9: Extension and depth of the top of the Lower Cretaceous, including faults and diapirs within the units. Data: GEUS.

3.3. Geothermics

Over the past four decades, the subsurface temperatures of the Danish Basin were widely investigated. Despite the presence of a homogeneous temperature vertical structure, the basin presents strong lateral variations, up to about 50 °C at 3,000 m of depth (Balling et al., 1981; Balling, 1992). The temperature gradients in the Norwegian-Danish Basin are mainly ranging between 27 and 30 °C/km (Balling et al., 1981; Balling, 1992; Nielsen et al., 2004). In general, temperatures vary from ca. 25–35 °C at 1,000 m, to over 55–75 °C at 2,000 m and 75–105 °C at 3,000 m. The temperature information originates from two sources: borehole temperature and theoretically modelled values. Temperature gradient were determined as mean gradient between surface and the actual depth of BHT information and they were corrected for the effect of paleoclimate and sedimentation (Balling et al., 1981; Balling, 1992).

The heat-flow density usually increases towards shallow depths due to the impact of the rocks radiogenic heat production. In shallow parts of the Danish Basin the heat flow is strongly influenced by paleoclimate temperature variations (i.e. cooling of the last glaciations; Balling, 1992) yielding values of only 35 to 45 mW/m². If this effect is corrected, the so called terrestrial surface heat flow provides the unperturbed heat flow from the Earth interior. Recent studies have provided values of 64–84 mW/m² for the terrestrial surface heat-flow (Nielsen et al., 2017). The temperatures and heat flow at the Moho were estimated, by Balling (1992) at 700–750 °C and 40–45 W/m², respectively.

3.3.1. Potential reservoirs in the Danish Basin

The thick Mesozoic succession was the target for hydrocarbon exploration since 1935. Data of borehole drilling and seismic campaigns show that the most promising geothermal reservoirs occur within the Triassic – Lower Cretaceous succession in the Danish Basin (Balling et al., 1981; Mathiesen et al., 2010). The principal sedimentary units of interest are the Gassum Formation and the Haldager Sand Formation, as well as the Bunter Formation. Different secondary potential reservoir are also present in the Skagerrak Formation, the F-II member of the Fjerritslev Formation, the Flyvbjerg Formation and Frederikshavn Formation (Balling, 1992; Mathiesen et al., 2010; Mahaler & Magtengaard, 2010; Nielsen et al., 2004; Petersen et al., 2008).

The Gassum Formation is enclosed by the thick marine mudstones of the Fjerritslev Formation. In North Jylland, the highest temperature gradient of this formation is at about 900 m and a reservoir temperature of 70–100 °C was predicted for this area. Lower values (50–70 °C) were predicted for the southern and eastern parts (Balling et al., 1981). The formation is currently used for geothermal energy, at a depth of ca. 1,200 m, in Thisted, northern Jylland and for natural gas storage at 1,550 m, in the Stenlille area

The Haldager Sand reservoir is surrounded by marine mudstones of the Flyvbjerg and Børglum Formations. Sandstones are present in the lower and upper part of the Flyvbjerg Formation and their thickness tend to increase towards the northern and eastern basin margin, where they may form an additional reservoir section (Petersen et al., 2008). The estimated temperature range is about 60–80 °C, with local increase up to about 100 °C, and decreasing to 30–50 °C at the northern margin (Balling et al., 1981).

Another potential reservoir unit is the upper part of the F-II member (Fjerritslev Formation) on the Skagerrak–Kattegat Platform. This unit is made up of muddy sandstones, which show potentially good characteristics along the Skagerrak–Kattegat Platform. The Flyvbjerg Formation contains shoreface sandstones in its lower and upper parts of the Upper Jurassic, thickening northwards. This formation is covered and isolated by its own marine mudstones and by the thick mudstones of the Børglum Formation.

The depths and the thickness of these reservoirs vary significantly in the basin. The uncertainty on the quality of the reservoir is strictly linked to the permeability, which varies laterally and vertically. Therefore, every reservoir study must be supplemented with specific surveys and local assessments to estimate local production potentials. The porosity of the sandy units in the Danish Basin decrease markedly with depth: from 30–35 % at 500–1,000 m, to 20–25 % at 2,000 m and 10–15 % at 3,000 m. The brine permeability decreasing trend is linked to decreasing porosity: from 300–3,000 mD for 30 % porosity, to 10–30 mD for 15 % porosity. This reduction is mainly caused by mechanical compaction and the formation of diagenetic minerals that reduce pore volume and pore connections. (Balling, 1992; Mahaler & Magtengaard, 2010; Nielsen et al., 2004). The water salinity shows a general increasing trend of about 10 % / km, but large variations are found (Mathiesen et al., 2010). At depths of about 2000–3000 m regional potential geothermal reservoirs normally show temperatures of 60–100 °C (Balling et al., 1981). Due to the diagenetic cementation and reduced pore space, the depth of exploitable reservoirs is limited to a range of 2.5–3 km. This limits the maximum temperatures to 80–90 °C. Therefore, the possibility of high-enthalpy systems remains precluded (Mahaler & Magtengaard, 2010). However, a general estimation of the geothermal potential is possible considering layers of sandstones at depths of 1,000–2,500 m, which are thicker than 25 m and sufficiently distributed (Nielsen et al., 2004).

4. Material and methods

4.1. Samples compilation






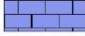


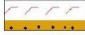

The samples used in this work were originally collected from the six wells reported in [Fig. 3.1](#), by the GEUS institute. The dataset consists of 43 core sections collected from the GEUS core storage in Copenhagen, by the help of Niels Balling (Aarhus University), Sven Fuchs (GFZ) and Rikke Weibel (GEUS). The samples were later sent to the GFZ institute, where they were catalogued, treated and analysed, following the procedures described in the following paragraph.

The rock samples' description presented in this paragraph is the result of a visual analysis carried out prior to the laboratory work. Such analysis was improved by comparing it with data from the well reports and the information provided by the GEUS institute.

4.1.1. *Aars-1*

The Aars-1 well ([Fig. 4.1](#)) was drilled near the city of Aars (North Jutland) by the Dansk Olie & Naturgas A/S society (DONG A/S) from November 1978 to August 1979. The GEUS provided the well report ([GEUS, 1979](#)). The aim of this drilling was to study the prospects of recovering geothermal energy from the Gassum Formation. As shown in [Fig. 4.1](#), 11 samples of the dataset (IDs: 1, 2, 3, 4, 5, 6, 7, 8, 8b, 9 and 10) were collected from this well:

- Samples 1 and 2 are representative of the Vested Formation. They appear as dark grey mudstone, slightly shaly, poorly consolidated. Silt is present in very thin layers.
- Sample 3 belongs to the Frederikshavn Formation. It is a dark grey, calcareous mudstone, well consolidated. Some calcareous fragments may suggest the presence of mollusc's fossils.
- Samples 4 and 5 belong to the Flyvbjerg member and consist of grey mudstones with fine-grained sand and a heterolithic bedding.
- Samples 6, 7, 8 and 8b belong to the Haldager Sand. They appear as whitish, medium-coarse grained, homogeneous sandstones. Very small lamellae of dark clay occur sporadically in samples 6 and 7.
- Samples 9 and 10 (Gassum Formation) show contrasting characteristics. Specimen 9 is a dark sandy mudstone, with heterolithic bedding, whereas specimen 10 is a whitish, coarse and very compact sandstone.

WELL	Aars-1	Lithology Legend	
LOCATION	6294870.65 N	 Boulder clay	 Limestone, clayey
ED50 UTM 32N	531114.52 E	 Claystein	 Limestone, argillaceous
LOGGER	DONG A/S	 Claystone, silty, calcareous	 Limestone
DATE	Nov 1979	 Claystone, calcareous	
		 Clay-Siltstone IB	
		 Silt-Sandstone IB	
		 Sandstone	

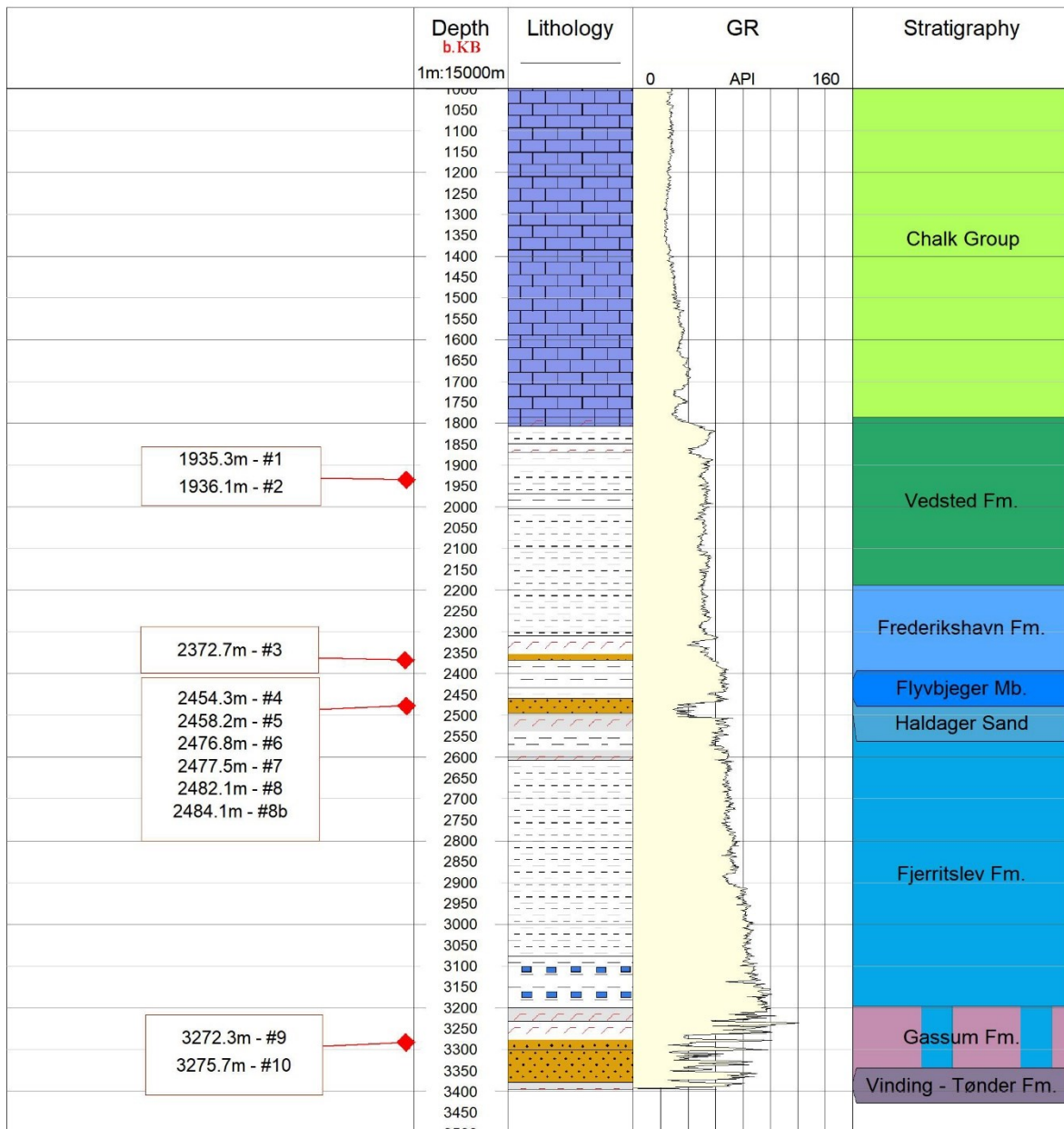

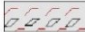


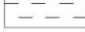






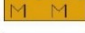
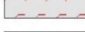




Figure 4.1: Log of the Aars-1 well (depth range: 1,000 – 3,400m). This log shows the intercepted lithologies, the GR measures and the relative formations. The red diamonds and the textboxes indicate the depth of each sample (depth [mbKB] - #ID). Data furnished by GEUS.

4.1.2. *Farsø-1*

This well is located in the homonym city of Farsø (North Jutland) and was drilled during 1982 by the DONG A/S and analysed by the GEUS. The aim of this drilling was to evaluate the geothermal potential of the sandy reservoirs, for low enthalpy systems (GEUS, 1982). Nineteen samples of the dataset were collected from this well (IDs: 11, 12, 13, 14, 15A, 15B, 16, 17, 17b, 17c, 17d, 18, 18b, 18c, 18d, 19, 19b, 20 and 20b; Fig. 4.2):

- Samples 11, 12 and 13 are from the Haldager Sand Formation. Specimen 11 is a light grey/yellow very fine-grained sandstone, with silt and dark clay lamellae in thin layers. It is poorly cemented. Specimen 12 is a relatively medium-grained sandstone, with barely evident laminations; specimen 13 is composed by very fine sand and mud intercalated in cross laminations.
- Specimen 14, 15A, 15B and 16 belong to the Fjerritslev Formation. They show similar characteristics: a mainly muddy composition, with barely evident tabular lamination, moderately compacted. Specimen 16 presents some differences: a relatively higher silt composition with a heterolithic bedding.
- The remaining specimens 17, 17b, 17c, 17d, 18, 18c, 18d, 19, 19b, 20 and 20b are all sandy samples belonging to the Gassum Formation. Specimen 17 and 17b are coarse-grained, whitish and homogeneous sandstones. The 17 is poorly cemented. Specimen 17c and 17d are white, fine-grained sandstones with dark mud and tabular (occasionally cross) lamination. The general cementation is good, although the layers of mud may represent weak points. Specimens 18, 18b and 18d are light grey, fine-grained sandstones. Dark mud is present in thin layers. The lamination is generally tabular. They are all well-cemented. In samples 19, 20 and 20b, the lithology is characterized by increasingly coarser sand and thinner mud layers. Sample 18c is the only rock of this group, which is composed mainly by homogeneous, grey mud.

WELL	Farsø-1	Lithology Legend	
LOCATION	56° 46' 53.04" 9° 21' 49.68"	 Calcareous marl	 Siltstone, dolomitic
LOGGER	DONG A/S	 Mudstone	 Silt-Sandstone IB
DATE	Jun 1982	 Claystein	 Sandstone, silty
		 Claystone, silty, calcareous	 Sandstone
		 Claystone, calcareous	 Sandstone, fs-ms
		 Clay-Siltstone IB	 Sandstone, ms
		 Siltstone	 Chalk
		 Siltstone, sandy	

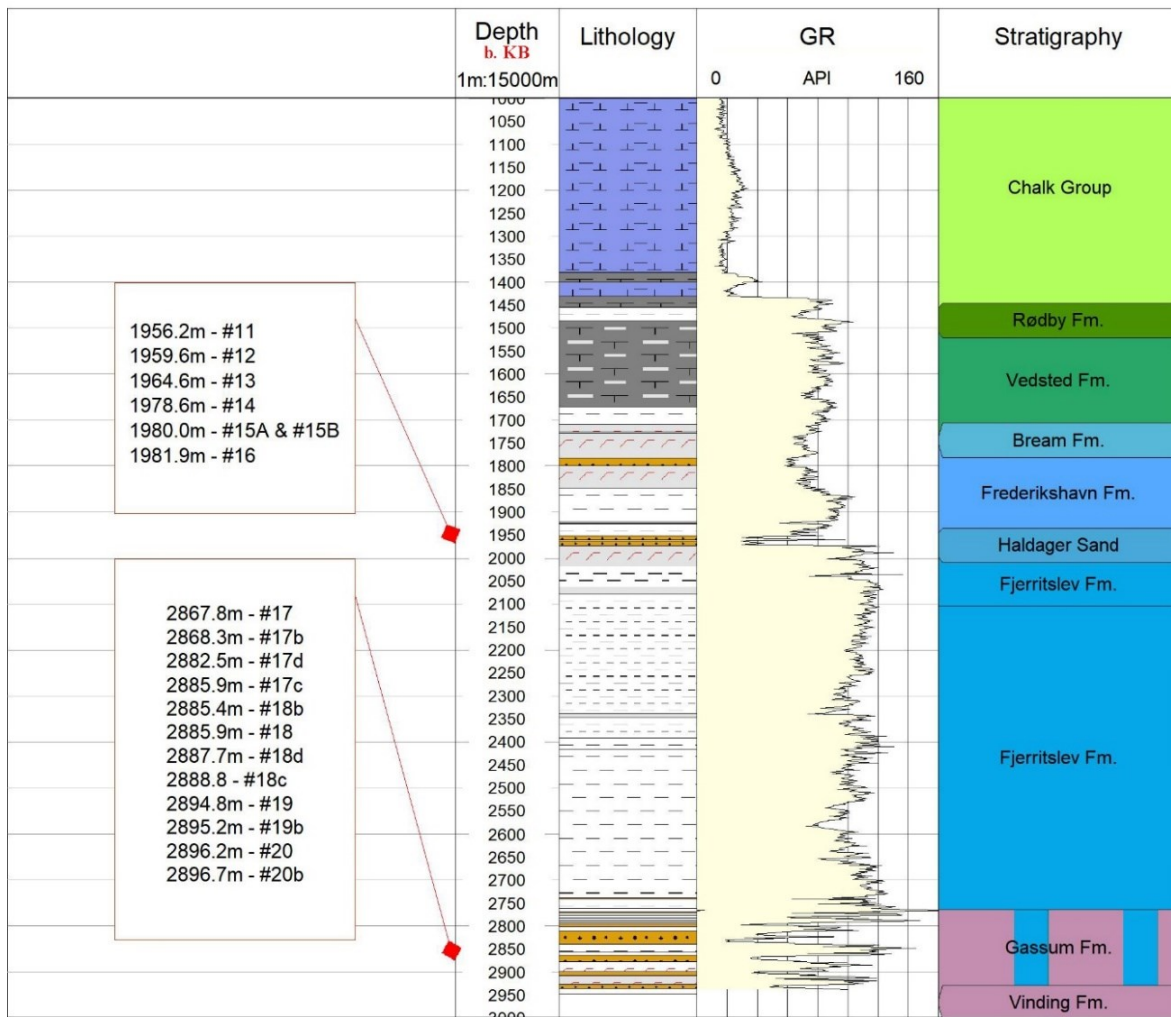


Figure 4.2: Log of the Farsø-1 well between 1,000 and 2,950m depth. This log shows the lithology intercepted, the GR measures and the relative formations. The red diamonds and the textboxes indicate the depth of each sample (depth [mbKB] - #ID). Data furnished by GEUS.

4.1.3. Stenlille-1

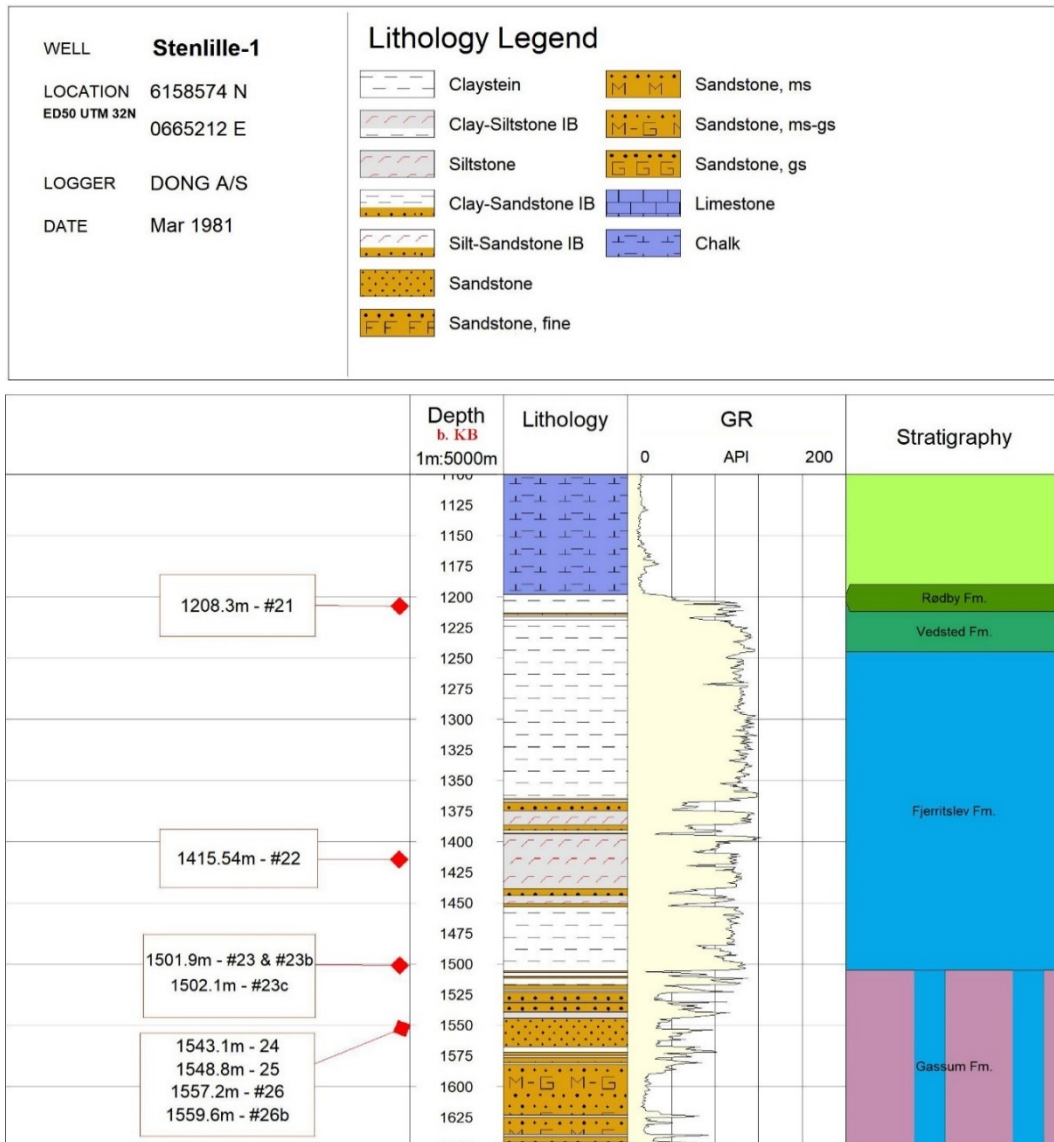


Figure 4.3: Log of the Stenlille-1 well between 1,100 and 1,625m depth. This log shows the lithology intercepted, the GR measures and the relative formations. The red diamonds and the textboxes indicate the depth of each sample (depth [mbKB] -#ID). Data furnished by GEUS.

This well was drilled in 1981 by the DONG A/S, in the former municipality of Stenlille (now part of the town of Sorø, Zealand). The purpose of this well was to analyse Gassum reservoir and the cap rocks above, in order to investigate the possibility of natural gas storing. Its maximum depth is 1,664 m. The well report is provided by GEUS (GEUS, 1981). Nine of the analysed in total belong to this well (IDs: 21, 22, 23, 23b, 23c, 24, 25, 26 and 26b; Fig. 4.3):

- Sample 21 is a dark, calcareous and homogeneous claystone. It belongs to the Vedsted Formation.
- Sample 22 is composed of fine-grained sand with a high content in organic mud, poorly cemented.
- Samples 23, 23b and 23c are grey and homogeneous calcareous claystones and belong to the Fjerritslev Formation.
- Samples 24, 25, 26 and 26b belong to the Gassum Formation. sample 24 is a very fine-grained sandstone. Samples 25, 26 and 26b are very similar: medium-grained,

homogeneous, and well cemented sandstones. Samples 26 and 26b sporadically present thin layers of clay.

4.1.4. Lavø-1, Sæby-1 and Gassum-1 samples

The remaining five samples were collected from Lavø-1, Sæby-1 and Gassum-1 wells (respectively [GEUS, 1995](#); [GEUS 1985](#); [GEUS 1951](#)). These rocks represent the Cretaceous Chalk Units.

- Samples 27 and 28 consist of white homogeneous calcareous limestones, respectively collected from the Sæby-1 well (at ca. 406 mbKB) and from Gassum-1 well (at ca. 265 mbKB). Both samples have a scarce consistence.
- Samples 29, 30 and 31 are grey limestones with variable presence of dark mud in layers. They were collected from Lavø-1 well ([Fig. 4.4](#)). Samples 29 and 30 show a modest lithification and higher content in mud, relatively to 31.

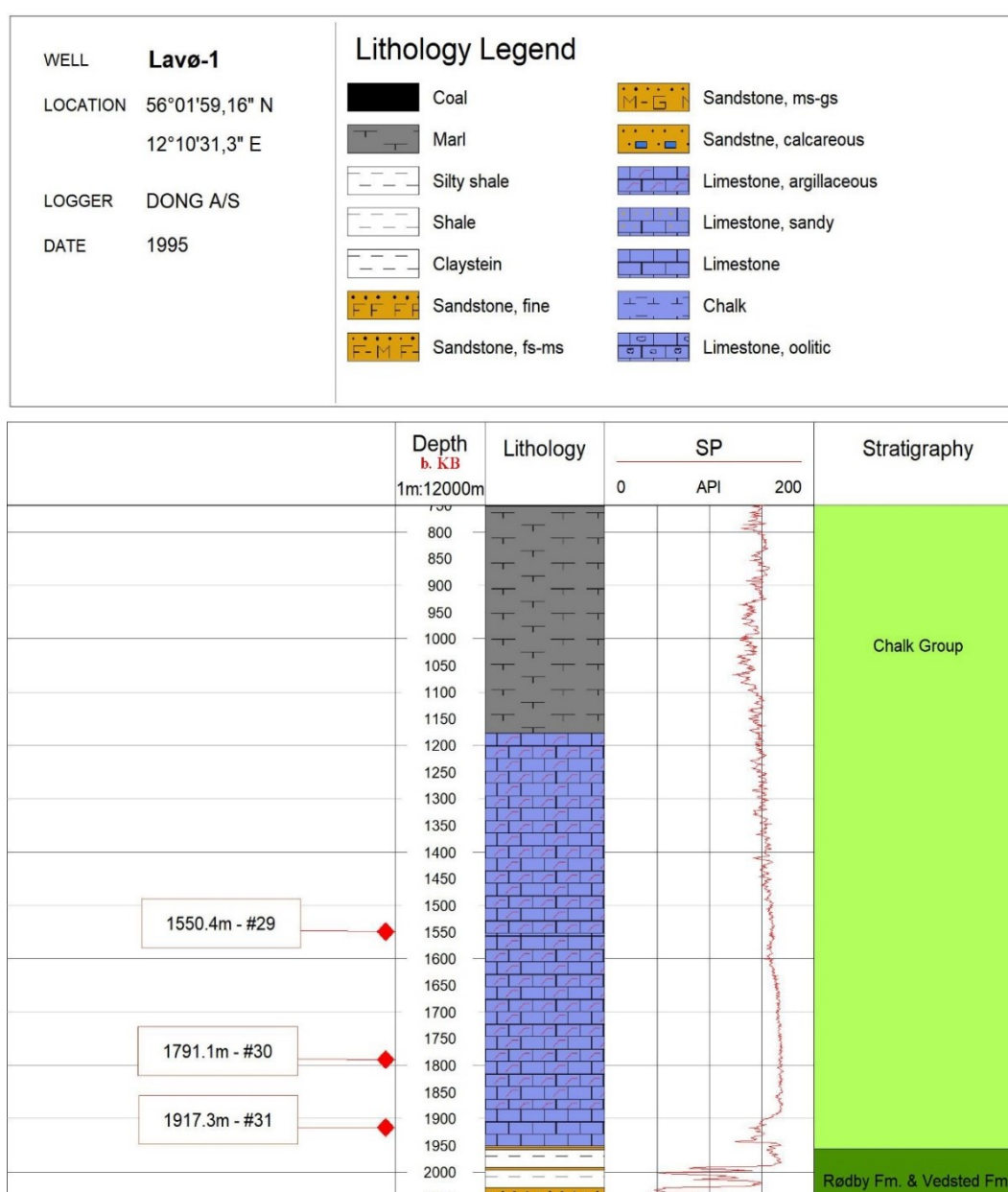


Figure 4.4: Part of the Lavo-1 well log. This log shows the lithology intercepted by the drilling, the GR measures and the relative formations of a depth range from 750 to 2,050mbKB. The red diamonds and the textboxes indicate the depth of each sample (depth [mbKB] - #ID). Data furnished by GEUS institute.

4.1.5. Classification by major components

The rocks of the compilation were catalogued by their major component into five different classes. Such classification was necessary to evaluate the relations between petrophysical properties and major lithological characteristics, and goes as follows:

- I. **Sandstones** (or ‘Sst’): samples which major component is visibly pure sand;
- II. **Argillaceous sandstones** (or ‘Sst argillaceous’): rocks mainly consisting in medium- or fine- grained sand with mud. The content in sand is greater than that of mud. A variable content in silt can be present;
- III. **Sandy mudstones** (or ‘Mst sandy’): muddy rocks with a minor but substantial content in silt or fine sand;
- IV. **Mudstones** (or ‘Mst’): rocks whose major component is pure mud;
- V. **Limestones** (or ‘Lst’): rocks composed of lithified calcareous mud;
- VI. **Claystones** (or ‘Clst’): rocks in which pure clay is visibly the main content.

For the graphs and the tables showed in Chapter 5 and Chapter 6, these lithologies are distinguished by a fixed colour code: yellow for Sst, orange for Sst argillaceous, green for Mst sandy, brown for Mst, blue for Lst and red for Clst. This classification was made based on visual analysis and well reports information. The GEUS institute provided an analogous classification of the samples, which was used only as an element for comparison. Therefore, the final classification (Tab 4.1) is independent from that provided by GEUS.

Table 4.1: list of samples used for this work and relative well, belonging formation and major lithological component (see text for details).

ID	Well	Formation	Major	ID	Well	Formation	Major
1	Aars-1	Vedsted	Mst	18	Farsø-1	Gassum	Sst argillaceous
2	Aars-1	Vedsted	Mst	18b	Farsø-1	Gassum	Sst
3	Aars-1	Frederikshavn	Mst sandy	18c	Farsø-1	Gassum	Mst sandy
4	Aars-1	Flyvbjerg	Mst sandy	18d	Farsø-1	Gassum	Mst sandy
5	Aars-1	Flyvbjerg	Mst sandy	19	Farsø-1	Gassum	Mst sandy
6	Aars-1	Haldager Sand	Sst	19b	Farsø-1	Gassum	Mst sandy
7	Aars-1	Haldager Sand	Sst	20	Farsø-1	Gassum	Sst argillaceous
8	Aars-1	Haldager Sand	Sst	20b	Farsø-1	Gassum	Mst sandy
8b	Aars-1	Haldager Sand	Sst	21	Stenlille-1	Vedsted	Clst
9	Aars-1	Gassum	Mst sandy	22	Stenlille-1	Fjerritslev	Mst sandy
10	Aars-1	Gassum	Sst	23	Stenlille-1	Fjerritslev	Clst
11	Farsø-1	Haldager Sand	Sst argillaceous	23c	Stenlille-1	Fjerritslev	Clst
12	Farsø-1	Haldager Sand	Sst	24	Stenlille-1	Gassum	Sst
13	Farsø-1	Haldager Sand	Mst sandy	25	Stenlille-1	Gassum	Sst
14	Farsø-1	Fjerritslev	Mst	26	Stenlille-1	Gassum	Sst
15A	Farsø-1	Fjerritslev	Mst	26b	Stenlille-1	Gassum	Sst
15B	Farsø-1	Fjerritslev	Mst	27	Sæby-1	Chalk units	Lst
16	Farsø-1	Fjerritslev	Mst	28	Gassum-1	Chalk units	Lst
17	Farsø-1	Gassum	Sst	29	Lavø-1	Chalk units	Lst
17b	Farsø-1	Gassum	Sst	30	Lavø-1	Chalk units	Lst
17c	Farsø-1	Gassum	Sst argillaceous	31	Lavø-1	Chalk units	Lst
17d	Farsø-1	Gassum	Mst sandy				

4.2. Laboratory analyses

As previously mentioned, the samples sent by GEUS were originally cylindrical core sections (about 12 cm of diameter), most of them cut in half by their major axis (Fig. 4.5a).

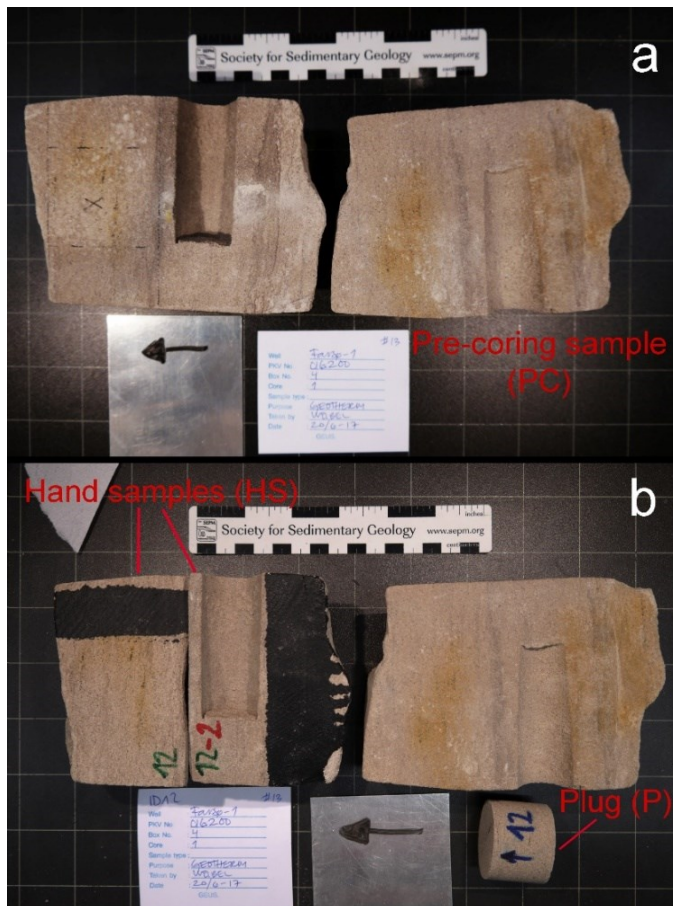


Figure 4.5: sample 12. a) Pre-coring sample, as it was received from the GEUS. b) Samples after the treatment: two hand samples (left) and a plug (bottom-right). The black paint on the hand samples is required for optical scanning (see 4.2.4 for details).

The length of each sample ranges approximately between 5 cm and 20 cm. These samples were later further cored to obtain several subsamples (Fig. 4.5b). The general procedure agreed by GFZ and the Danish institute, in fact, provided for a coring of small cylinders ('P' in Fig. 4.5b) of 4 cm in diameter and 3 cm in height, from 25 original samples. These plugs are a prerequisite for further analysis with the divided-bar apparatus, which will be carried out by the Aarhus University, as well as for future autoclave measurements at the GFZ. Twenty cylinder samples were successfully obtained using a water-drilling rig, whereas plugging of the remaining samples was not possible due to their scarce compaction. Moreover, additional samples with straight and smooth surfaces were sawed from the remaining parts of the cores for the optical scanning measurements (details in the following paragraph). The plugging and the sawing procedures took place both in the GFZ laboratories.

Therefore, the subsamples analysed in the laboratory are 101, divided as follows:

- Twelve samples analysed before the coring procedures, labelled as 'Pre-coring' samples (or 'PC');
- Twenty cylinders obtained from the coring procedure, labelled as 'Plugs' (or 'P');
- Sixty-nine subsamples, labelled as 'Hand samples (or 'HS'), consisting of sawed samples of the original cores and scraps from plugging procedures.

For this project, several measurements were conducted, aiming to the investigation of the following characteristics:

- Dry and saturated masses ("submerged mass" and "saturated mass");
- Volume;
- Effective porosity;
- Density (density of the matrix and bulk density in saturated and dry conditions);
- Thermal conductivity at dry and saturated conditions;
- Thermal diffusivity at dry and saturated conditions.

Additional information on how the data acquired from the subsamples were merged for each sample are described in 4.3.2. For various reasons, explained in the following paragraphs, it was not possible to carry out every measurement on every subsample of the dataset. This lack of data was partly resolved by the data processing. This procedure is explained in the next paragraph. Measurement and treatment of the samples took place in the GFZ laboratories, from September 2017 to December 2017.

4.2.1. *Drying process*

In order to reach the dry conditions, each sample needed to be dried. This process was preceded by an initial mass measure, representing undefined saturation conditions after a long stocking period in the core storage facility. The masses were measured with two different scale (Fig. 4.6a,b), depending on the sample size. Larger and heavier samples, such as pre-coring and hand samples, were weighted using a Mettler PM2000 (Fig. 4.6b). Smaller samples (mass < 200 g, e.g. the plugs) were weighted with a Sartorius scale (Fig. 4.6a). The accuracy of such measurements is 0.1 g for the Mettler and 0.01 g for the Sartorius scale.

The samples were subsequently located in a Vacucell Vacuum Oven (Fig. 4.7) at 60 °C and $P < 0.2$ bar, in order to remove the water in the pores. This phase required a minimum period of 48 hours. Nevertheless, the masses were checked daily, taking into account their decreasing trend. When a mass constancy is obtained, the dry conditions are reached. Therefore, the last value of mass measured is considered the dry mass of the sample.

The PC samples were analysed before the scheduled coring phase. Only twenty of these samples were dried and analysed, due to the limited amount of time available and a longer drying time.

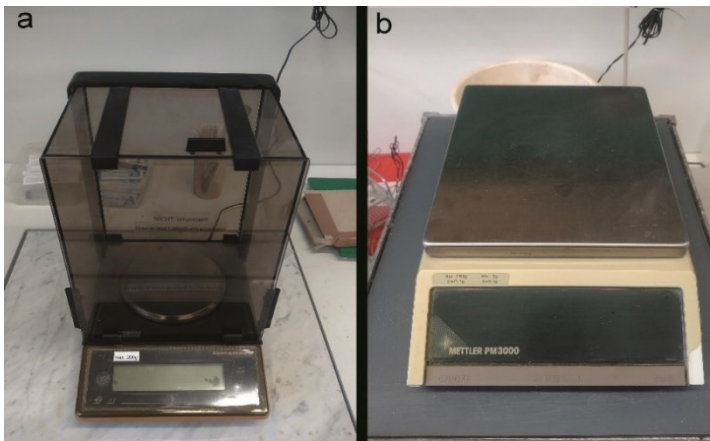


Figure 4.6: a) Sartorius balance, used for measuring the mass of the plugs; b) Mettler PM3000 Balance, used for measuring the mass of hand samples and pre-coring samples.



Figure 4.7: Vacucell Vacuum Oven, used for drying the samples.

4.2.2. Saturation procedure

The samples were saturated with pure water or isooctane (2,2,4 Trimethylpentane). The isooctane was used for clays and muddy samples, in order to prevent the expected clay swelling and the consequent destruction of the sample. In fact, the water absorption of clays and subsequent ion exchange (due to the polarity of the water molecule), leads to the expansion and possible destruction of these kind of samples. On the contrary, the isooctane's molecule is apolar and avoids this phenomenon, entering in the pores without altering consistently the structure of the rock.

The saturated conditions of the rocks are achieved using the system shown in Fig. 4.8. The method consists in using a sealed dryer, containing the samples submerged in the saturating fluid. Several samples can be treated at the same time, depending on the size of both rocks and dryer used. The desiccator is under vacuum and two pipes connect it to an aspirating pump and a funnel (containing the saturating fluid). Two valves on the pipes permit to regulate the flux of air and fluids.

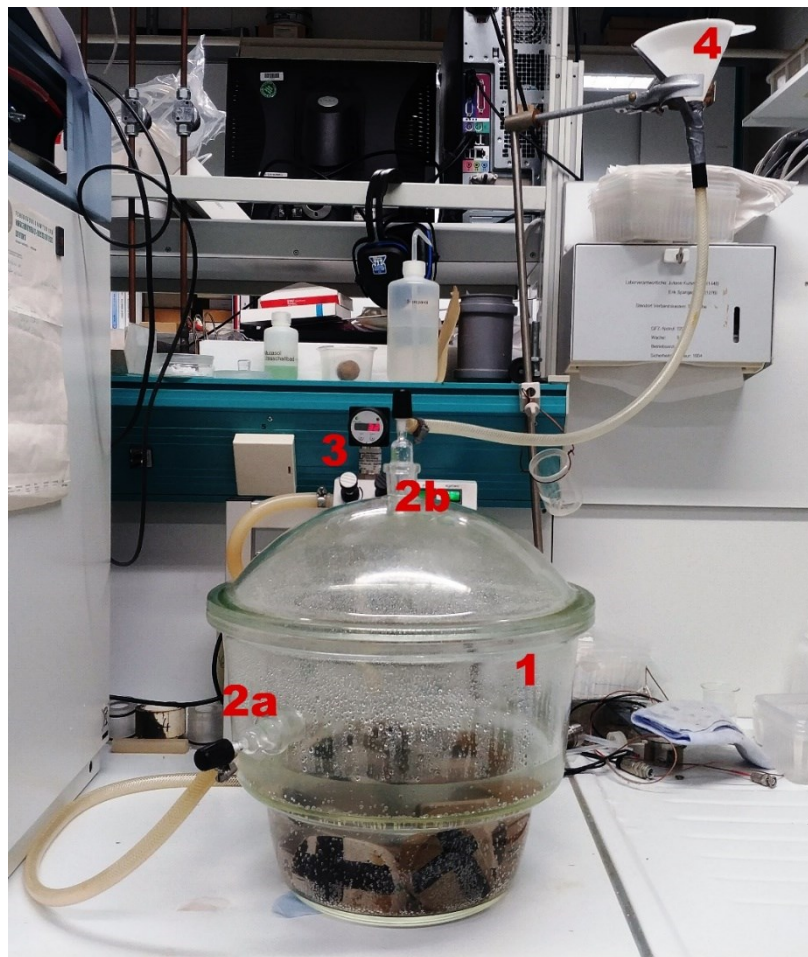


Figure 4.8: System used for the saturation of the samples. 1) Desiccator with samples submerged in water; 2a,b) nozzles of the desiccator, connected to the pipes (black caps: valves); 3) aspirating pump – behind the desiccator; 4) funnel.

For this method, the following procedures were followed:

- The samples are placed in the desiccator, which is later closed with its top and connected to the pipes. Both the top and the pipes are sealed with a baysilone paste (fat lubricant);
- The upper valve (regulating the flux from the funnel) is closed, while the connection to the pump is completely opened;

- The funnel is filled with the saturating fluid and the pump is activated;
- When the pressure reaches a fixed value (4–6 mbar for water or 20 mbar for isooctane), the valve of the funnel is opened, in order to fill the desiccator with fluid. (It is important to keep the funnel always full in order to avoid air infiltrations);
- Once the samples are completely submerged, the valves are closed and the pump is switched off.

In case of isooctane saturation, the under vacuum conditions are kept for only 2 hours and then the pressure is brought back to 1.013 bar. Samples are left submerged for about 48 hours (using pure water as saturating fluid) or 24 hours (using isooctane) to ensure the full saturation. The plugs have not been saturated, since their integrity has to be assured for the further measures provided by the GEUS.

4.2.3. Archimedes' method

The Archimedes' method was adopted in order to obtain different parameters:

- Volume (V);
- Porosity (Φ);
- Matrix density (d_m);
- Bulk densities in dry (d_d) and saturated (d_s) conditions.

This method involves the measurement of two kind of masses of a saturated sample: the mass of the saturated rock on the scale's plate (m_s) and the mass of a saturated rock submerged in its saturating fluid (m_i). Both these masses were measured using the Mettler scale (Fig. 4.6b). The measurement of m_i was possible placing the sample on a plate hooked to scale and immersed in the saturating fluid.

Due to the high volatility of isooctane, each measure with this fluid was carried out under a fume hood and keeping the samples the shortest time possible out of the fluid.

Given the saturating fluid density (d_f) and the dry mass (m_d), it is possible to define the porosity as

$$V_p = \frac{m_s - m_d}{d_f} \quad (4.1)$$

$$V = \frac{m_s - m_i}{d_f} \quad (4.2)$$

$$\Phi = \frac{V_p}{V} * 100 \quad (4.3)$$

Where V_p is the pore volume and V is the sample's volume. The different densities are calculated as

$$d_d = \frac{m_d}{V} \quad (4.4)$$

$$d_s = \frac{m_s}{V} \quad (4.5)$$

$$d_m = \frac{d_s - \frac{V_p}{V} * d_f}{1 - \frac{V_p}{V}} \quad (4.6)$$

The maximum relative uncertainties calculated are 0.5 % for the volume and 1 % for porosity and density values.

In different cases, a significant mass loss of the samples was recorded after the submersion period, especially in case of saturation with isooctane. In these cases, the drying procedure was repeated and the dry mass measured again. As already mentioned, this measurements were carried out only on the hand samples.

4.2.4. Optical Scanning method

The analysis of thermal properties such as thermal conductivity (TC) and thermal diffusivity (TD) was done by direct measurement in the laboratory, using the Optical Scanning method (OS). This technique was developed by Dr. Yuri Popov (Moscow State Geological Prospecting Academy) and is one of the most diffused methods for the evaluation of thermal properties of the rocks. It is a transient-state, non-destructive method that works at ambient conditions (20–25 °C; 1atm) and permits to measure the bulk thermal conductivity (BTC) and the bulk thermal diffusivity (BTD) of a rock. Both dry and saturated samples can be analysed.

Other widely used techniques are e.g. the Divided Bar and the Line Source methods; Popov et al. (1999), Popov et al. (2012) and Popov et al. (2016) provide a comparison between these three methods.

4.2.4.1. Theoretical background

The OS is based on the determination of the maximum temperature rise induced on the surface of a sample by a known heat source (Popov et al., 1985; Popov et al., 1999). As shown by the schematic representation of the instrument in Fig. 4.9, a sample's surface is heated by a heat source, moving along a scan line. Three infrared sensors (1, 2 and 3 in Fig. 4.6) record different temperatures: the first one (1) is placed before the heat source and records the temperature of the undisturbed sample (ambient temperature); the second sensor (2) is located behind the heater at a fixed distance (x_0), and records the temperature of the sample after being heated.

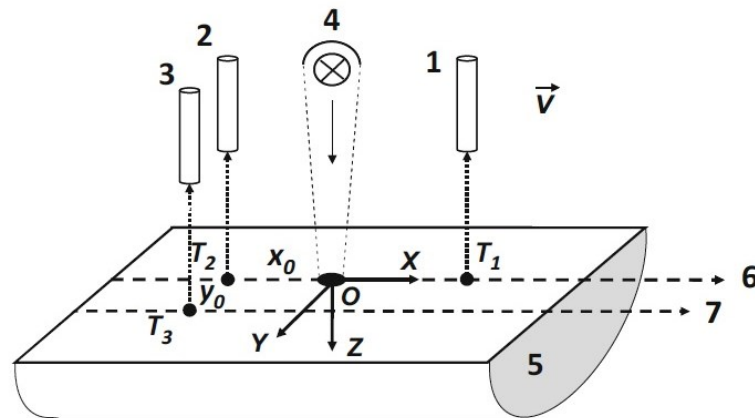


Figure 4.9: essential element of the optical scanning method. 1, 2, 3: infrared sensors; 4: heat source; 5: sample; 6: scan line (Popov et al., 2016).

The heat source and first two sensors are aligned along the scanline. The third sensor (3) is placed behind the heat source at a distance $R = \sqrt{x_0^2 + y_0^2}$, where y_0 is the lateral displacement from the scan line axis (6). Both sensors and heat source move along the scan line at a constant velocity (v). Therefore, TC and TD are defined from the following equations, as reported by Popov et al. (2016):

$$T_2 - T_1 = \frac{q}{2\pi x_0 \lambda} \quad (4.7)$$

$$T_3 - T_1 = \frac{q}{2\pi \lambda R} \frac{v(R-x_0)}{2\alpha} \quad (4.8)$$

where:

- λ is the thermal conductivity
- α is the thermal diffusivity
- T_1 , T_2 and T_3 are the temperatures recorded respectively by sensor 1, 2 and 3
- q is the incidental heat on the sample

According to Popov et al. (1985), these parameters can be defined provided the use of two reference standards of known λ_R and α_R , aligned along the scanline and measured together with the samples. Thus, the equations previously considered would become:

$$\lambda = \frac{\lambda_{R1} * (T_{2R1} - T_{1R1}) * \lambda_{R2} * (T_{2R2} - T_{1R2})}{2(T_2 - T_1)} \quad (4.9)$$

$$\alpha = \frac{\alpha_{R1} * \ln\left(\frac{\lambda_{R1} * (T_{3R1} - T_{1R1})}{\lambda_{R2} * (T_{3R2} - T_{1R2})}\right)}{\ln\left(\frac{\lambda_{R1} * (T_{3R1} - T_{1R1})}{\lambda_{R2} * (T_{3R2} - T_{1R2})}\right) + \frac{\alpha_{R2} - \alpha_{R1}}{\alpha_{R2}} * \ln\left(\frac{\lambda_{R1} * (T_{3R1} - T_{1R1})}{\lambda_{R2} * (T_{3R2} - T_{1R2})}\right)} \quad (4.10)$$

It is important to point out that these quantities are tensors and each measure is a mean value of TC and TD of the scan, oriented perpendicularly to the scan line.

Three principal axes (A, B and C in Fig. 4.10) of thermal conductivity and diffusivity can be defined for each rock, depending on its layering. In cases of pure isotropy of the rock, these axes are equal to each other. It is possible to define three main components of λ and α as:

- λ_{perp} and α_{perp} for axis A
- $\lambda_{||1}$ and $\alpha_{||1}$ for axis B
- $\lambda_{||2}$ and $\alpha_{||2}$ for axis C

Perpendicular (*perp*) and parallel ($||_{1,2}$) are therefore referred to the orientation of the vector with respect to the foliation of the rock.

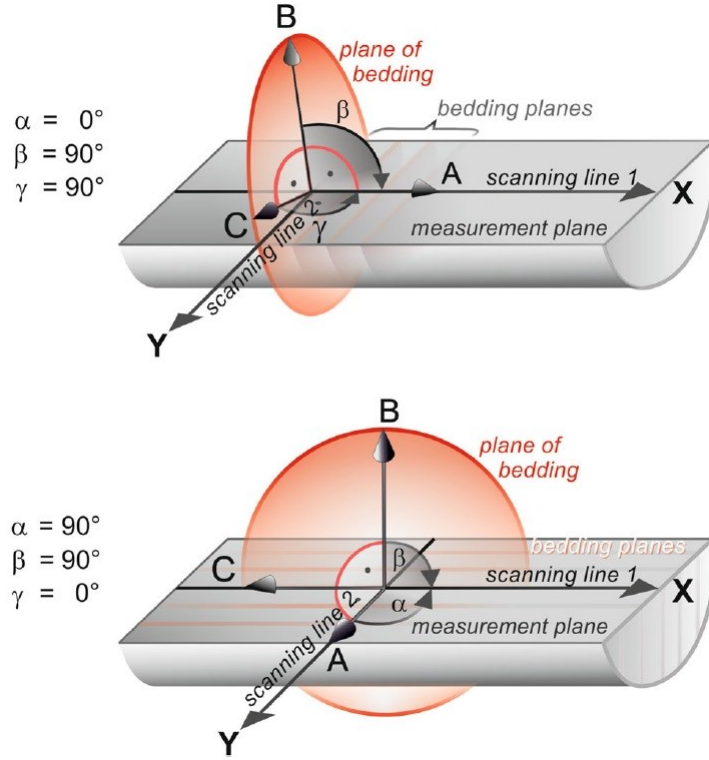


Figure 4.10: two scanning directions and their relation to bedding of the sample. A, B and C are main axes of TC and TD. A is perpendicular to the bedding planes. B and C lie on the plane of bedding and are perpendicular to each other. α , β , γ are the angles between A, B and C and the scanning line (Popov et al., 2016).

Finally, the measurement requires the application of an optical coating on the sample's scan line that reduces the effect of varying optical reflection coefficients of the components of the rock. It can be a layer of black paint or black tape, with a width $> 2\text{cm}$. The application of paint preceded the drying procedure, while the tape was applied before every measuring phase. An example of a stripe of black paint on the sample's surface is showed in Fig. 4.5b.

4.2.4.2. Required corrections

The surfaces of a sample are not always parallel to the main axes A, B and C. In this case, the measured value is defined "apparent" (λ_{app} and α_{app}) and is related to main axes by the following equation, provided by Popov & Mandel (1998):

$$\lambda_{app} = \sqrt{\lambda_{perp} * \lambda_{||1} * \cos^2\gamma + \lambda_{perp} * \lambda_{||2} * \cos^2\beta + \lambda_{||1} * \lambda_{||2} * \cos^2\alpha} \quad (4.11)$$

where α , β and γ are the angles between the scan line and the axes A, B and C respectively (Fig. 4.9). The same equation is applied for TD. Given three non-collinear and non-coplanar directions, located on two non-parallel planes, Eq. (4.11) permits to obtain the main values from a set of three equations with three unknowns (Popov & Mandel 1998; Popov et al., 1999). However, this type of conversion was not applied in this work. In fact, the cutting of the samples permitted to obtain results corresponding to the main axes A, B and C (or were assumed so, at the sample's scale).

In addition, it is necessary to apply a correction in case of analyses with TCS of cylindrical surfaces. In fact, the curved surface of a cylinder defines an underestimation of the TC. The

BTD values measured do not show this underestimation. This correction is applied using the following empirical equation:

$$\Delta\lambda = 0.17e^{-0.03d} \quad (4.12)$$

where $\Delta\lambda$ is the quantity to add to the measured value, and d is the diameter of the cylinder in mm. This is a geometric correction, which does not take into account the possible effect of the lithology. The equation was obtained by comparing measurements of TC from several cylindrical surfaces with the one of the flat surfaces of the same samples. The samples considered are acrylic cylinders cut in half along their major axis, of different diameters. Despite the fact that the correction identified is small and mostly lower than the uncertainty of the measure itself, it is necessary to improve it with further studies, on different materials.

4.2.4.3. Measuring procedures

The scanner used for the measurements is the Thermal Conductivity Scanner (TCS) produced by Lippmann and Rauhen GbR (Fig. 4.11). The optical head of the TCS contains three infrared cameras as sensors and an electric lamp as heat source. It moves under the scan line (identified by the red stripes in Fig. 4.11). The TCS is connected to a computer, where a dedicated software, “TCS”, permits to control the machine.

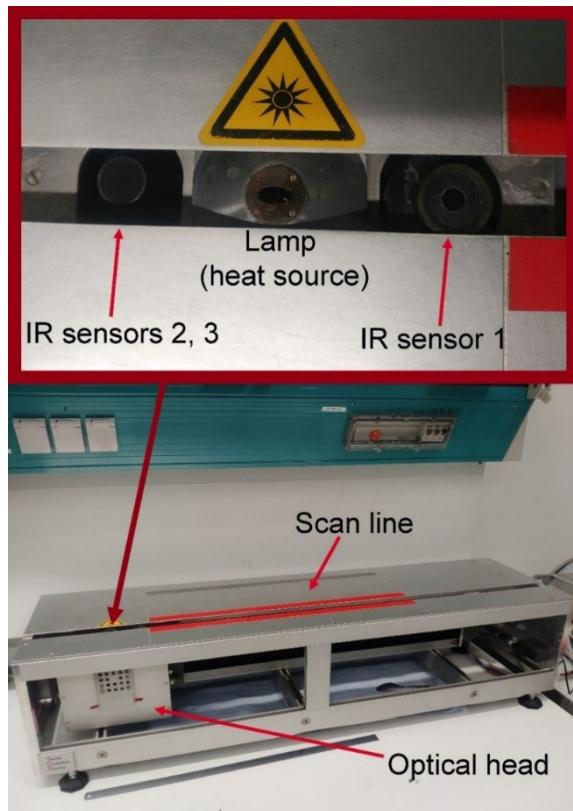


Figure 4.11: Thermal Conductivity Scanner used for this project. The red box shows the essential part contained by the optical head (explained in 4.3.4.1).

The parameters measured are the bulk TC and bulk TD. It is possible to run the scanner in the single 'TC' mode or in the combined 'TC+TD' mode. In the first case, only the sensors, 1 and 2, are activated, providing TC measurements with 3 % of accuracy. In the second case, all sensors are activated and the results produced are TC and TD values, with an accuracy of 5 % (such percentages are declared by the manufacturer).

The samples are aligned along the scan line with the analysed surface facing downwards, together with two reference standards, one at the beginning and one at the end of the row of samples. Despite the presence of the optical coating stripe, the actual width of the measurement is approximately 1–2 mm.

The reference standards consist in various samples of different nature. Their thermal properties are well known. Tab. 4.2 shows the standards used for this work. The single 'TC' mode requires a pair of standards of the same material with the same thermal properties. In order provide

the best results, their TC and TD should be as close as possible to those expected from the samples. On the contrary, for the combined 'TC+TD' mode, two different standards must be used, in order to define a range in which the thermal properties of the samples should fit. These ranges are already defined and can be selected from the software. If the TC and the TD of the samples differ too much from these conditions, a new appropriate set of standards

is chosen. When the scan of the machine is completed, the software shows two ('TC') or three ('TC+TD') temperature lines. On these lines, it is possible to define the position of the standards and the samples. For each sample it is possible to specify a series of information, such as the orientation of the layering with respect to the scanning line and the conditions of the sample (dry or saturated).

Table 4.2: Standards adopted for the measurements in this project. The properties are declared by the provider (TCS manufacturer).

Name	Material	TC [W/m*K]	TD [10^{-6} m ² /s]
'B1' – 'B2'	Technical glass	1.094	0.550
'C1' – 'C2'	Fused quartz	1.35	0.827
'D1' – 'D2'	Marble	2.93	1.21
'D3' – 'D4'	Marble	3.71	1.61
'E1' – 'E2'	Titanium Alloy	6.25	2.74
'C113'	Gabbro	2.41	1.02

Subsequently, the software calculates the following values for every scanned direction on a sample:

- Mean TC and TD;
- Minimum and maximum values of TC and TD detected;
- G (%) factor = standard deviation/mean;
- Inhomogeneity factor = (Max value – Min value)/mean.

Of the calculated parameters, only the mean TC and TD values were strictly needed in this work, while the other data were considered as additional indicators of the quality of the measures.

Along every direction of the samples, three non-collinear measurements (1–5 mm distant between each other) were carried out. Their arithmetic mean represents the TC and TD for the specific direction considered. This way provides representative values of the heterogeneities on the rock surface and reduces the error on a single measurement by a factor of $\sqrt{3}$.

In conclusion, it is worth to point out that the saturated samples needed to be submerged in their fluid after every single scanning. Nevertheless, for isooctane-saturated samples, a lightly decreasing trend of TC and an increasing TD was recorded anyway. The hypothesized cause is an unmanageable replacement of the alkane fluid with air, due to the evaporation of isooctane under ambient room conditions. However, this variation is always lower than the overall standard deviation of the mean and thus it is believed not to influence significantly the final results.

4.3. Data processing

The data acquired in the laboratory were processed in order to:

- Calculate the matrix thermal conductivity and diffusivity values;
- Complete the dataset in case of missing direct measurements (where possible);
- Calculate values representative of the samples (from subsamples measurements);
- Calculate the anisotropy;
- Calculate the specific heat capacity.

All these operation, together with the laboratory work, led to the definition of a final dataset, which was analysed as reported in the following chapter

4.3.1. Geometric mean model

The processing of the data acquired in the laboratory involved, in a first phase, the use of mixing models. Generally, these techniques permit to determine indirectly the thermal properties of a rock. Some of the most commonly used methods are the arithmetic mean, the geometric mean and the harmonic mean models, which are simple methods based on the assumption of a two-phase rock system: rock matrix and pore fluid. The arithmetic and harmonic mean are also known as parallel and series models, respectively. In the first case, a composite rock with grains arranged in a parallel orientation to the direction of heat flow is assumed. The harmonic mean instead assumes a rock which grains are oriented perpendicularly to the orientation of heat flow (Clauser, 2006; Fuchs et al., 2013; Robertson, 1988; Woodside & Messmer, 1961a). See also Fuchs et al. (2013), Fuchs et al. (2015) and Ray et al. (2015) for further details on different common mixing models and a comparison between them.

The geometric mean model, used in this work, is an empirical model that assumes a chaotic disposition of the grains. It was firstly evaluated by Woodside & Messmer (1961a,b) and shows a good reliability in modelling of sedimentary rocks. This method permits to calculate the matrix TC (λ_m or MTC) and matrix TD (α_m or MTD) from the measured bulk values Eq. (4.12). From these calculated properties, it is then possible to define the BTC and the BTD assuming different saturating fluids in the rock. The geometric mean model for thermal conductivity is

$$\lambda_b = \lambda_m^{1-\varphi} * \lambda_p^\varphi \quad (4.12)$$

$$\lambda_m = \left(\frac{\lambda_b}{\lambda_p^\varphi} \right)^{\frac{1}{1-\varphi}} \quad (4.13)$$

where φ is the porosity, λ_p is the thermal conductivity of the saturating fluid and λ_b is the bulk thermal conductivity. λ_b refers to dry or saturated conditions depending on the fluid considered in the specific equation.

The thermal diffusivity calculations required two additional factors to include in Eq. (4.14) and (4.15): f and β (Goto & Matsubayashi, 2009):

$$\beta = \frac{\rho_p c_p}{\rho_m c_m} \quad (4.14)$$

$$f = \frac{\beta^\varphi}{1 + (1 - \beta) * \varphi} \quad (4.15)$$

where $\rho_p c_p$ and $\rho_m c_m$ are the volumetric heat capacities of saturating fluid and matrix. Thus, the geometric mean for thermal conductivity would become

$$\alpha_b = f * \alpha_p^\varphi * \alpha_m^{1-\varphi} \quad (4.16)$$

Such factors represent a correction originally applied by Goto & Matsubayashi (2009) for marine water sediments and their application is discussed in Chapter 6.

The different calculations carried out with this model involved the use of tabulated petrophysical properties of different materials. The values used in this project are listed in Tab. 4.3 and their application is specified in the following part of this work, where necessary.

Table 4.3: tabulated petrophysical properties considered in this work for geometric mean model and data analysis. These values are referred to ambient conditions. Data collected from several authors and reported in: ^aFuchs et al. (2015), ^bFuchs et al. (2013), ^cClauser (2006), ^dBlumm & Lindemann (2005), ^eWatanabe (2003). “||” and “Perp” refer to measurements parallel and perpendicular to the direction of maximum thermal conductivity of a mineral (see Clauser (2006) for further details).

Phase	ρ [kg/m ³]	c [J/(kg*K)]	TC (λ) [W/(m*K)]	TD (α) [10 ⁻⁶ m ² /s]
<i>Air</i>	1.225 ^a	1004 ^a	0.025 ^b	19 ^a
<i>Water</i>	998 ^c	4180 ^c	0.604 ^b	0.143 ^d
<i>Isooctane</i>	688 ^c	2136 ^e	0.095 ^e	0.065 ^e
<i>Quartz</i>	2650 ^a	740 ^a	7.7 ^a 10.17 ^a [] 6.15 ^a [Perp]	3.8 ^a 7.14 ^a [] 3.3 ^a [Perp]
<i>Illite</i>	2750 ^a	796 ^a	1.8 ^a	0.82 ^a
<i>Calcite</i>	2710 ^a	820 ^a	3.4 ^a	1.62 ^a

4.3.2. Final data set

The laboratory work provided one or more petrophysical properties for every subsample of the collection. Therefore, for the final dataset required in this work, a single, representative value for every sample was calculated for every petrophysical property. Porosity and densities were measured on one selected subsample, for each sample and the measurement obtained was considered representative of the entire specimen. On the contrary, the bulk thermal conductivity and diffusivity measurements of each sample, were treated as follows:

- I. The 3 direct measurements of a subsample's surface were averaged in order to get one single value, representative of a specific direction ($\parallel 1$, $\parallel 2$ or *perp*; see also 4.2.4.3.);
- II. MTC and MTD were calculated for each subsample's surface from bulk measures, using the geometric mean model;
- III. BTC and BTD measurements from isooctane-saturated samples were converted to water-saturated equivalents using the geometric mean model;
- IV. Where direct measures were not possible in one of the conditions (dry or saturated), a converted value of BTC or BTD was calculated (e.g. in case of samples' destruction during saturation process). This was possible using the geometric mean model.
- V. The resulting data from the different subsamples' surfaces were averaged together in order to obtain values representative of the relative sample of origin. In this way, three values ($\parallel 1$, $\parallel 2$ and *perp*) of matrix and bulk thermal properties have been obtained for each sample.

The measurements that required the conversions described in steps III and IV are showed in Appendix B.

Finally, two additional properties were calculated: the anisotropy ('A'), using Eq (4.17) and Eq. (4.18), and specific heat capacity (*c* or 'SHC') using Eq. (4.19).

$$A_{\lambda} = \frac{\lambda_{\parallel}}{\lambda_{perp}} \quad (4.17)$$

$$A_{\alpha} = \frac{\alpha_{\parallel}}{\alpha_{perp}} \quad (4.18)$$

$$c = \frac{\lambda}{\rho * \alpha} \quad (4.19)$$

4.3.3. Software

The processing of data described in this paragraph was carried out using Microsoft Excel 2015. The same software was used to produce all graphs shown in the following chapters ("Results" and "Discussions and conclusions") and analyse the data.

With the data provided by Dr. Sven Fuchs and GEUS institute, it was possible to produce the maps shown in Chapter 3 ("Overview of the study area") using ArcGIS 10.1 (Esri).

The well logs images shown at the beginning of this chapter were produced using WellCAD 5.0 (ALT- Advanced Logic Technology) and were possible thanks to the data provided by the GEUS institute.

5. Results

The laboratory analyses and the data processing involved 38 samples of the entire collection. Five samples (1, 17d, 18d, 21 and 23c) of the initial compilation were destroyed during the plugging procedure, therefore it was not possible to carry out any of the measurements. For two samples (22 and 23) only the porosity and the densities measurements were possible, due to the absence of smooth surfaces for TCS measurements and to the impossibility of sawing the samples without destroying them. A printout of the final dataset is shown in the Appendix A and B. The resulting data obtained are here shown under two main perspectives:

1. The relations between petrophysical properties and the lithological classification of the samples (see 4.1.5. for the details on the lithology classes identified);
2. A comparison between the petrophysical data of the different formations analysed, within the limits of the sample available.

5.1. Petrophysical properties and lithology

5.1.1. Porosity and density

The results of the measurements of porosity and density are plotted as cumulative distributions for each lithological class: Fig. 5.1 shows the effective porosity, whereas Fig. 5.2a,b,c shows bulk densities, dry and saturated conditions, and matrix density. The uncertainty of both porosity and density measurements is 1 %.

The measured effective porosity of each lithological class (Fig. 5.1) approximately plots within a certain range of porosity, except for the limestones, which define two separated “groups”. In particular:

- The mudstones and the sandy mudstones values between 4 % and 12 %.
- The argillaceous sandstones present a range of porosity from 12 % to 22 %.
- The sandstones present a wider distribution, from 8 % to 28 %.
- The limestones’ porosities are distinguished in low porosity (4 %, 6% and 9 %) and high porosity (28 % and 32 %) rocks.

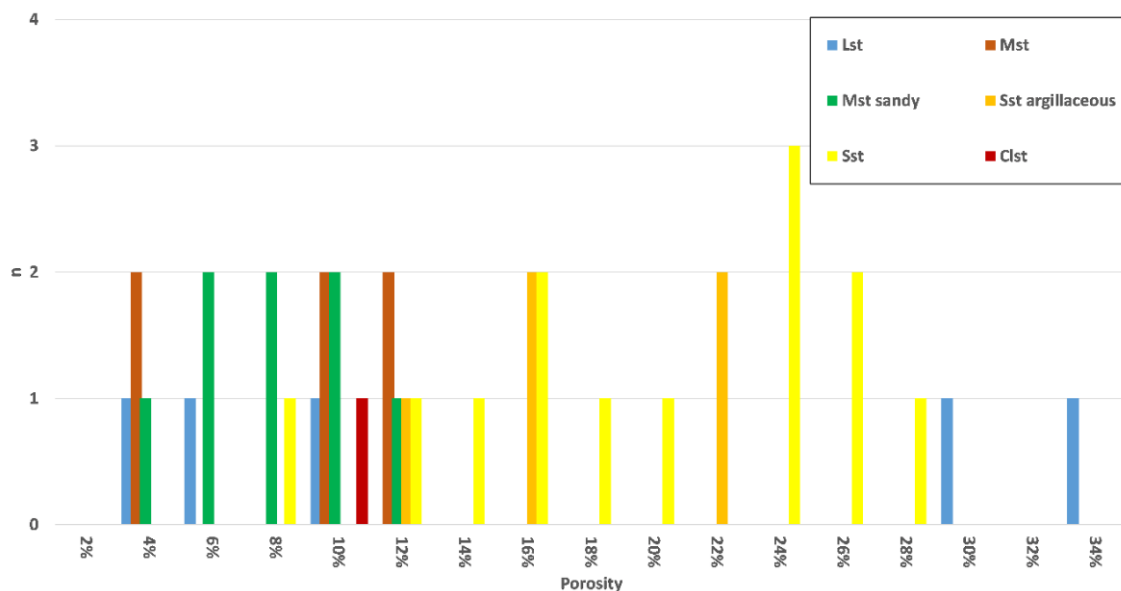


Figure 5.1: effective porosity distribution per lithological class.

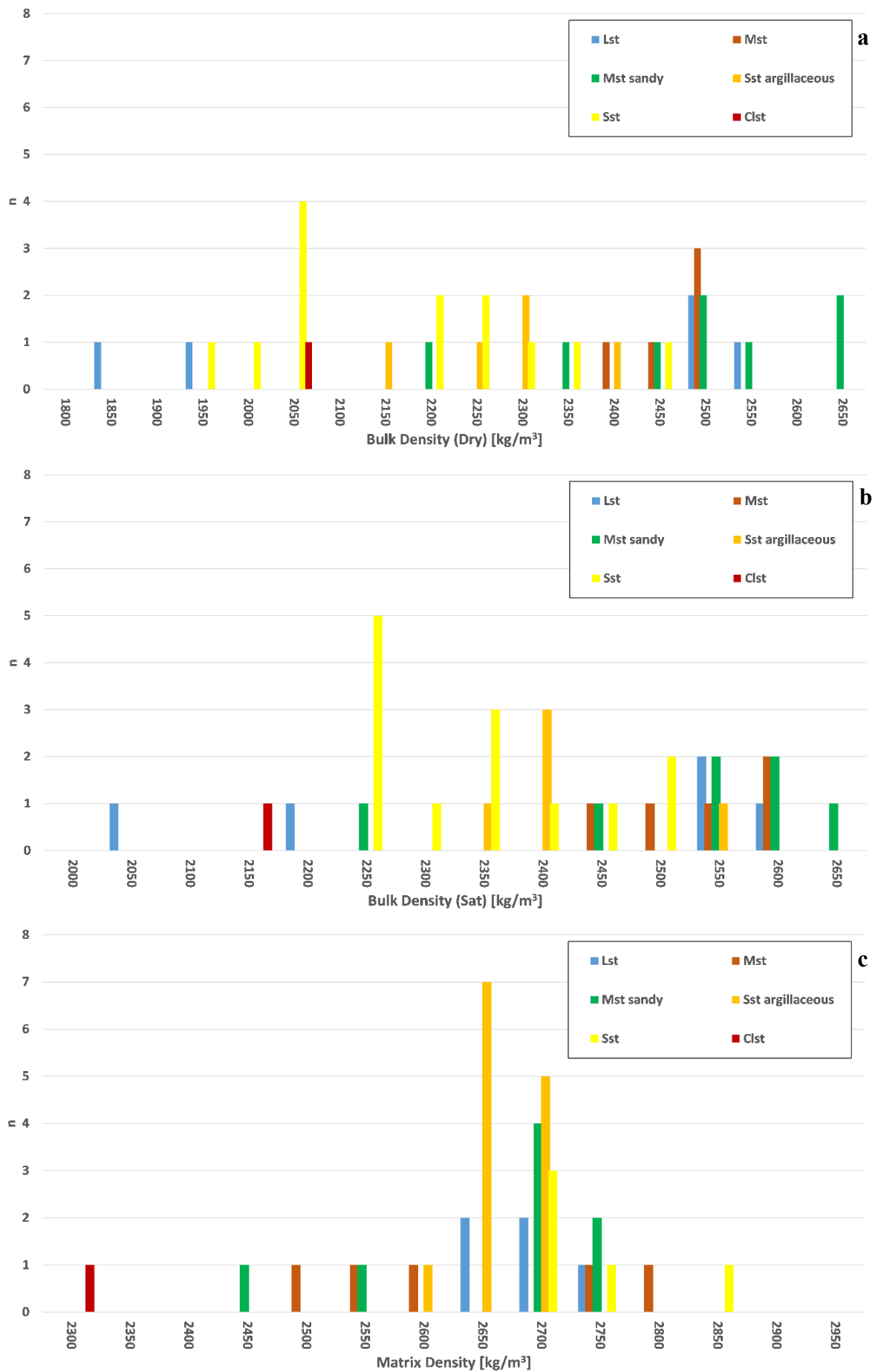


Figure 5.2: distribution of bulk density of dry rocks (a), saturated rocks (b), and matrix density (c), per lithology.

The densities of the different lithology classes show wide distributions of values. In particular, from the bulk densities of dry rocks (Fig. 5.2a) and saturated rocks (Fig. 5.2b) it is possible to distinguish ranges of values for each lithology, which are distributed as summarised in Tab. 5.1.

Table 5.1 mean values and ranges, plotted as (Min – Max), for bulk densities in dry and saturated rocks. The relative uncertainty of each measurement is 1%.

Lithology	Density (dry) [kg/m³]	Density (saturated) [kg/m³]
<i>Claystone</i>	2060	2160
<i>Limestones</i>	2240 (1810 – 2550)	2360 (2030 – 2570)
<i>Mudstones</i>	2460 (2400 – 2480)	2500 (2440 – 2570)
<i>Sandy mudstones</i>	2460 (2170 – 2620)	2520 (2240 – 2660)
<i>Argillaceous sandstones</i>	2260 (2130 – 2340)	2400 (2340 – 2510)
<i>Sandstones</i>	2140 (1950 – 2430)	2320 (2210 – 2500)

The lowest density values of 1810 kg/m³ and 2030 kg/m³, for dry and saturated conditions respectively, belong to the sample 28, which is a limestone. The highest values belong to the sandy mudstone 19b, which has a density of 2620 kg/m³ in dry conditions and 2660 kg/m³ in saturated conditions.

Contrarily to bulk density, most of the samples' matrix densities (Fig. 5.2c) cluster around 2650 – 2750 kg/m³. In particular, the mudstones spread in a wide range between 2500 kg/m³ and 2760 kg/m³; the sandy mudstones plot between 2420 kg/m³ and 2720 kg/m³, with a mean of 2640 kg/m³. The argillaceous sandstones are in the 2660 kg/m³ – 2840 kg/m³ range, while the sandstones plot between 2600 kg/m³ and 2660 kg/m³. The lowest matrix density detected is 2280 kg/m³, measured on the claystone (sample 23), whereas the highest value was identified on the sample 22, which has a matrix density of 2838 kg/m³.

5.1.2. Bulk thermal conductivity and bulk thermal diffusivity

The bulk thermal conductivities and bulk thermal diffusivities measured with the TCS and calculated with the geometric mean are shown together in Fig. 5.3. These graphs are representative of the entire dataset obtained in this work and shows the distribution of the measurements from every surface of every sample, per lithological class. Therefore no distinction between parallel and perpendicular values was done. The uncertainty of each single measurement considered here is specified in Appendix B.

Each of the five rows of Fig. 5.3 (two graphs per row) refers to one lithological class, from limestones to sandstones; the left column shows thermal conductivity, while thermal diffusivity is shown in the right column. In each of the histograms, the orange bars represent dry samples and the blue, semi-transparent bars represent saturated conditions (pure water). As previously mentioned, the iso-octane-saturated measurements were converted to pure water saturated equivalents using the geometric mean model.

Samples in saturated conditions define distributions which mean is always higher than that of dry conditions. This is valid for both thermal conductivity and thermal diffusivity. The investigated range of BTC in dry conditions (or 'dry TC') goes from a minimum of 1.08 W/(m*K) for limestones, to a maximum of 3.65 W/(m*K) for sandstones. In saturated conditions ('sat TC') the measured values range from a minimum of 1.80 W/(m*K) for the mudstones to a maximum of 5.47 W/(m*K) for sandstones.

For BTC, the distributions in dry and saturated conditions are generally similar in shape, except for the limestones, which plot around 2.75 W/(m*K) for saturated conditions contrarily to the wider distribution in dry conditions. Moreover, mudstones and sandy mudstones show a smaller difference between the distributions in dry and saturated conditions, relatively to the sandy classes. In fact, the mean difference between sat and dry TC is about 0.6 W/(m*K) for both muddy rock types, while it grows to 1.6 W/(m*K) and almost 2 W/(m*K) for sandstones and argillaceous sandstones, respectively.

The BTD measured in dry conditions ('dry TD') shows a range from 0.57 mm²/s, for the limestones, to 1.83 mm²/s for the sandstones. Limestones and sandstones represent also the minimum and the maximum values for saturated conditions ('sat TD'): respectively, 0.83 mm²/s and 2.38 mm²/s. The BTD's distributions are contained in smaller ranges of values than BTC and define very small differences between dry and saturated conditions. Nonetheless, it is evident a stronger difference between the two conditions for sandy samples, compared to the muddy ones.

Finally, for both TC and TD, a general increasing trend from muddy to sandy samples is evident. This trend is highlighted in Fig. 5.4, where the distributions of sat TC (Fig. 5.4a) and sat TD (Fig. 5.4b) of each lithology are plotted together. Such distinction is also present in dry conditions, although it is less evident.

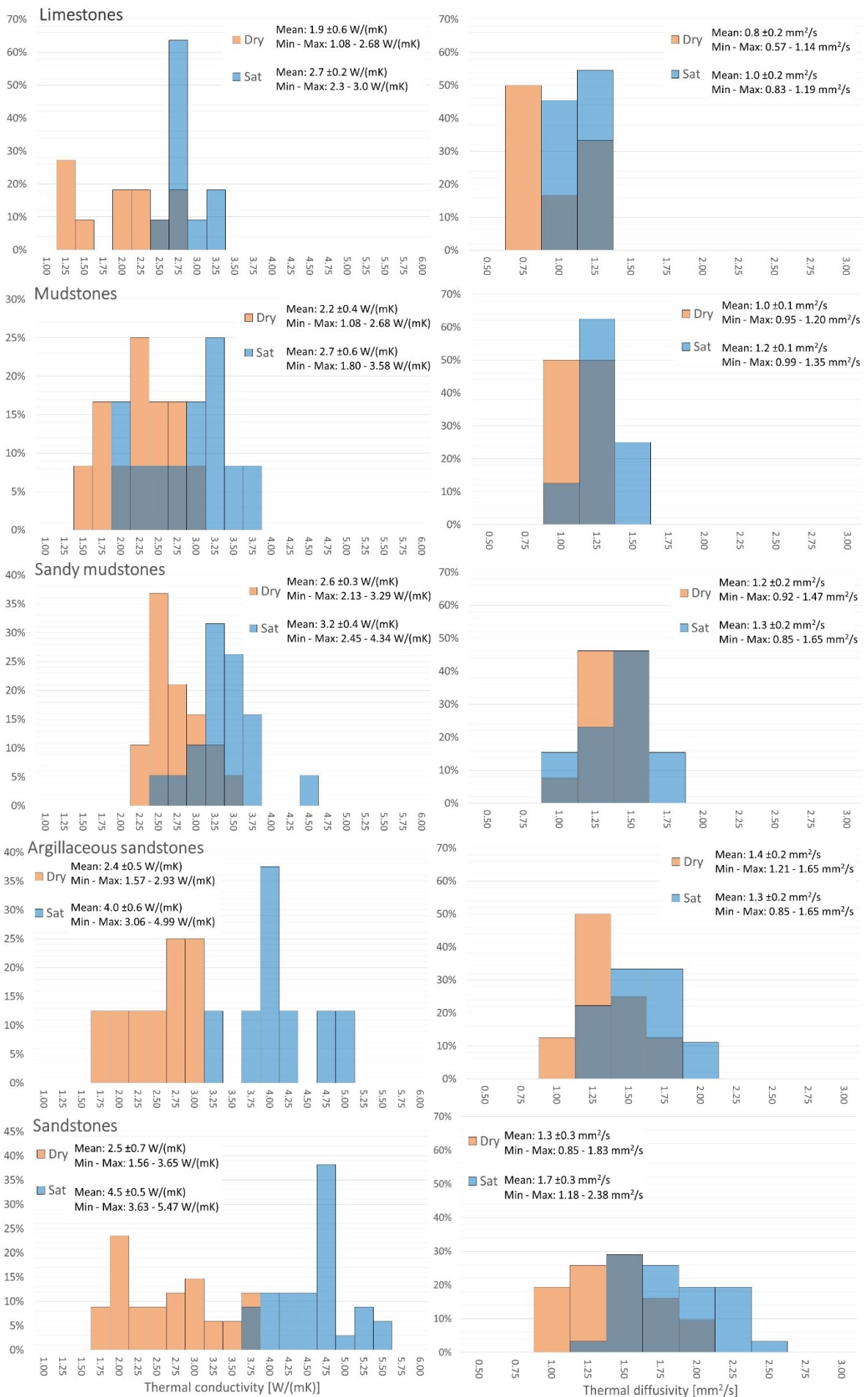


Figure 5.4: (previous page): frequency distribution of TC and TD for dry (orange bars) and saturated (blue-transparent bars) samples. The TC is showed in the left column and the TD is showed in right column. N. of measurements for TC (sat and dry): 11 Lst, 12 Mst, 19 Mst Sandy, 8 Sst Argillaceous, 34 Sst. N. of measurements for TD: 12 Lst, 8 Mst, 13 Mst Sandy, 8 Sst Argillaceous, 31 Sst.

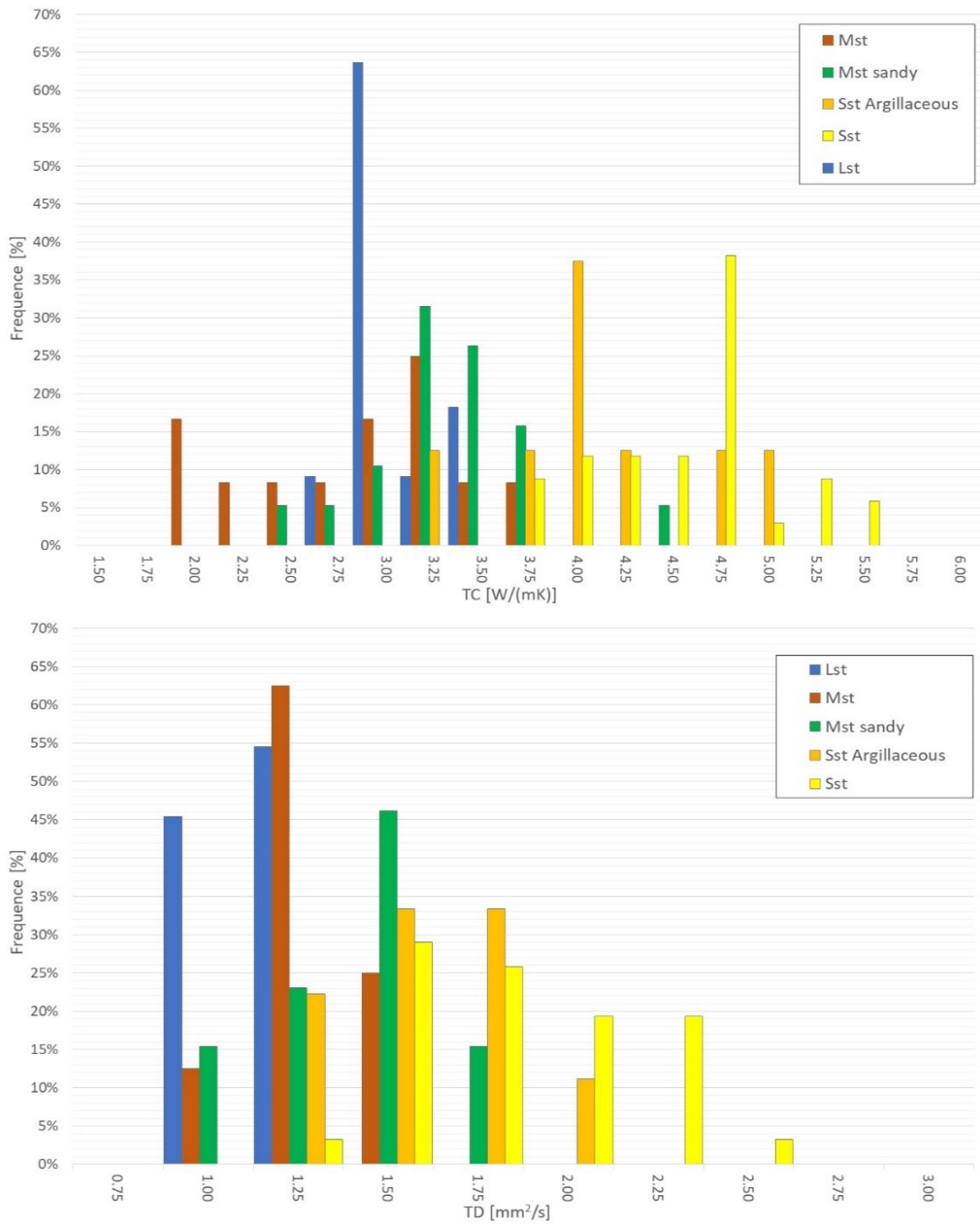


Figure 5.3: cumulative distribution of thermal conductivity (a) and thermal diffusivity (b) for saturated samples.

5.1.3. Specific heat capacities

The specific heat capacity (SHC) was calculated for every sample in which thermal conductivity, thermal diffusivity and density were all determined. Fig. 5.5 shows the SHC for dry and saturated samples (orange and blue bars, respectively), and for the matrix of the rock (grey bars). The matrix values were calculated at a later stage using the matrix thermal conductivity and diffusivity, the obtaining of which is defined in 5.1.6. The averaged relative uncertainty for these values is 10 %. Two main observations can be done for most samples:

- The higher specific heat capacity of pure water, compared to that of air, leads to a higher bulk SHC for saturated samples.
- The SHC for dry samples and that of the matrix are similar.

The mean SHC for dry samples is 870 J/(kg*K) with a minimum value of 570 J/(kg*K) and a maximum of 1290 J/(kg*K) identified for samples 19 and 19b respectively. The mean value for saturated samples grows to 1070 J/(kg*K). In this case, the maximum and minimum values are 640 J/(kg*K) and 1610 J/(kg*K) calculated for samples 3 and 11. As previously mentioned, the matrix values have a distribution analogous to that of dry samples, but with slightly lower values: 540 J/(kg*K) and 1090 J/(kg*K) as minimum and maximum for samples 19 and 7, respectively, and a mean value of 860 J/(kg*K).

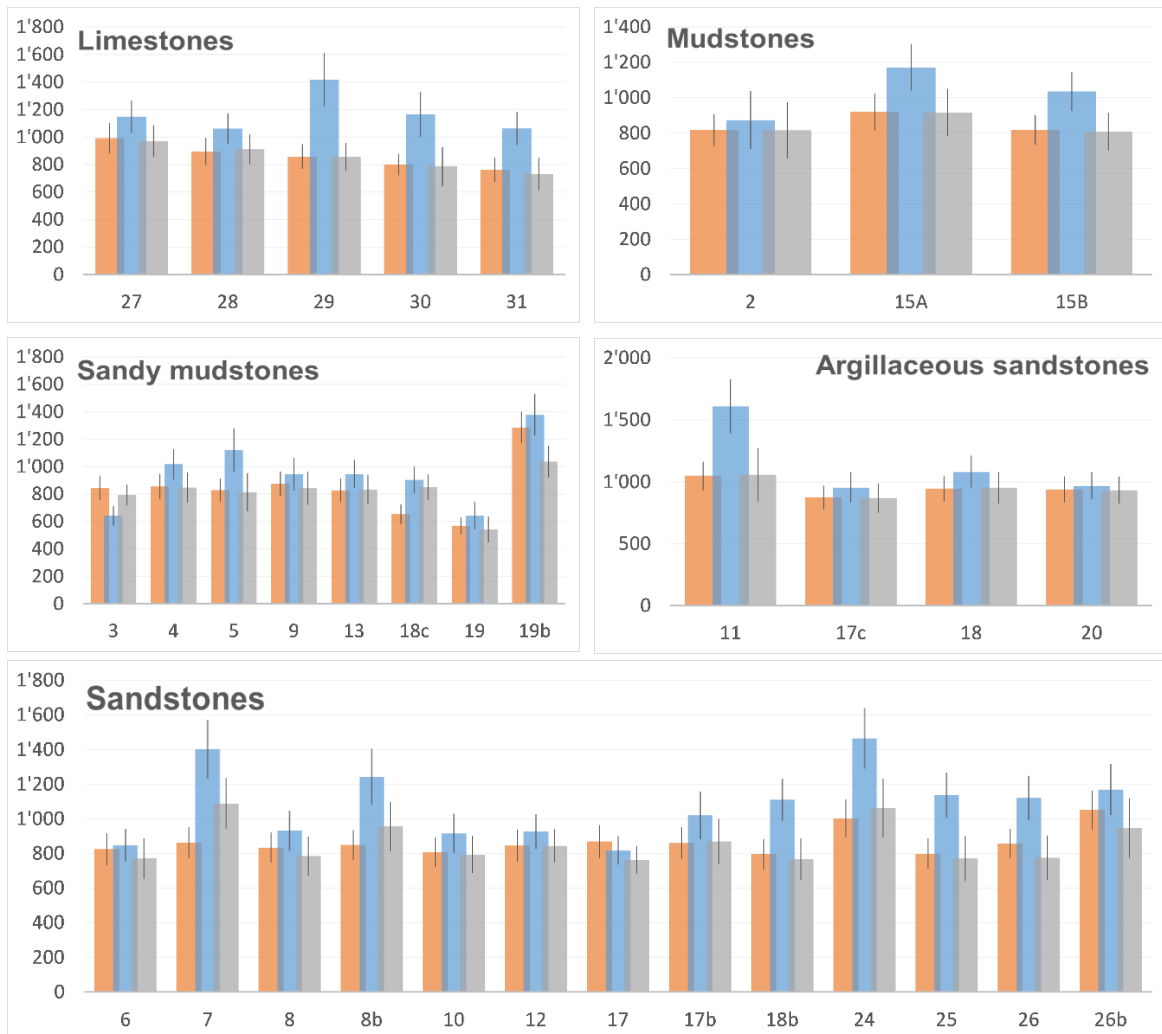


Figure 5.5: Specific heat capacity of dry (orange bars), saturated (blue bars) rocks and matrix (grey bars). For each sample, parallel and perpendicular values are averaged in one single sample. The X axes represents the ID of the sample, the Y axes are the SHC values in J/(kg*K).

5.1.4. Anisotropy

The thermal anisotropy was studied for each condition (dry and saturated) and lithology. The two parallel values ($\lambda_{||1}$ and $\lambda_{||2}$) were averaged in a single value. The anisotropies are shown in Fig. 5.6 plotting parallel against perpendicular values for each sample. The anisotropy for both TC (5.6a,b) and TD (5.6c,d) are plotted, for saturated and dry conditions (Fig. 5.6a,c) and the different lithology classes (Fig. 5.6b,d). Three reference lines of anisotropy are plotted: $A=1.2$, $A=0.8$ and $A=1$. The sample is considered purely isotropic when $A=1$.

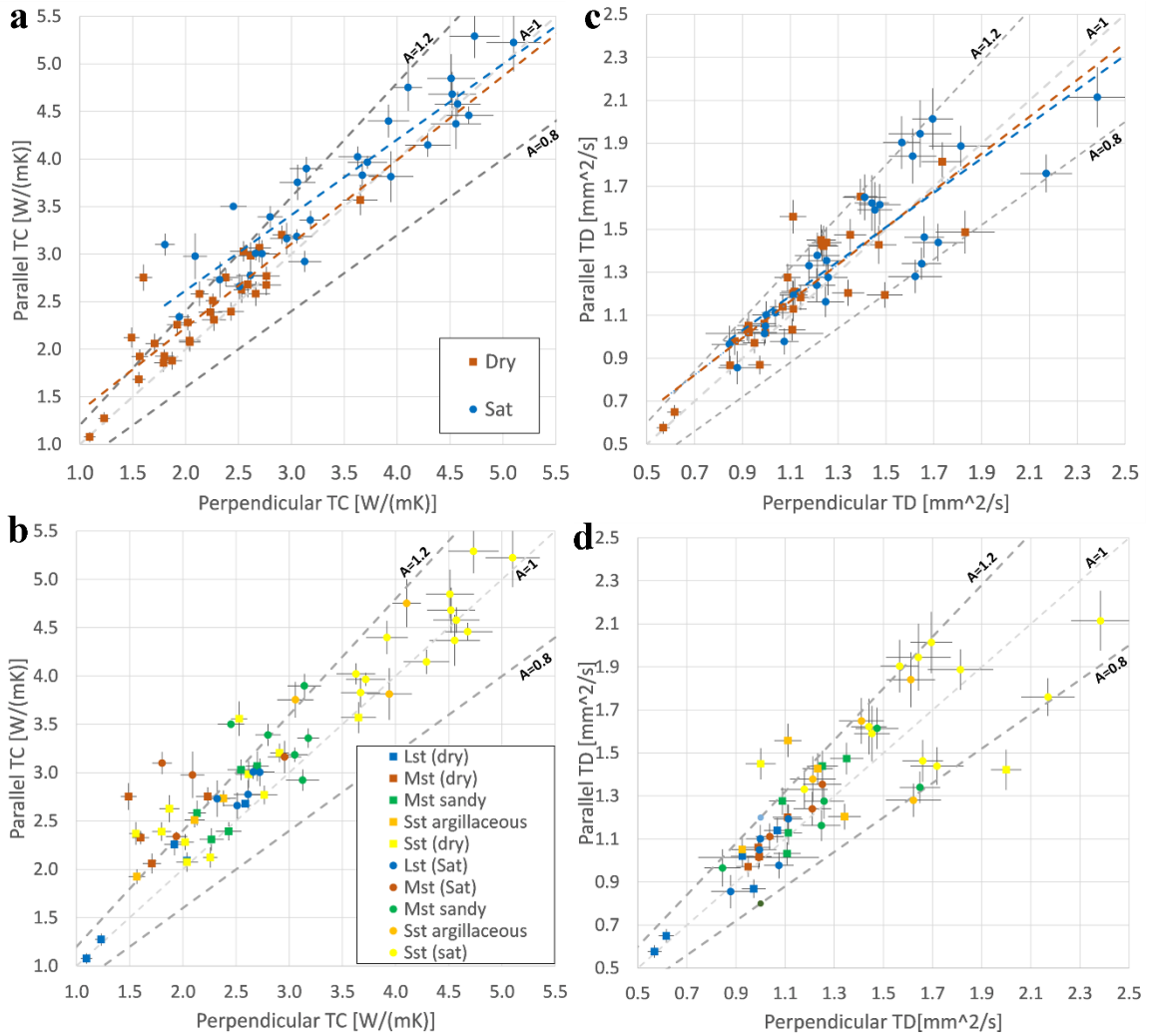


Figure 5.6: Anisotropy of rock samples for TC (left) and TD (right). a, c: distinction between dry and saturated rocks. Parallel values are mean between Par1 and Par2. b, d: distinction between dry (squares), saturated (circles) and lithologies.

For both TC and TD, almost all samples fall in the anisotropy range of 1.2 and 0.8. The TC shows that the majority of $\lambda_{||}$ is higher than the perpendicular one, defining an anisotropy greater than 1. On the contrary, the TD has a scattered distribution around $A=1$.

A decreasing trend of anisotropy with increasing thermal conductivity is evident. This trend is more noticeable in saturated rocks. The distribution of TD suggests a similar tendency, nevertheless it is not as clear as for the TC, due to the scattering of the data. This effect is mainly caused by the combination of two factors:

- I. Generally higher isotropy of sandy rocks compared to muddy and limey rocks
- II. Higher TC and TD for the sandy samples

The highest anisotropy ($A=1.7$) was identified in sample 15A (Mst), whereas the lower values generally belong to the Sst group. In these graphs is also possible to appreciate the distributions of TC and TD for the different lithological classes and saturating fluids, as already shown by the histograms in 5.1.2.

5.1.5. Geometric mean model application on bulk thermal properties

It is possible to compare the measured thermal properties obtained from the laboratory work with the geometric mean model. In order to do so, the samples' thermal properties were compared to those of ideal porous media obtained using the geometric mean. Fig. 5.7a and Fig. 5.7b show this comparison for BTC and BTd, respectively, plotting the bulk thermal property of a rock against its effective porosity.

The ideal porous media values were calculated considering the thermal properties of minerals ($\lambda_m; \alpha_m$) and fluids ($\lambda_p; \alpha_p$) listed in Tab. 4.3. The porosity (ϕ) values considered range from 0 % to 35 %. The mineralogical composition of the ideal reference samples is known:

- Pure quartz
- 50% of quartz and 50% of illite
- Pure calcite
- Pure illite

They are plotted as black-to-grey curves in the graphs. The laboratory measurements are plotted as coloured dots, distinguished by their lithological class. No distinction between the values of parallel and perpendicular axes is shown.

The measured values in Fig. 5.7 (dry conditions) are all direct measurements. In fact, these graphs can give an idea of the fitting of the geometric medium model to real cases. In contrast, a consistent number of measurements of Fig. 5.8 (saturated conditions) were converted from dry TC and TD (details in Appendix B).

Two main aspects can be analysed in Fig. 5.7. The first one is the decreasing trend of both BTC and BTd with increasing porosity defined by the geometric mean model. The majority of the samples analysed has the same trend, especially for sandstones, argillaceous sandstones and sandy mudstones. This is evident for both thermal conductivity and thermal diffusivity. On the contrary, the mudstones do not follow this trend, presenting a BTC and BTd that remain generally constant with increasing porosity, whereas the limestones show a different decreasing trend, inconsistent with the calcite curve. Nonetheless, there are only a few samples of mudstones and limestones available for a reliable comparison.

The second aspect concerns the lithology and compositions. The calculated curves, in fact, act as compositional end members and the measured values generally fit these model curves:

- The sandstones plot around the quartz reference.
- The argillaceous sandstones and the muddy sandstones plot above and under the “50 % quartz + 50 % illite” curve, respectively.
- Most of the mudstones plot above the “Illite” curve, near the sandy mudstones group.
- The limestones values plot coherently with the “Calcite” curve, except for the BTC of the highly porous samples, which is much higher than that calculated for calcite.

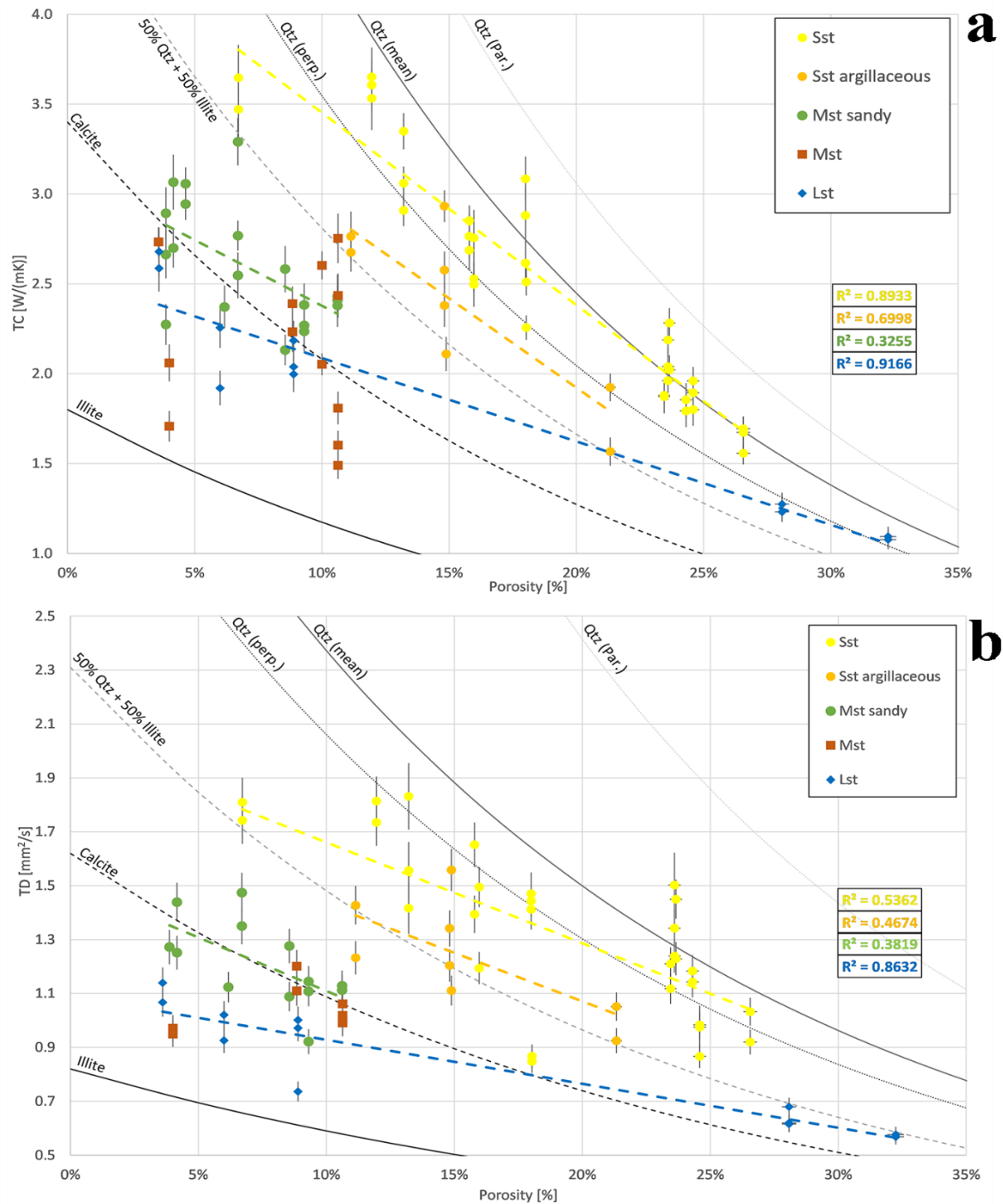


Figure 5.7: Bulk thermal conductivity (a) and bulk thermal diffusivity (b) in dry conditions, plotted against the relative porosity of each sample. The coloured dots represent the measured samples, the black-to-grey curves represent ideal samples of known composition (see text for details).

Fig. 5.8 shows the same comparison of Fig. 5.7 for saturated conditions, considering both measured and converted values. In this case, the distributions of measured and calculated values are very similar to those shown in Fig. 5.7. In fact, the data obtained from the samples plot close to the relative reference curves and a decreasing trend is generally recorded. However, the trends detected by BTC and BTM of limestones and the BTC of sandy mudstones are of growth with porosity, contrary to what was expected.

Finally, comparing dry with saturated conditions graphs (Fig. 5.7 and Fig. 5.8) it is possible to notice that the distributions of thermal properties per lithology are generally similar to each other. Such analogy is supported also by the similar distribution of values between dry and saturated conditions showed in Fig. 5.3.

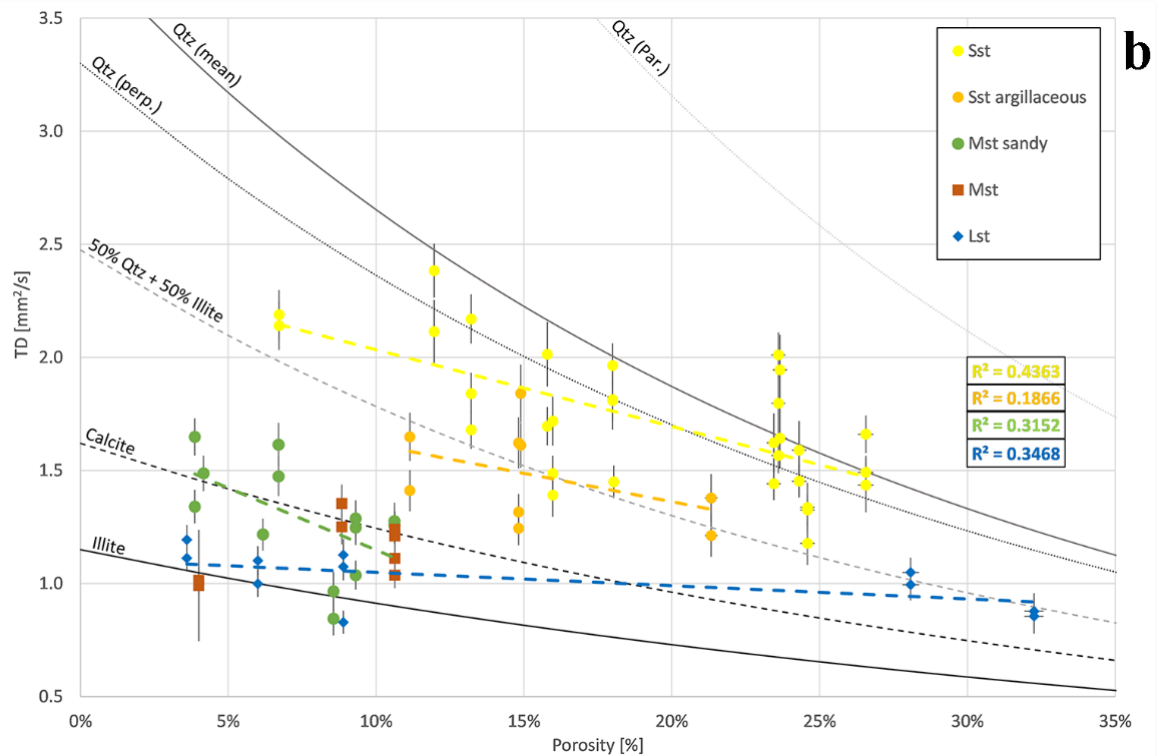
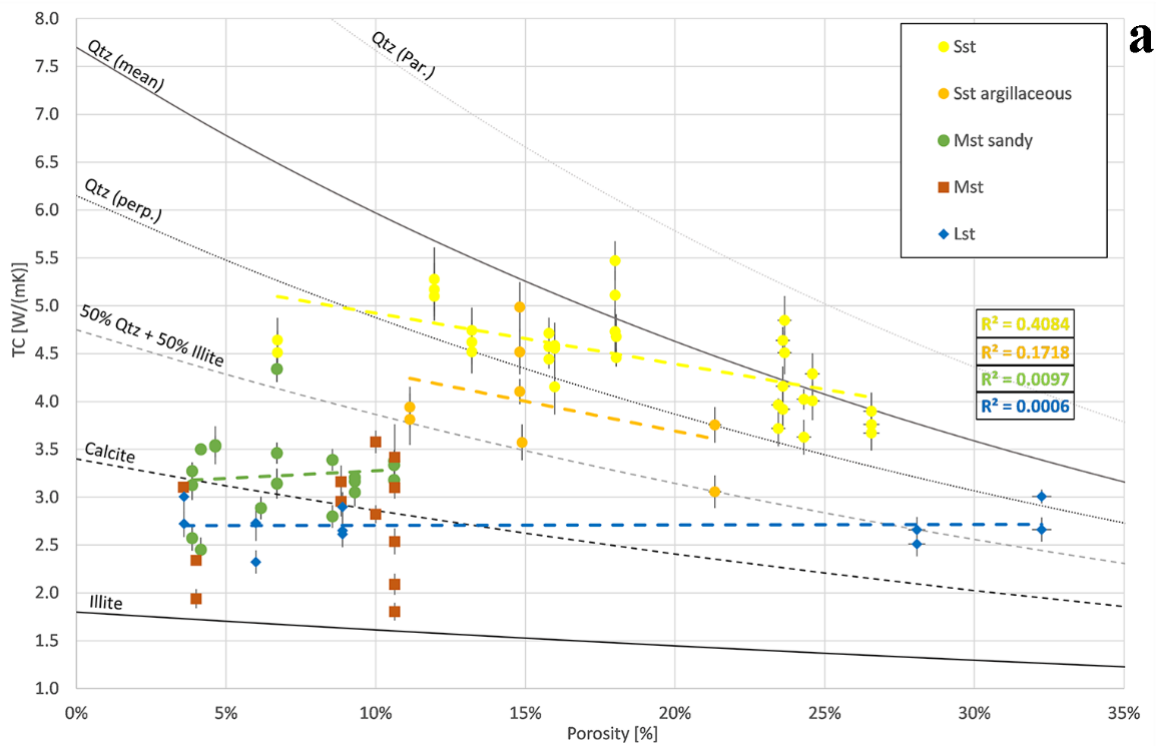


Figure 5.8: Bulk thermal conductivity (a) and bulk thermal diffusivity (b) in saturated conditions, plotted against the relative porosity of each sample. The coloured dots represent the measured samples, the black-to-grey curves represent ideal samples of known composition (see text for details)

5.1.6. Matrix thermal properties from geometric mean model

A further fundamental application of the geometric mean model is the possibility to calculate the matrix thermal conductivity ('MTC') and matrix thermal diffusivity ('MTD'), using the measured values. For thermal diffusivity, the correction of Goto & Matsubayashi (2009) was applied. For the f factors calculation, mean values of bulk SHC were considered.

One matrix value was calculated from each α_b and λ_b measured in the laboratory, on saturated and dry subsamples. The TD and TC of the fluid phases are listed in Tab. 4.3. A summary of the distribution of the matrix values, subdivided by lithological class is shown in Tab. 5.2.

Table 5.2: Minimum, maximum and mean values of matrix thermal conductivity ($W/(m^*K)$; upper number) and matrix thermal diffusivity (mm^2/s ; lower number) for each lithological class.

Lithology	Max – Min	Mean \pm St. deviation
<i>Limestones</i>	6.5 – 2.5	4.0 \pm 1.4
	2.3 – 1.0	1.6 \pm 0.5
<i>Mudstones</i>	4.4 – 1.9	3.1 \pm 0.8
	1.7 – 1.1	1.4 \pm 0.3
<i>Sandy mudstones</i>	4.8 – 2.7	3.7 \pm 0.5
	2.0 – 1.3	1.7 \pm 0.2
<i>Argillaceous sandstones</i>	6.9 – 4.7	5.4 \pm 0.8
	3.0 – 1.8	2.3 \pm 0.4
<i>Sandstones</i>	9.3 – 5.0	7.0 \pm 1.0
	4.8 – 2.3	3.3 \pm 0.6

Analogously to the analysis conducted in the previous subparagraph (Fig. 5.7 and Fig 5.8), the relation between the matrix thermal properties, the effective porosity and the nature of the rocks is here presented. This comparison and analysis is shown in Fig 5.9. Here, the MTC and MTD are considered to be directly dependent on the mineral composition of the rock, once removed the effect of the fluids in the pores. These properties were plotted against the effective porosity, which is dependent on the lithology of the rock considered (as also shown by the distributions in Fig. 5.1). In both graphs of Fig. 5.9, each sample's thermal property is represented by a mean between parallel (\parallel) and perpendicular (*perp*) values. Four coloured lines define ideal end members, reporting the values of MTC and MTD of single minerals (listed in Tab. 4.3). The distributions of MTC and MTD are generally similar with each other: the lithological classes plot in singular, distinguishable groups. Moreover, every group plots relatively close to a reference line:

- The sandstones are distributed around the “Qtz” line. The distribution for matrix thermal diffusivity is relatively more dispersed than the matrix thermal conductivity.
- Sandy mudstones and argillaceous sandstones define groups that are close to the “0.5 Qtz + 0.5 Illite” line.
- The mudstones plot close to the sandy mudstones group, but have lower MTD and MTC on average.

- The limestones define two separated groups: three low porosity samples with MTC and MTD lower than that of the calcite, and two highly porous samples with MTC and MTD higher than calcite.

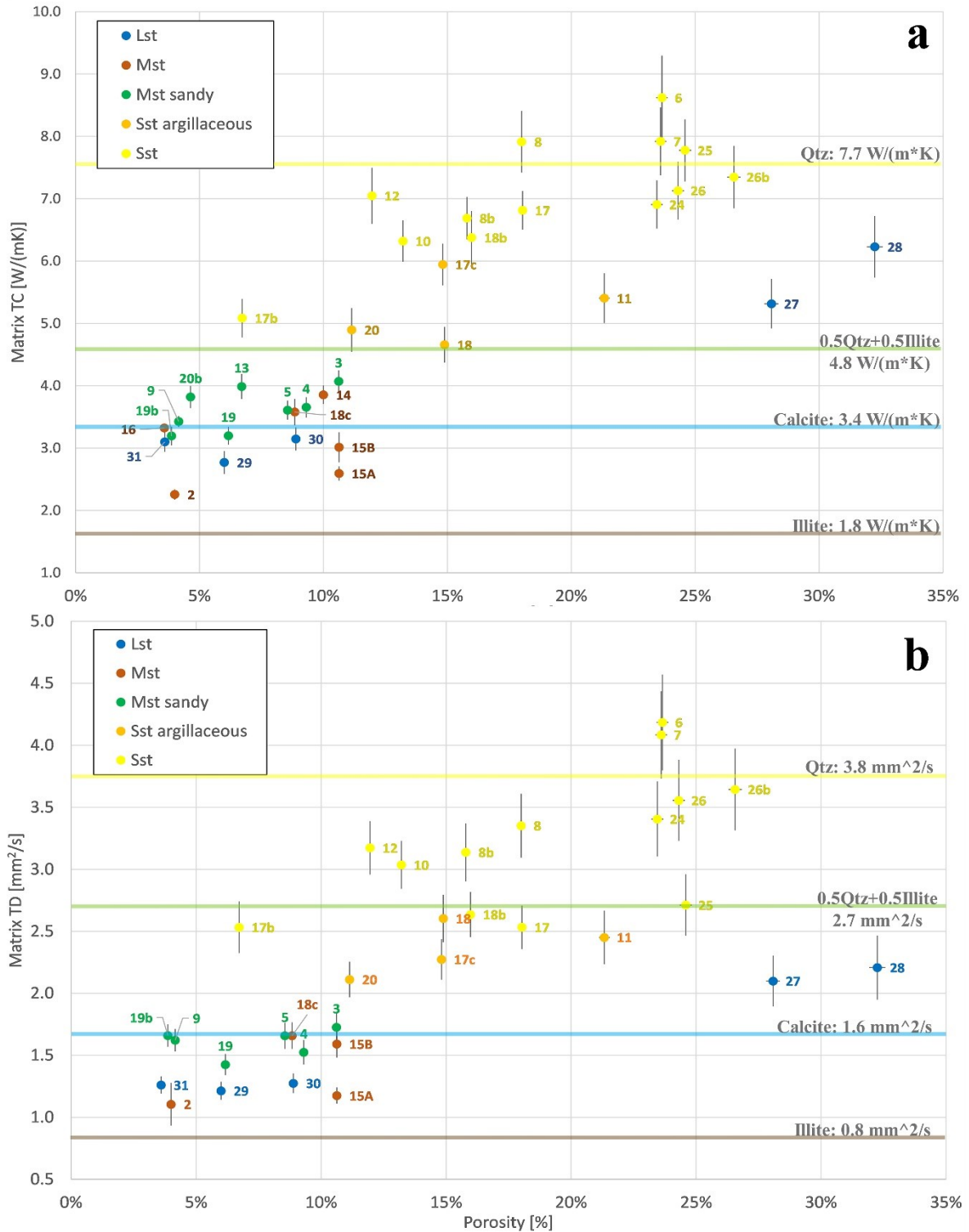


Figure 5.9: Matrix thermal conductivity (a) and diffusivity (b) plotted against the effective porosity of each sample. The coloured lines represent values of TC and TD of minerals (see Tab 4.3 and text for details).

5.2. Characteristics by formations

On the basis of the analysed rock samples, an overview of the petrophysical properties of the investigated formations is given in [Tab 5.3](#). This table shows and compares the mean values of porosity and thermal properties and includes the relative ranges of the values by plotting their minimum and maximum. The rock samples were distinguished by their lithological class and origin (well).

In the dataset, the Gassum Formation's sandstones are represented by 8 samples, collected from Aars-1, Farsø-1 and Stenlille-1. When comparing the three origins, it is possible to identify two distinct ranges of porosity and thermal properties: one represented by the sandstones collected from Aars-1 and Farsø-1 (which are close to each other; see [Fig. 3.1](#)), and one represented by the sandstones of Stenlille-1. On average, the samples of Stenlille-1 have an effective porosity 12 % higher than other wells' rocks. These sandstones present also lower values of BTC and BTD: the mean difference is 1.2 W/(m*k) and 0.7 W/(m*k) for dry and saturated TC, and 0.4 mm²/s for both dry and saturated TD. However, the opposite is true for MTC and MTD, where the differences are 1.1 W/(m*k) and 0.6 mm²/s, respectively.

The Haldager Sand Formation's sandstones collected from Aars-1 and Farsø-1 show characteristics that are more similar to each other, relatively to the Gassum sandstones. The single sample collected from Farsø-1 shows a lower effective porosity and higher values of the thermal properties than those collected from Aars-1. In this case the difference is 0.7 W/(m*K) for the BTC, 0.4 mm²/s for BTD and MTD, and 0.4 W/(m*K) for the MTC.

The three samples of argillaceous sandstones of the Gassum Formation have a generally lower porosity and higher bulk thermal conductivity and diffusivity, in dry and saturated conditions, than the Haldager Sand's one. In particular, the mean difference for BTC (sat and dry) is 0.8 W/(m*K). The BTD defines smaller differences: 0.3 mm²/s for dry BTD and 0.2 mm²/s for sat BTD. Although, the matrix thermal conductivity of the samples from both formations are similar, with a small difference of 0.2 mm²/s for the MTD.

The sandy mudstones of Gassum, Haldager Sand, Flyvbjerg and Frederikshavn Formations define a wide range of porosities, from a minimum of 4 % to a maximum of 11 %. On the contrary, the thermal properties range is more limited, in spite of the variability of origin, nature and formation of these samples.

The mudstone sample of the Vedsted Formation fits in the range defined by the mudstones of the Fjerritslev Formation. Although, the thermal conductivity shows stronger differences than the thermal diffusivity. MTC and MTD show the greater spread: the MTC of the Vedsted mudstone is almost 1 W/(m*K) lower than the Fjerritslev ones, while its MTD is almost 0.3 mm²/s lower.

As already highlighted by the graphs showed in the previous paragraphs, the limestones of the Chalk units show a strong variability of density, porosity and thermal properties. In particular, the deeper limestones of Lavø-1 have a lower porosity than the shallower one. Both BTC and BTD dry of Lavø-1 are higher than the one of the other two samples, while the saturated limestones do not show such difference. On the contrary, the limestones of Sæby-1 and Gassum-1 show a significantly higher range of MTC and MTD

Table 5.3 Mean values of the formations of effective porosity, bulk thermal conductivity (dry and saturated conditions) and matrix thermal conductivity. The samples' formations are distinguished between their lithological classifications and origin (belonging well). The lithology classes are distinguished by the background colours of the table, which reflect the same colour code used in the previous graphs.

Form.	Well	Depth range [mbgl]	Porosity (Min - Max)	BTC dry [W/(m*K)]			BTC sat [W/(m*K)]			BTD dry [mm ² /s]			BTD sat [mm ² /s]			MTC [W/(m*K)]			MTD [mm ² /s]			n
				Mean	Min Max	A	Mean	Min Max	A	Mean	Min Max	A	Mean	Min Max	A	Mean	Min Max	A	Mean	Min Max	A	
Gassum	Aars-1	3275.7	13%	3.11	2.91 3.55	1.1	4.63	4.52 4.74	1.0	1.60	1.42 1.83	0.8	1.90	1.68 2.17	0.8	6.42	6.04 6.81	1.1	2.91	2.53 3.40	0.8	1
	Farsø-1	2867.8 2885.4	14% (7% - 18%)	2.81	2.26 3.65	1.1	4.51	4.15 4.68	1.0	1.33	0.85 1.81	0.9	1.73	1.39 2.19	0.8	6.13	4.95 6.29	1.0	2.54	2.30 2.92	0.8	3
	Stenlille-1	1543.2 1559.6	25% (23% - 27%)	1.80	1.56 1.96	1.1	3.92	3.63 4.29	1.0	1.05	0.87 1.21	1.1	1.45	1.18 1.66	1.0	7.39	6.76 8.13	1.1	3.32	2.49 3.72	1.1	4
Haldager Sand	Aars-1	2476.8 2484.1	20% (16% - 24%)	2.49	1.96 3.08	1.1	4.65	3.92 5.47	1.1	1.41	1.23 1.65	1.1	1.83	1.57 2.01	1.1	7.78	6.46 9.25	1.1	3.74	2.82 4.48	1.2	4
	Farsø-1	1959.6	12%	3.60	3.53 3.65	1.0	5.18	5.10 5.28	1.0	1.77	1.73 1.81	1.0	2.25	2.11 2.38	0.9	7.03	6.92 7.09	1.0	3.17	3.15 3.20	1.0	1
Gassum	Farsø-1	2883 2896	14% (11% - 15%)	2.57	2.11 2.93	1.1	4.16	3.57 4.99	1.1	1.31	1.11 1.56	1.2	1.53	1.24 1.84	1.0	5.46	4.66 6.87	1.1	2.28	1.83 2.99	1.1	3
Haldager Sand	Farsø-1	1956.2	21%	1.75	1.57 1.92	1.2	3.41	3.05 3.75	1.2	0.99	0.92 1.05	1.1	1.30	1.21 1.38	1.1	5.40	4.70 6.11	1.3	2.45	2.25 2.65	1.2	1
Gassum	Aars-1	3272.3	4%	2.88	2.07 3.07	1.1	2.98	2.45 3.50	1.4	1.35	1.25 1.44	1.1	1.49			3.43	3.07 3.78	1.2	1.62	1.54 1.70	1.1	1
	Farsø-1	2888.9 2896.7	6% (4% - 9%)	2.60	2.23 3.06	1.0	3.13	3.57 3.54	1.0	1.18	1.11 1.27		1.36	1.22 1.65	0.9	3.44	2.73 3.86	1.0	1.61	1.43 1.84	0.9	4
Haldager sand	Farsø-1	1964.6	7%	2.87	2.55 3.29	1.1	3.65	3.14 4.34	1.2	1.41	1.35 1.47	1.1	1.54	1.47 1.61	1.1	4.12	3.60 4.80	1.1	1.88	1.79 1.98	1.1	1
Flyvbjerg	Aars-1	2454.3 2458.2	9% (8.5% - 9%)	2.32	2.13 2.58	1.1	3.12	2.80 3.39	1.1	1.11	0.92 1.28	1.1	1.08	0.85 1.29	1.0	3.64	3.23 3.98	1.1	1.57	1.29 1.80	1.1	2
Frederikshavn	Aars-1	2372.7	11%	2.41	2.38 2.43	1.0	3.30	3.18 3.38	1.1	1.12	1.11 1.13	1.0	1.27	1.26 1.28	1.0	4.09	4.03 4.14	1.0	1.73	1.71 1.74	1.0	1

Table 5.3 (Continued).

Form.	Well	Depth range [mbgl]	Porosity (Min - Max)	BTC dry [W/(m*K)]			BTC sat [W/(m*K)]			BTD dry [mm ² /s]			BTD sat [mm ² /s]			MTC [W/(m*K)]			MTD [mm ² /s]			n
				Mean	Min Max	A	Mean	Min Max	A	Mean	Min Max	A	Mean	Min Max	A	Mean	Min Max	A	Mean	Min Max	A	
<i>Fjerritslev</i>	<i>Farsø-1</i>	1978.6 1981.9	9% (4% - 11%)	2.18	1.49 2.75	1.6	2.81	1.80 3.58	1.6	1.02	0.99 1.06	1.0	1.15	1.04 1.24	1.0	3.23	1.88 4.36	1.6	1.38	1.13 1.61	1.1	4
<i>Vedsted</i>	<i>Aars-1</i>	1936.1	4%	1.88	1.71 2.06	1.2	2.14	1.94 2.34	1.2	0.96	0.95 0.97	1.0	1.00	0.99 1.01	1.0	2.26	2.04 2.48	1.2	1.11	1.09 1.12	1.0	1
<i>Chalk units</i>	<i>Saeby-1</i>	405.9	28%	1.25	1.23 1.27	1.0	2.59	2.51 2.66	1.1	0.64	0.62 0.68	1.1	1.02	1.00 1.05	1.1	5.32	5.23 5.40	1.0	2.10	1.98 2.21	1.1	1
	<i>Gassum-1</i>	264.6	32%	1.09	1.08 1.09	1.0	2.83	2.66 3.01	1.1	0.57	0.57 0.58	1.0	0.87	0.86 0.88	1.0	6.23	6.00 6.46	1.1	2.21	2.17 2.25	1.0	1
	<i>Lavø-1</i>	1550.4 1791.1 1917.3	6% (4% - 9%)	2.24	1.96 2.68	1.1	2.71	2.32 3.00	1.1	0.98	0.74 1.14	1.0	1.06	0.83 1.19	1.0	3.04	2.53 3.38	1.1	1.24	1.01 1.41	1.0	3

6. Discussions and conclusions

The data acquired in this work represent the result of a new study on thermophysical properties of the sedimentary rocks of the Danish Basin. The information obtained permit to analyse different fundamental aspects:

- The applicability of the geometric mean model to thermal diffusivity and the behaviour of this thermal property within an air-saturated rock;
- The use of matrix thermal properties and porosity to obtain information related to the composition and nature of the rock, in the absence of a mineralogical analysis ;
- An estimate of the variability of thermal properties within the Mesozoic sedimentary units of the Danish Basin, also supported by the data available in the literature, and in various saturation conditions.

The samples analysed in this study were selected from the GEUS institute basing on the availability of other information such as temperature at depth or other geophysical data. The data and samples here investigated are clearly not sufficient for a complete characterization of the sedimentary bodies identified in the wells. Nonetheless, these results will be integrated to further analyses of the GEOTHERM project and used for this purpose.

6.1. Bulk thermal diffusivity and geometric mean model

The geometric mean model represent a simple yet reliable way to calculate the bulk thermal conductivity of sedimentary rocks, when the mineralogical composition and the porosity are known or assumed, as already demonstrated by several authors (e.g. Clauser, 2006; Fuchs et al., 2013; Robertson, 1988). The goodness of fit between the geometric mean model and the measurements of thermal conductivity obtained with the TCS is represented in Fig. 5.7a. On the contrary, the measurements of thermal diffusivity show an opposite trend to what was initially calculated with the “classic” geometric mean model (substituting α to λ in Eq. (4.12)). In fact, given the high value of thermal diffusivity of air (19 mm²/s), a strong increasing trend of bulk thermal diffusivity with porosity was expected for dry rocks, as shown by the green curves in Fig. 6.1.

However, the measurements show a decreasing trend with increasing porosity (Fig. 5.7b). This behaviour fits with the geometric mean model corrected with the f factor, shown in Eq. (4.14) and represented in Fig. 5.7b and Fig. 6.1 (orange curves). Goto & Matsubayashi (2009) developed this correction for calculations of thermal diffusivity of sediments saturated with marine water. The effect of the f factor for pure water saturation is relatively small (Fig. 6.2), whereas it is significantly greater for air saturation, as shown in Fig. 6.1. The good fitting between corrected geometric mean model and measured values in Fig. 5.7b and Fig. 5.8b confirms the applicability of the correction. This is also supported by the small differences between the MTD values calculated from dry TD and sat TD measurements, using the corrected geometric mean model (Fig. 6.3).

A possible explanation of what was observed in this work is here proposed. The β factor is the ratio between the specific heat capacities of the saturating fluid and the rock matrix. Thus, this factor quantifies the contribution of a saturating fluid with respect to the matrix of a rock in retaining thermal energy. The f factor relates this ratio to pore (ϕ) volume and solidity ($1 - \phi$) of the rock.

The elevated thermal diffusivity of air is due to a particularly small specific heat capacity, which is four orders of magnitude smaller than that of a rock matrix. In fact, this means that

the air in the pores tends to diffuse heat immediately towards the matrix, which retains the majority of the thermal energy. To a first approximation, the air in the pores would act as a “barrier”, also due to its low thermal conductivity, leading to a concentration of the heat flow in the rock matrix. Therefore, the insulating property of air in the pores would reduce its contribution to the overall diffusion of heat in the rock by a quantity expressed by the f factor.

In conclusion, the correction applied is considered reliable and has been applied in this work for all the values of TD calculated or converted using geometric mean model.

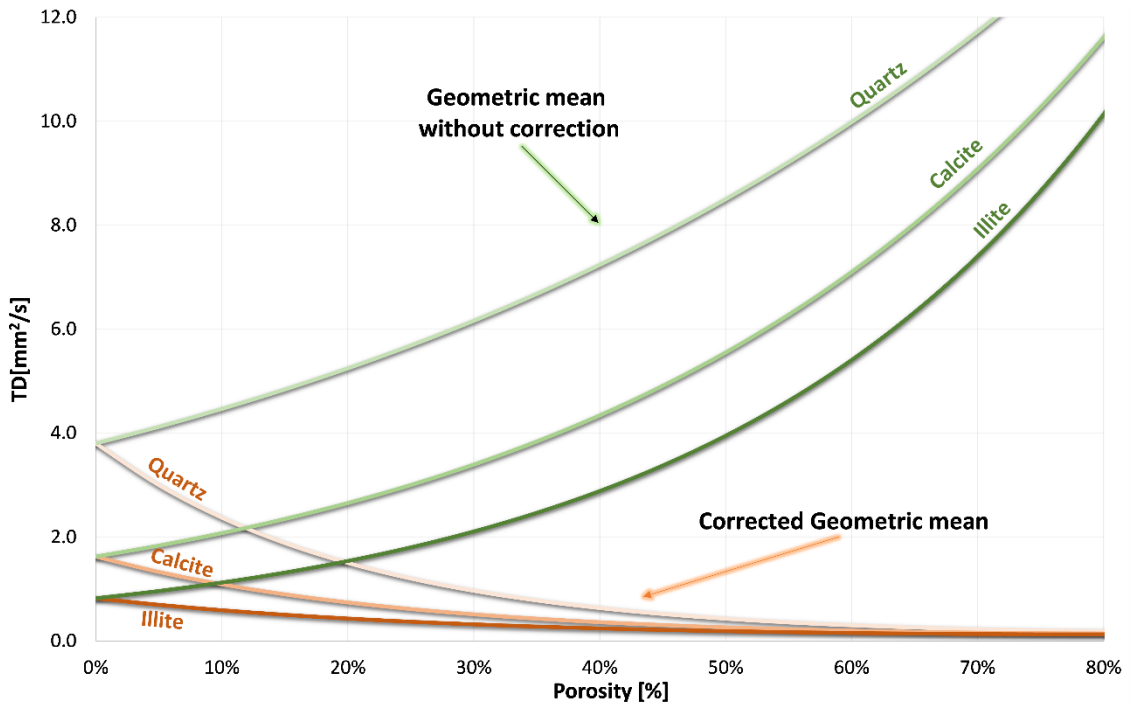


Figure 6.2: Calculation of bulk thermal diffusivity in air saturation conditions, using geometric mean with and without correction from Goto & Matsubayashi (2009). The matrix values considered are listed in Tab. 4.3.

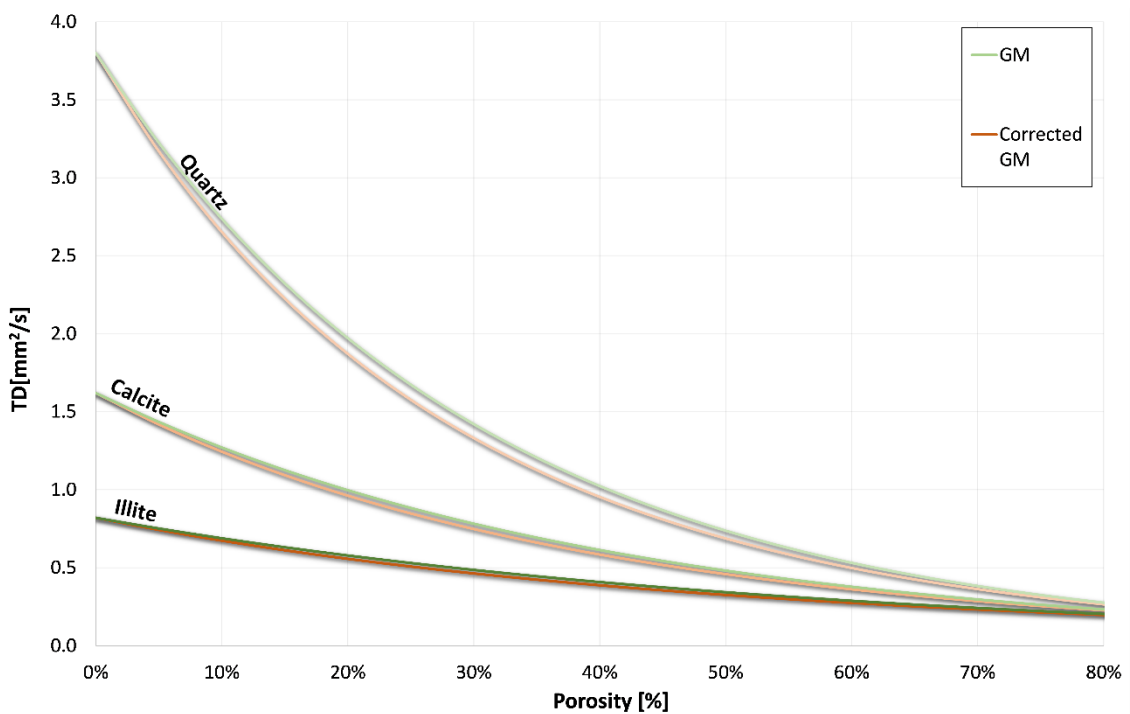


Figure 6.2: Calculation of bulk thermal diffusivity in pure water saturation conditions, using geometric mean with and without correction from Goto & Matsubayashi (2009). The matrix values considered are listed in Tab. 4.3.

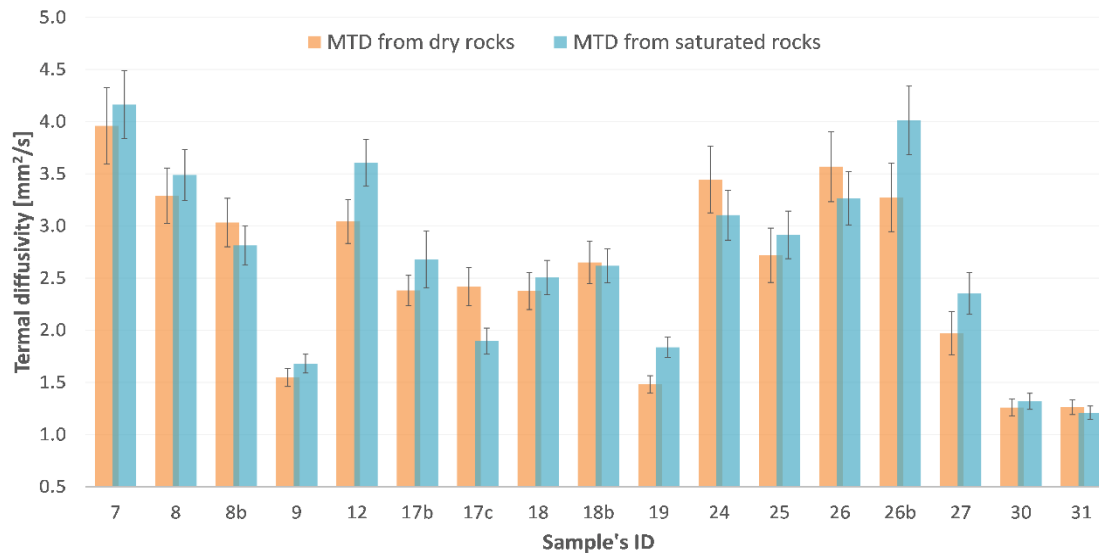


Figure 6.3: comparison between MTD values obtained from direct measures of dry samples (pink bars) and saturated samples (blue bars).

6.2. Matrix thermal properties as indicators of the composition of the rocks

The application of the geometric mean model to the bulk thermal properties using Eq. (4.13) for λ_m and Eq. (4.16) transposed to α_m , allowed to calculate the contribution of the sole rock matrix. Therefore, the contribution of the overall mineral composition is estimated, considering negligible the effect of isolated pores. In addition to the matrix thermal conductivity and diffusivity, the representation proposed in Fig. 5.9 and Fig. 6.4 takes into account the effective porosity distributions and its dependency from the lithology. In Fig. 6.4 the clusters identified by the measurements are highlighted with the specific colours of the relative lithologies.

From these graphs, it is possible to investigate qualitatively the mineralogical composition of the rock samples analysed. Therefore, in case of lack of a specific mineralogical analysis, this representation can be used for:

- The evaluation of the relative content in quartz or clay minerals between different samples;
- A qualitative estimate of the content of a specific mineral in a rock whose major composition is known (e.g. the evaluation of clay content in a clean sandstone);
- Eventually, a comparative method to investigate the lithology of a sample.

Consequently, this method allowed to make several observations, described below.

The anomalous values of the highly porous limestones (samples 27 and 28) plot here as dots clearly distant from the calcite line. This configuration suggests a consistent quartz content in the matrix, which determines the shift of TC and TD from the calcite's line towards that of quartz. On the contrary, the three remaining samples of limestones plot slightly below the calcite line, suggesting the presence of a small, yet significant, quantity of clay.

Moreover, it is possible to notice the presence of different sandstones that plot above the mean TC and TD of quartz. Although they appear as clean sandstones from the visual analysis of the samples, the graphs show that they are totally composed of quartz crystals. For these samples, a further evaluation is required to clarify this effect.

Finally, one sandstone, the 17b, plots outside the relative cluster. This sample clearly shows a coarse-grained sand composition. Nonetheless, its relatively small effective porosity and thermal properties suggest the presence of clay minerals in the interstices of the rock. Unfortunately, the scarce reliability of the matrix density values (as specified in 6.3) does not permit to make further evaluations on the composition of the matrix of the rocks.

It is possible to conclude that the investigated petrophysical properties and the method here proposed can be used to obtain important information on rock composition and nature, which can be useful when a mineralogical analysis is missing, as in the case of this work.

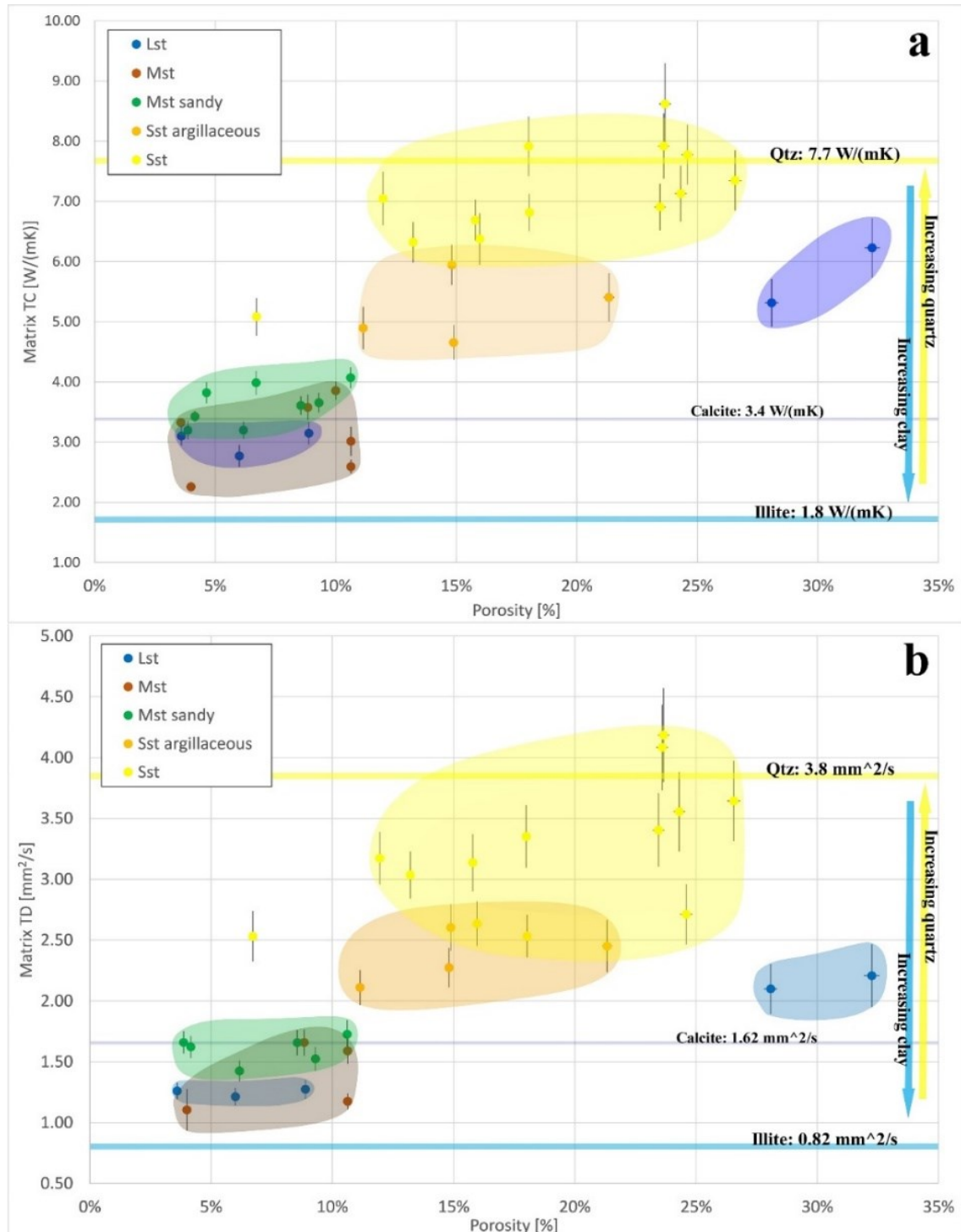


Figure 6.4: Matrix thermal conductivity (a) and diffusivity (b) plotted against effective porosity of the rocks. Tabulated values of TC and TD of quartz, calcite and illite minerals plot in the graph as horizontal lines and act as reference values. The “Increasing quartz” and “Increasing clay” arrows show the interpretation of this graph (details in the text). The coloured areas have the only purpose to highlight the clusters of data for each lithology.

6.3. Variability of the investigated properties and comparison with literature

The distributions of bulk thermal conductivity and bulk thermal diffusivity defined by the rock samples measured (Fig. 5.3) clearly show that each lithological class is characterized by specific ranges of values. In addition, the information on the anisotropy of the rock samples derived from thermal conductivity (Fig. 5.6) clearly shows that the sandy samples are generally more isotropic than muddy ones, as expected. However, the thermal diffusivity does not confirm this behaviour.

These characteristic distributions are also identified for effective porosity and, to a lesser degree, for bulk densities. On the contrary, the matrix density does not follow the same trend. These values may be affected by error, due to the measurement method adopted. In fact, the Archimedes method (4.2.3) permits to measure only the effective porosity, thus the effect of the isolated pores on the matrix density measurements are ignored. This could lead to a measurement error, which is bigger for low permeability rocks (such as mudstones and sandy mudstones). However, from a comparison of matrix SHC with dry SHC (Fig. 5.5), it is noted that the difference is small in almost all cases. This is in accordance with the Kopp's law (Clauser, 2006; Robertson, 1988; Woodside & Messmer, 1961a) where the small contribution of air is added to the matrix SHC following Eq. (6.1):

$$(\rho_b c_b) = (1 - \varphi)(\rho_m c_m) + \varphi(\rho_p c_p) \quad (6.1)$$

where b , m and p subscripts define bulk, matrix and fluid, respectively. Therefore, this suggests that the error associated to matrix density does not influence significantly the specific heat capacity values.

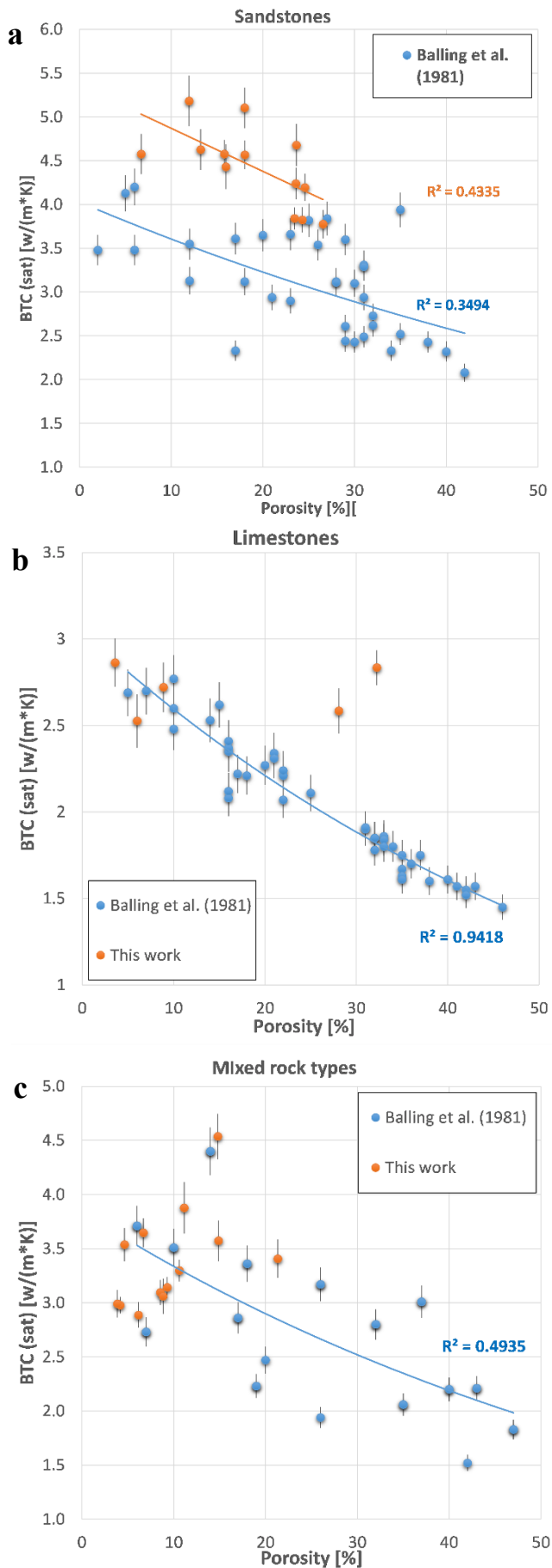
Furthermore, contrarily to thermal properties, porosity and bulk density, the SHCs do not identify clusters of characteristic values.

6.3.1. Variability within the Danish Basin

It is possible to compare the thermal conductivity from this work with those already published in literature by Balling et al. (1981) and Balling et al. (1992). These authors carried out several measures of BTC and effective porosity of the rocks of the Danish Basin, considering the entire stratigraphic sequence (from Zechstein to Upper Cretaceous – Tertiary units). Thus, they provide an overview of the overall stratigraphic sequence. The samples are analysed with the line source method, in water saturated conditions. This transient state technique works at ambient conditions and provides data that are comparable to the values from the Optical Scanning (for further details about this technique see Balling et al. (1981)). The porosity was determined using the Archimedes' method as well.

From a set of 178 samples of the sedimentary units in the Danish Basin, the mean value is 2.49 W/(m*K), with 68 % of the samples lying between 1.5 and 3.0 W/(m*K). As pointed out by the authors, the lithology types investigated by this work cover 95 % of the Danish post-Permian sediments. The rock samples were distinguished according to a lithological classification similar to that carried out this work:

- Limestones
- Sandstones
- “Mixed” rock types, which includes “Siltstones, fine grained sandstones, clayey sandstones and sandy claystones”
- Claystones



The mean conductivity of the rock types ranges from about 2.0 W/(m*K) for limestones to 3.1 W/(m*K) for sandstones, while the fine-grained and "mixed" rock types have a mean value of 2.6 W/(m*K). Fig. 6.5a,b,c shows the trend of the sat BTC of the data analysed in this work (orange dots) and the data provided by Balling et al. (1981; blue dots). Based on the lithological classification, the comparison is possible for sandstones (Fig. 6.5a), limestones (Fig. 6.5b) and the "mixed" groups (compared to Argillaceous sandstones and Sandy mudstones together; Fig. 6.5c).

Generally, it is possible to observe that sample properties of this work plot in the higher BTC – lower porosity interval, relatively to the values from literature. The reason for this is that the majority of the samples studied in this work belong to depths greater than 1500 m. In fact, the effective porosity in the Danish Basin tends to decrease with depth, while the bulk thermal conductivity has a general increasing trend (Balling et al., 1981).

From the comparison of the sandstones in Fig. 6.5a, it is possible to see that the rock samples of this work present higher values of sat TC. On average, the difference between these two dataset is about 1 W/(m*K). This may be due to a difference between the analysed sandstones and those analysed by Balling et al. Nonetheless, mineralogical analyses are needed to confirm this hypothesis and explain the consistent difference.

The comparison with limestones in Fig. 6.5b shows that three of the five samples fit well in the cluster of data from literature. On the contrary, the two samples of limestones with higher porosity plot markedly outside the cluster. A possible explanation of this trend is reported in paragraph 6.2.

Figure 6.5: Bulk thermal conductivity vs effective porosity of samples from this work (orange dots) and samples from Balling et al. (1981). Further details in the text.

The argillaceous sandstones and the sandy mudstones (Fig. 6.5c) plot coherently with the mixed rock types from literature. In both Fig. 6.5b and Fig. 6.5c, the trendlines of the data of this work are not plotted, due to the scarce number of samples, which would give a non-reliable regression.

Balling et al. (1992), instead, provide an evaluation of the mean bulk thermal conductivity of rocks at different depth intervals. They measured the BTC at saturated conditions on 21 core sections, collected from Aars-1, Farsø-1, Saeby-1, Gassum-1 and Lavø-1. The data provided in this work are direct measurements using the line source (indicated as ' λ_{perp} ' and ' $\lambda_{||}$ ') or mean values calculated with the geometric mean model (indicated as ' λ ').

Tab. 6.1 and Tab. 6.2 show the comparison between data from literature (upper numbers) and data of this work (lower numbers). The results of this thesis have been "adapted" to those tabulated, basing on the depth range investigated by Balling et al. (1992). In fact, the BTCs provided in the literature are compared with averaged BTCs from samples with a corresponding source depth. In addition, tabulated ' λ ' values are compared with BTC obtained averaging λ_{perp} and $\lambda_{||}$. For the Chalk units additional data from Balling et al. (1981) were available (Tab. 6.2).

In some cases the two dataset are significantly different, as for the Flyvbjerg Formations in Aars-1 and Fjerritslev Formation in Farsø-1. These differences may be due to the different rock types considered in the two studies.

Table 6.1: Bulk thermal conductivity vs effective porosity of samples from this work (orange dots) and samples from Balling et al. (1981). Further details in the text.

<i>Aars-1</i>				
<i>Formation</i>	<i>Depth [mbKB]</i>	λ_{perp}	$\lambda_{ }$	λ
<i>Vedsted</i>	1932 – 1938.2	1.54 ±0.04	2.4 ±0.03	
	1936.05	1.94 ±0.10	2.34 ±0.05	
<i>Frederikshavn</i>	2370 – 2377	2.7 ±0.06	3.14 ±0.02	
	2372.71	3.18 ±0.10	3.36 ±0.1	
<i>Flyvbjerg</i>	2453 – 2462	1.96 ±0.12	2.76 ±0.15	
	2454.3 – 2458.2	2.93 ±0.13	3.25 ±0.09	
<i>Haldager Sand</i>	2477.4 – 2485.7			5.16 ±0.22
	2476.8 – 2484.1			4.65 ±0.20
<i>Gassum</i>	3270.8 – 3277.5			4.15 ±0.32
	3272.3 – 3275.7			4.63 ±0.23
<i>Farsø-1</i>				
<i>Haldager Sand</i>	1958.2-1966.7			4.83 ±0.3
	1956.2 - 1964.6			4.16 ±0.20
<i>Fjerritslev</i>	1975.2-1981			4.09 ±0.43
	1978.6-1981.9			2.81 ±0.13
<i>Gassum</i>	2885.4-2903.4	2.89 ±0.3	3.4 ±0.13	
	2886 - 2897	3.63 ±0.19	3.50 ±0.18	

Table 6.2: Comparison of bulk thermal diffusivity (saturated conditions) with data published by Balling et al. (1981) and Balling et al. (1992). Further information in the text.

<i>Formation</i>	<i>Well</i>	<i>Depth [mbKB]</i>	λ_{perp}	$\lambda_{ }$	λ	
<i>Chalk units</i>	<i>Sæby-1</i>	405.87	2.51 ±0.13	2.66 ±0.13		<i>Balling et al. (1992)</i>
		390 – 408	1.95 ±0.03	1.98 ±0.02		
	<i>Gassum-1</i>	209.1			1.84	<i>Balling et al. (1981)</i>
		264.56			2.83 ±0.10	
	<i>Lavø-1</i>	1521.7			2.6	
		1550.35			2.53 ±0.15	
	<i>Lavø-1</i>	1762.7			2.7	
		1791.14			2.72 ±0.14	
	<i>Lavø-1</i>	1918.7			2.73	
		1917.26			2.86 ±0.14	

It can be concluded that the variability of these bulk properties varies considerably even within the same depth range, as well as with composition. Similarly, lateral variability is noted within the same formation and lithology, as shown by the representation of [Tab. 5.3](#). The influencing factors of these thermal properties are various. Nonetheless, when considering the same P–T conditions and the same saturating fluid, mineralogical composition and porosity represent the fundamental elements that influence these variations.

6.3.2. Variability with saturating fluid

The effect of the different pore fluids on the bulk thermal properties of the same rock can be shortly analysed by comparing the differences between dry and saturated BTC and BTD, as shown in [Fig. 6.6a,b,c](#). This is in fact a representation of the difference between [Fig. 5.8](#) and [Fig. 5.7](#). A representation of this variability is also visible by comparing the histograms presented in [Fig. 5.3](#). In general, as expected, the greater the pore volume of a rock, the greater the variation of BTC and BTD with different fluids in the pores. For BTC, the trend is clear, whereas for BTD, the values are more scattered. The combination of both BTC and BTD on the rocks' thermal property can be estimated from [Fig. 6.6c](#), where the difference between saturated and dry SHC is plotted against the porosity of the sample.

It can be deduced that in a porous rock, the effect of the variation of the saturating fluid on BTC increases with effective porosity according to the trend shown in [Fig. 6.6a](#). In particular, the registered difference between the bulk thermal conductivities of rocks saturated in pure water and dry rocks grows of 0.1 W/(m*K) each 1 % of porosity, on average. In turn, the BTD ([Fig. 6.6b](#)) shows an analogous trend, which is however more scattered. Therefore, its dependence from the saturating fluid appears less predictable. Further measurements are certainly required to verify this phenomenon.

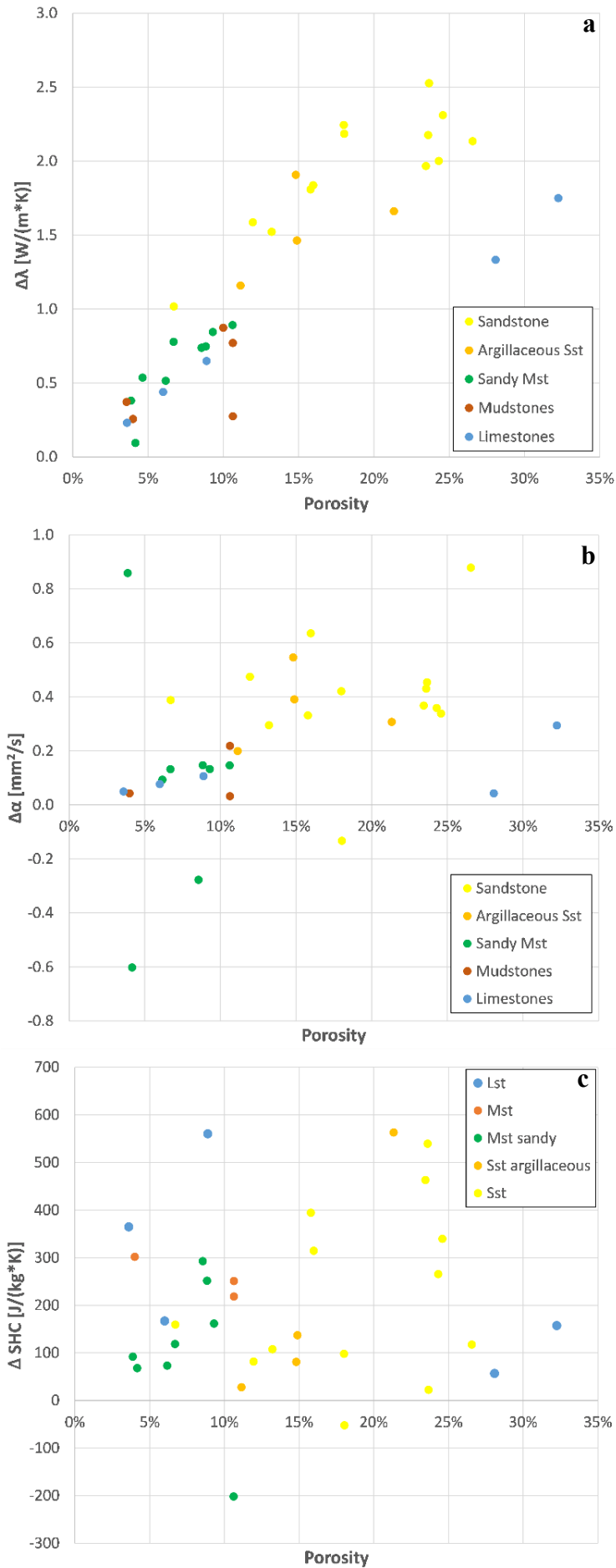


Figure 6.6 Difference between saturated and dry values of BTC (a), BTD (b) and bulk SHC (c) plotted against effective porosity of the relative rock sample.

6.4. Summary of the main results

The Danish Basin presents a series of formations and sedimentary units that were targeted as potential exploitable geothermal systems. The GEOTHERM project aims to study this by defining the geothermal potential at a national scale. For this purpose, some of the main geological elements to define are the relevant petrophysical properties of the rocks (thermal conductivity, diffusivity, and heat absorption capacity). Therefore, the present study dealt with analysing these properties and investigating their variability, taking into account the factors that mainly influence them. In summary, the herein this work presents:

- New data on thermal conductivity and thermal diffusivity at ambient conditions of rocks in the Danish Basin. These data intend to integrate and improve the dataset already published in the literature by Balling et al. (1981) and Balling et al. (1992). In particular, the majority of the analysed rocks were taken at depths between 1500m and 3000m, where favourable conditions for geothermal applications are present.
- Direct measurements of bulk and matrix thermal diffusivity, by means of the Thermal Conductivity Scanner.
- Information that will be integrated into further analyses and will be used in the following Work Packages of the GEOTHERM project.

From the analysis of the lab results and the processing carried out subsequently, it was possible to make important observations, which are here reported:

- The geometric mean model used for thermal conductivity is not sufficient to calculate the expected bulk thermal diffusivity of a rock sample. This is particularly evident for dry rocks, where the thermal properties of air in the pores seems to reduce the contribution in heat diffusion rather than increasing it, as it was expected. Goto & Matsubayashi (2009) apply a correction that takes into account the differences between the specific heat capacities of the phases which are in contact in a rock sample. Although it was applied on marine water saturated samples, its effectiveness is here demonstrated also in the case of air and pure water saturation. The here proposed cause of the behaviour of the dry bulk thermal diffusivity is ascribed to the insulating property of air, which tend to reduces significantly the diffusion of heat in the pores.
- The lithologies recognized from the visual analysis of the samples define clear ranges of the petrophysical properties, as expected. These ranges are coherent with the data from literature (Balling et al., 1981), which are representative of the general distribution of saturated bulk thermal conductivity and effective porosity in the entire basin. Some differences have been found for limestones and sandstones. These differences may be due to a different mineralogical composition between the samples investigated here and those analysed by Balling et al. However, further mineralogical information would be needed to confirm this explanation for the sandstones samples.
- The presence of different saturating fluids can significantly affect the bulk thermal properties of a rock. In case of thermal conductivity, a linear increase of the difference between pure water and air saturation was observed. On the contrary, the thermal diffusivity shows an analogous behaviour but more dispersed data points.
- The geometric mean model is a useful tool to evaluate the matrix thermal properties of the rocks from the bulk properties of the rocks and that of the saturating fluids. By comparing MTC or MTD with effective porosity of each sample, the different rocks plot in specific clusters. These clusters are related to the overall mineral composition and lithology of the samples. From a comparison of these data with the tabulated

thermal properties of minerals it is possible to make qualitative estimates on the general mineralogical composition of a rock.

Appendix A

Porosity and density measurements

ID	Major lithological composition	Bulk density			Matrix density
		Porosity	Dry [kg/m ³]	Sat [kg/m ³]	
1	Mst	25%	2000	2180	2680
2	Mst	4%	2400	2440	2500
3	Mst sandy	11%	2170	2240	2420
4	Mst sandy	9%	2440	2510	2700
5	Mst sandy	9%	2320	2410	2540
6	Sst	24%	2010	2250	2640
7	Sst	24%	2010	2240	2630
8	Sst	18%	2160	2340	2640
8b	Sst	16%	2210	2370	2620
9	Mst sandy	4%	2540	2570	2650
10	Sst	13%	2300	2430	2650
11	Sst argillaceous	21%	2130	2340	2700
12	Sst	12%	2340	2460	2650
13	Mst sandy	7%	2490	2550	2670
14	Mst	10%	2480	2550	2760
15A	Mst	11%	2480	2510	2580
15B	Mst	11%	3420	3490	3820
16	Mst	4%	2430	2470	2520
17	Sst	18%	2160	2340	2640
17b	Sst	7%	2430	2500	2610
17c	Sst argillaceous	15%	2270	2370	2660
17d	Mst sandy				
18	Sst argillaceous	15%	2280	2380	2680
18b	Sst	16%	2230	2340	2650
18c	Mst	9%	2480	2570	2720
18d	Mst sandy				
19	Mst sandy	6%	2500	2560	2660
19b	Mst sandy	4%	2620	2660	2720
20	Sst argillaceous	11%	2390	2500	2690
20b	Mst sandy	5%	2600	2630	2730
21	Clst				
22	Mst sandy	21%	2240	2390	2840
23	Clst	10%	2060	2160	2280
23c	Clst				
24	Sst	23%	2030	2260	2650
25	Sst	25%	2000	2250	2650
26	Sst	24%	1970	2210	2600
26b	Sst	27%	1950	2220	2650
27	Lst	28%	1930	2160	2680
28	Lst	32%	1810	2030	2670
29	Lst	6%	2450	2520	2620
30	Lst	9%	2470	2530	2710
31	Lst	4%	2540	2570	2640
Relative uncertainty:			1%		

Appendix A: Effective porosity and density measurements.

Red value: outlier.

Yellow values: values of effective porosity assumed basing on lithology and depth, due to errors during porosity measures.

Appendix B

Thermal conductivity and thermal diffusivity measurements

ID	Thermal Conductivity [W/(m*K)]				Thermal Diffusivity [mm ² /s]				
	Dry Conditions		Saturated conditions		Dry Conditions		Saturated conditions		
	$\lambda_{perp} \pm$	$\lambda_{ } \pm$	$\lambda_{ 2} \pm$	$\lambda_{perp} \pm$	$\lambda_{ } \pm$	$\lambda_{ 2} \pm$	$\alpha_{perp} \pm$	$\alpha_{ } \pm$	$\alpha_{ 2} \pm$
2	1.71	0.09	2.06	1.94	0.10	2.34	0.95	0.05	1.01
3	2.43	0.12	2.38	3.18	0.10	3.34	1.11	0.06	1.28
4	2.27	0.11	2.38	3.05	0.15	3.21	1.11	0.06	1.29
5	2.13	0.09	2.58	2.80	0.12	3.39	1.09	0.05	1.97
6	2.02	0.08	2.28	4.51	0.23	4.85	1.23	0.06	1.94
7	2.04	0.10	2.19	3.92	0.20	4.64	1.24	0.06	2.01
8	2.62	0.12	3.08	4.73	0.24	5.47	1.47	0.07	1.80
8b	2.76	0.12	2.69	4.57	0.22	4.44	1.39	0.07	1.96
9	2.70	0.11	3.07	2.45	0.13	3.50	1.25	0.06	2.01
10	2.91	0.09	3.35	4.52	0.23	4.62	1.83	0.12	1.84
11	1.57	0.08	1.92	3.06	0.17	3.75	0.92	0.05	1.38
12	3.65	0.16	3.61	5.10	0.26	5.28	1.73	0.09	2.11
13	2.55	0.13	3.29	3.14	0.16	4.34	1.35	0.07	1.61
14	1.60	0.08	2.60	1.80	0.09	3.10	0.99	0.05	1.11
15A	1.49	0.07	2.75	2.09	0.11	3.42	0.99	0.05	1.24
15B	1.49	0.07	2.44	2.09	0.11	3.42	0.99	0.05	1.24
16	2.26	0.07	2.51	4.68	0.23	4.46	0.85	0.04	1.45
17	2.38	0.12	3.47	4.10	0.13	4.64	1.34	0.07	2.19
17b	2.38	0.12	2.93	3.57	0.19	4.99	1.11	0.06	1.62
17c	2.11	0.09	2.93	4.56	0.24	4.15	1.50	0.07	1.61
18	2.53	0.08	2.50	4.56	0.24	4.15	1.50	0.07	1.72
18b	2.23	0.11	2.39	2.96	0.16	3.16	1.11	0.06	1.25
18c	2.66	0.13	2.89	3.13	0.16	3.27	1.23	0.06	1.65
19	2.76	0.14	2.67	3.94	0.21	3.81	1.23	0.06	1.41
19b	2.76	0.14	2.67	3.94	0.21	3.81	1.23	0.06	1.41
20	1.87	0.09	1.88	3.72	0.19	3.97	1.12	0.06	1.44
20b	1.80	0.09	1.96	4.29	0.21	4.29	0.87	0.04	1.18
24	1.79	0.09	1.86	3.63	0.18	4.02	1.14	0.06	1.45
25	1.56	0.06	1.69	3.67	0.18	3.76	0.92	0.05	1.66
26	1.23	0.06	1.27	2.51	0.13	2.66	0.62	0.03	1.00
26b	1.09	0.05	1.08	2.66	0.13	3.01	0.57	0.03	0.88
27	1.92	0.10	2.26	2.32	0.12	2.73	0.93	0.05	1.00
28	2.04	0.10	2.18	2.61	0.14	2.90	0.97	0.05	1.07
29	2.59	0.13	2.68	2.72	0.14	3.00	1.07	0.05	1.11
30									
31									

Appendix B: Thermal conductivity and thermal diffusivity measurements. Blue values are converted using geometric mean model. Purple values are converted from iso-octane-saturated conditions to water-saturated using geometric mean model.

References

- Balling, N., Kristiansen, J.I., Breiner, N., Poulsen, K.D., Rasmussen, R. and Saxov, S., 1981. Geothermal measurements and subsurface temperature modelling in Denmark. *GeoSkifter* 16, Aarhus University: 172.
- Balling N., Priisholm S., Christensen O. W., 1988. Denmark. In: Haenel R., Staroste E. (Eds.), *Atlas of Geothermal resources in the European Community, Austria, and Switzerland*. Commission of the European Communities, Directorate-General for Science, Research and Development, Geothermal Energy Research: 74.
- Balling, N., 1992. Denmark. In: Hurtig, E., Cermak, V., Haenel, R. and Zui V. (Eds), *Geothermal Atlas of Europe, Explanatory Text*, 25-28. Hermann Haack Verlagsgesellschaft m.b.H., Gotha: 156.
- Balling N., Nielsen S. B., Christiansen H. S., Christensen L. D., Poulsen, S. 1992. The subsurface thermal regime and temperature of geothermal reservoirs in Denmark. Synthesis report to Commission of the European Communities. Contract EN3G-0029-DK. Department of Earth Sciences, Geophysical Laboratory, University of Aarhus, Denmark.
- Balling N., Hvid J.M., Mahler A., Møller J.J., Mathiesen A., Bidstrup T., Nielsen L. H. 2002. Denmark. In Hurter, S., Haenel, R. (Eds), *Atlas of geothermal resources in Europe*. Luxemburg: European Commission Office for Official Publications of the European Communities, 93 p.
- Blumm J., & Lindemann A., 2003. Characterization of the thermophysical properties of molten polymers and liquids using the flash technique. *High Temp. High Press*, 35(36): 627–632.
- Clauser C., 2006. Geothermal energy. In: K. Heinloth (Ed), *Landolt-Börnstein, group VIII: Advanced Materials and Technologies, Vol. 3: Energy Technologies, Subvol. C: Renewable Energies*. Springer Verlag, Heidelberg-Berlin, pp. 493–604.
- Clauser C., 2009. Heat transport processes in the Earth's crust. *Surveys in Geophysics*, 30(3): 163–191.
- Clauser C., 2011. Thermal storage and transport properties of rocks, II: thermal conductivity and diffusivity. In Harsh Gupta (Ed), *Encyclopedia of solid earth geophysics*: pp. 1431–1448.
- Danish Energy Agency, 2014. Energy scenarios for 2020, 2035 and 2050. https://ens.dk/sites/ens.dk/files/Analyser/energiscenarier_uk.pdf. March 2014.
- EGEC – European Geothermal Energy Council, 2017. Geothermal market report, Key Findings 2016, 6th edition, Brussels, 17p. EGEC website: www.egec.org.
- Eugeno-S Working Group, 1988. Crustal structure and tectonic evolution European of the transition between the Baltic Shield and the North German Caledonides (the EUGENO-S Project). *Tectonophysics*, 150(3): 253–348.

- Fuchs S., & Förster A., 2010. Rock thermal conductivity of Mesozoic geothermal aquifers in the Northeast German Basin. *Chemie Der Erde-Geochemistry*, 70: 13–22.
- Fuchs S., Schütz F., Förster H.-J., Förster A., 2013. Evaluation of common mixing models for calculating bulk thermal conductivity of sedimentary rocks: correction charts and new conversion equations. *Geothermics*, 47: 40–52.
- Fuchs S., Balling N., & Förster A., 2015. Calculation of thermal conductivity, thermal diffusivity and specific heat capacity of sedimentary rocks using petrophysical well logs. *Geophysical Supplements to the Monthly Notices of the Royal Astronomical Society*, 203(3): 1977–2000.
- GEUS, 1951. Gassum-1, Gassum-1, Final report (Report No. 7408). Copenhagen, Denmark.
- GEUS, 1979. Aars-1A. Geothermal exploration well. Completion report. Michelsen O. (Ed). Copenhagen, Denmark.
- GEUS, 1981. Stenlille-1, Stenlille-1, Geological well completion report (Report No. 7887). Christensen O. W. (Ed). Copenhagen, Denmark.
- GEUS, 1982. Farsø-1 Completion report. Søren P., Byrne L. (Eds). Copenhagen, Denmark.
- GEUS, 1985. Sæby-1, Final well report – Geology and shows (Report No. 10789). Exiog, England.
- GEUS, 1995. Lavø-1, Lavø-1, Completion report (Report No. 8523). Randers, Denmark.
- Goto S., Matsubayashi O., 2009. Relations between the thermal properties and porosity of sediments in the eastern flank of the Juan de Fuca Ridge. *Earth, planets and space*, 61(7): 863–870.
- Mahler A., Magtengaard J., 2010. Country update report for Denmark. In DONG Energy, World Geothermal Congress, Bali, Indonesia, pp. 25–29.
- Mathiesen A., Nielsen L. H., Bidstrup T., 2010. Identifying potential geothermal reservoirs in Denmark. *Geological Survey of Denmark and Greenland Bulletin*, 20(1): 19–22.
- Michelsen, O., Nielsen, L.H., 1993. Structural development of the Fennoscandian Border Zone, offshore Denmark. *Marine and Petroleum Geology* 10, 124–134.
- Michelsen, O., Nielsen L. H., Johannessen P. N., Andsbjerg J., Surlyk F., 2003. Jurassic lithostratigraphy and stratigraphic development onshore and offshore Denmark. *Geological Survey of Denmark and Greenland Bulletin* 1, 145–216.
- Mogesen T. E., Korstgård J. A., 2003. Triassic and Jurassic transtension along part of the Sorgenfrei-Tornquist Zone, in the Danish Kattégat: In: Ineson, JR & Surlyk, F. (Eds): *The Jurassic of Denmark and Greenland. Review of Survey Activities*, 1: 439–458.
- Nielsen L.H., 2003. Late Triassic – Jurassic development of the Danish Basin and the Fennoscandian Border Zone, southern Scandinavia. In: Ineson, J.R. & Surlyk, F.

- (Eds), The Jurassic of Denmark and Greenland. Geological Survey of Denmark and Greenland Bulletin 1: 459–526.
- Nielsen, L.H., Mathiesen, A. & Bidstrup, T., 2004. Geothermal energy in Denmark. Geological Survey of Denmark and Greenland Bulletin 4, 17–20.
- Nielsen L. H., Andersen M. S., Balling N., Boldreel L. O., Fuchs S., Hjuler M. L., Kristensen L., Mathiesen A., Olivarius M., Weibel R., 2017. The geothermal energy potential in Denmark-updating the database and new structural and thermal models. In EGU General Assembly Conference Abstracts, Vol. 19, p. 7296.
- Petersen H. I., Nielsen L. H., Bojesen-Koefoed J. A., Mathiesen A., Kristensen L., Dalhoff F., 2008. Evaluation of the quality, thermal maturity and distribution of potential source rocks in the Danish part of the Norwegian–Danish Basin. Geological Survey of Denmark and Greenland Bulletin, 16: 1-27.
- Popov Y. A., Berezin V. V., Semionov V. G., & Korosteliy V. M., 1985. Complex detailed investigations of the thermal properties of rocks on the basis of a moving point source. *Izv Phys Solid Earth*, 21(1), 64-70.
- Popov Y., Mandel A. M., 1998. Geothermal study of anisotropic rock masses. *Izvestija, Physics of Solid Earth c/c of fizika zemli-rossiiskaia akademiia nauk*, 34, No 11: 903–915.
- Popov Y. A, Pribnow D.F.C., Sass J.H., Williams C.F., Burkhardt H., 1999. Characterization of rock thermal conductivity by high-resolution optical scanning. *Geothermics* 28(2), 253–276.
- Popov Y., Bayuk I., Parshin A., Miklashevskiy D., Novikov S., Chekhonin E., 2012. New methods and instruments for determination of reservoir thermal properties. In *Proceedings, Thirty-Seventh Workshop on Geothermal Reservoir Engineering Stanford University, Stanford, California*.
- Popov Y., Beardsmore G., Clauser C., Roy S., 2016. ISRM suggested methods for determining thermal properties of rocks from laboratory tests at atmospheric pressure. *Rock Mech. Rock. Eng.* 49, 4179–4207.
- Ray L., Förster H.-J., Förster A., Fuchs S., Naumann R., Appelt O., 2015. Tracking the thermal properties of the lower continental crust: Measured versus calculated thermal conductivity of high-grade metamorphic rocks (Southern Granulite Province, India). *Geothermics* 55: 138–149.
- Robertson, E.C., 1988. Thermal properties of rocks (Open-File Report 88-441). US Geological Survey, Reston, VA: 97p.
- Røgen B., Ditlefsen C., Vangkilde-Pedersen T., Nielsen L. H., Mahler A., 2015. Geothermal energy use, 2015 country update for Denmark. In *Proceedings world geothermal congress. Melbourne, Australia*: 9p.
- Vejbæk O. V., 1989. Effects of asthenospheric heat flow in basin modelling exemplified with the Danish Basin. *Earth and Planetary Science Letters* 95, 97–114.

- Watanabe H., 2003. Thermal Conductivity and Thermal Diffusivity of Sixteen Isomers of Alkanes: $C_n H_{2n+2}$ ($n= 6$ to 8). *Journal of Chemical & Engineering Data*, 48(1): 124–136.
- Woodside W., Messmer J., 1961a. Thermal conductivity of porous media. I. Unconsolidated sands. *Journal of Applied Physics* 32, 1688–1699.
- Woodside W., Messmer, J., 1961b. Thermal conductivity of porous media. II. Consolidated rocks. *Journal of Applied Physics* 32, 1699–1706.
- Van Wees J. D., Boxem T., Angelino L., & Dumas P., 2013. A prospective study on the geothermal potential in the EU. *Geoelect Report* 13, 96p.